ON IMPACT DAMPERS FOR NON - LINEAR AND SELF - EXCITED VIBRATING SYSTEMS
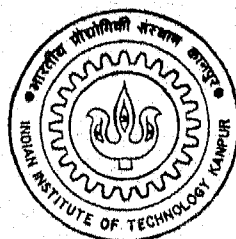
by

SHYAMAL CHATTERJEE

DEPARTMENT OF MECHANICAL ENGINEERING
INDIAN INSTITUTE OF TECHNOLOGY KANPUR
August, 1995

On Impact Dampers for Non-Linear and Self-Excited Vibrating Systems

A Thesis submitted
in partial fulfilment of the requirements
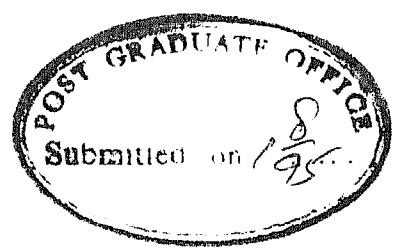*for the degree of*

Doctor of Philosophy

by
Shyamal Chatterjee

to the
DEPARTMENT OF MECHANICAL ENGINEERING
INDIAN INSTITUTE OF TECHNOLOGY
KANPUR
August 1995

Dedicated to

my beloved

parents and sister

CERTIFICATE

This is to certify that the present work titled **ON IMPACT DAMPERS FOR NON-LINEAR AND SELF-EXCITED VIBRATING SYSTEMS** by Mr. Shyamal Chatterjee has been carried out under our supervision and that, it has not been submitted elsewhere for a degree.

(A. Ghosh)

Professor

(A. K. Mallik)

Professor

Department of Mechanical Engineering

Indian Institute of Technology, Kanpur

ACKNOWLEDGEMENTS

It is a rare piece of fortune to have Professor A.K. Mallik and Professor A. Ghosh as my thesis supervisors. Only 'thank you' would be too cold a word to express my deep sense of gratitude. So let it be never expressed but felt for ever.

My sincere thanks are due to Professor N. Vays of our vibration lab.

I specially thank Professor A.K. Mallik for introducing me to the field of Non-linear Vibrations. Frequent visits of Professor J.K. Bhattacharyya to our laboratory were a continuous source of inspiration for our studies on CHAOS. I would also like to thank Professor M.R.M. Rao for his advanced courses on O.D.E. and Liapunov stability. I am very happy having Professor V. Gupta as one of my teachers. His friendly attitude to us can never be forgotten.

What, if I didn't have Ravindra, Rajiv, Chandrashekhar around me! It would have been simply impossible for me to live and work in the cool of our vibration lab. They kept it warm. They all were the sources of vibration, energy, fun, enjoyment and so on.

Soumya, Anirvan, Biswajit, Indra, Sudipta, Rahul, Biswaroop, Atanu and others brought chaotic order in my hall four days. It was they who made my six years stay at IITK, so short.

My special thanks are due to Mr. M. M. Singh for his kind assistance.

And my little, window-side table - you never felt tired bearing my load and sharing my frustrations, my pains, my joys. How do I acknowledge you! Or how do I express my love to you, my

cute, red cycle for carrying my weariness along the asphalt roads of IITK. I enjoyed your company on the way of my journey from the glass-doors of the C.C. to the bed of my dreams in so many dark silent nights.

Thanks every one I know.

Shyamal

SYNOPSIS

Linear/non-linear vibration neutralisers (absorbers), designed for controlling the vibrations of lightly damped systems are available in various forms. The hardware design of vibration neutralisers consists of a secondary mass connected to the primary vibrating body by a linear elastic member. It is known that a non-linear coupling force between the primary and secondary masses greatly enhances the effectiveness of a vibration absorber. An impact damper, in the form of a loose secondary mass provides a clearance type non-linear coupling force. This clearance eventually gives rise to repeated impacts between the primary and secondary masses and the vibration is attenuated mainly through the transfer of momentum. The simple constructional features of an impact damper make it very attractive for use in real life systems. Impact dampers have been successfully used to control the vibrations of various linear systems with well separated modal frequencies. The theoretical design methodologies of an impact damper are also developed based on the assumption that the primary system is linear. However, the non-linearity present in the primary system tends to show up its prominence when the system is strongly excited and needs to be controlled. Moreover, the oscillatory characteristics of certain systems, such as self-excited systems, are fundamentally non-linear. The major objective of the present thesis is to study the performance and design of an impact damper for non-linear systems. Three different

types of models of non-linear systems viz.,

(i) harmonically driven Duffing's oscillator,

(ii) autonomous van der Pol oscillator and

(iii) harmonically excited van der Pol oscillator

are considered in details. Besides the design of an impact damper, studies on various complicated dynamical responses of the systems under consideration are also carried out in the light of the bifurcation theory and chaotic dynamics. A brief outline of the contents of the thesis is given below.

The systems under consideration can be classified as piecewise smooth, non-linear systems. In chapter 2, the equivalent linearization procedure has been extended for such systems and is termed as the equivalent piecewise linearization (EPL) method. The efficacy of the method, as compared to the simple harmonic balance method (HBM), for piecewise smooth, non-linear systems has been demonstrated by considering a Duffing's oscillator with motion limiting stops (Vibroimpacting oscillator). The stability analysis of the solutions is also presented. All the analytical results are verified by numerically integrating the equations of motion.

In chapter 3, the design and performance of an impact damper for controlling the high-amplitude vibration of a harmonically excited, Duffing type primary system are discussed. Again, the results are obtained by the HBM, EPL and numerical integration. A detailed parametric study is carried out to demonstrate the effects of various parameters. The procedure for arriving at an optimal design is presented. The question of controlling the

subharmonic response has also been addressed to. Finally, the possibility of using the impact damper discontinuously in an active manner has been demonstrated. In this mode, the impact damper is shown to act as a migration controller which changes the initial conditions so as to bring the original system within the basin of attraction of a lower amplitude solution. Thus the feature of multiple stable solutions of a non-linear primary system is put to use.

In chapter 4, the performances of an impact damper towards controlling the autonomous (limit cycle amplitude) and harmonically entrained forced oscillations of self-excited oscillators, are discussed separately. In the latter case, after a detailed parametric study, an empirical relation for the optimum design is established. A sensitivity analysis of the design with reference to the self-excitation and forcing parameters is included.

In chapter 5, a study of bifurcations and chaos in self-excited, autonomous oscillators with an impact damper is presented. Results have been obtained by considering various models of the self-excitation mechanism. The major emphasis is on the detection of the types of bifurcations which are independent of the exact nature of the model. In this chapter, a numerical technique for analysing the eigen properties of the numerically integrated response has been proposed.

In chapter 6, different routes to chaos for a forced, van der Pol oscillator with an impact damper have been investigated. Some

uncommon intermittency routes to chaos have been detected. Finally in chapter 7, the overall conclusions and some suggestions for future works are included.

The major conclusions of the present thesis are listed below.

(i) The proposed EPL technique contains information in both time and frequency domains and consequently gives better results than the HBM which is simply a frequency domain technique. This method is particularly suitable for obtaining the time domain response of a class of piecewise smooth, non-linear systems.

(ii) An impact damper is effective, both in passive and active on-off forms, for controlling the vibration of non-linear systems having Duffing type restoring force characteristics. Both the primary and secondary resonances can be controlled. A simple formula is obtained for providing an initial design and it has been shown how to improve upon to obtain a final design.

(iii) An impact damper can be used to control both free and forced self-excited vibrations. Sensitivity of the designed performance towards the inaccuracy of the estimated model parameters is to be incorporated in the design rules. An empirical design formula for an impact damper attached to a forced van der Pol oscillator is provided after a detailed parametric study. The role of the coefficient of restitution for various situations has been clearly brought out.

(iv) Various instabilities occur in an autonomous self-excited system with an impact damper. The gross bifurcation superstructure of the systems under consideration is more or less independent of

the exact nature of the model of the self-excitation. A numerical technique has been developed for analysing the eigen properties of the stable solutions.

(v) The dynamics of a harmonically driven van der Pol oscillator with an impact damper is rich with different types of intermittency catastrophes viz., type II, type III etc. A new type of intermittency after a subcritical, symmetry-breaking pitchfork bifurcation is seen to exist in the system under consideration. Several instabilities of the system has a close resemblance to the hydrodynamic instabilities such as Rayleigh-Benard convection.

CONTENTS

CAPTIONS FOR FIGURES

C H A P T E R - 1

INTRODUCTION

1.1 Introduction

A rich variety of qualitatively different phenomena may be exhibited by a non-linear system. Such complex behaviour can never be predicted through the corresponding linearized system. In the last fifteen years, there is an explosion of literature related to the study of non-linear systems in various branches of physics and engineering. While the mathematician and physicists are attempting to analyse and categorise various non-linear phenomena, the engineers are trying to use these phenomena towards improving the performance of practical systems.

A mechanical vibrating system is often modelled through a combination of spring, mass and dashpot where the spring represents the restoring force and the dashpot represents the dissipative force. If the restoring and/or the dissipative forces present in the system are represented by some non-linear functions of the motion variables, then the system is called non-linear. Mostly these functions are considered to be smooth in nature. Such smooth non-linearity may arise due to large motion, material non-linearity and coupling of different modes of motion etc. But there are situations where an abrupt change in the restoring and/or dissipative forces or in the state of the system takes place. Such an abrupt change automatically brings in non-linearity

in the system, even if the nature of the restoring and dissipative forces basically remain linear. Speaking in mathematical terms, such non-linearity is introduced through the non-analytic nature of the restoring and dissipative forces which appear in the differential equations describing the model of the system. Such a system is often called a non-differentiable or piecewise smooth system.

The latter kind of non-linearity is present in a variety of man-made devices which engineers cannot afford to overlook. Connected components with unavoidable clearances in the joints, machining conditions during intermittent cutting, backlash in meshing gears, rotor-bearing mounting with clearance, colliding machine components such as impact hammers etc. are some common examples in this category. Sometimes clearances and impacts are deliberately introduced for improving the system performance. In the field of vibration control, the typical examples included the motion limiting stops such as elastic fenders for moored ships, vibration arresters for heat-exchanger tubes.

The use of a secondary system, elastically connected to a primary system, for controlling the near resonance, high amplitude oscillation of the latter is quite common. Such a secondary system is normally referred to as a dynamic vibration neutraliser(DVN). The analysis and design of such DVN's based on linear theory, in various forms, are widely reported in the literature on engineering vibrations. The idea of using a non-linear DVN for better effectiveness has also been proposed. But in practice, the introduction of a desired and controllable non-linearity in a

system is by no means an easy task. It is possibly the clearance which can generate non-linearity in a system in an easy and controllable fashion. Based on this idea, an impact damper is conceived where a loose secondary mass undergoes repeated collisions with the primary system and in the process reduces the unwanted vibration of the primary system.

Though the non-linearities may be effectively used for the purpose of vibration control, one must also remember that a non-linear system may become unstable in a number of ways to mar the system characteristics. This aspect of stability deserves serious attention at least in a qualitative sense. Recent studies of qualitative non-linear dynamics have shown ample promise to throw light on a number of complicated behaviours frequently observed in laboratory experiments and practical situations. For example, the noise in an apparently simple looking system (working in a more-or-less deterministic dynamic environment) may have its origin in the simple non-linearity provided by the clearance.

One of the major objectives of the present thesis is to investigate the role of an impact damper in controlling the vibration of inherently non-linear systems. Design philosophies and methodologies have been discussed for a class of non-linear oscillators such as Duffing's oscillator and van der Pol oscillator. Besides the aspects relating to vibration control, the characteristics of the complex behaviour exhibited by such non-linear systems with clearances and impacts have been studied in the light of the bifurcation theory and chaotic dynamics.

1.2 Literature Review

Systems having clearances and impacts have been modelled and studied by several authors. It has also been understood that at the level of mathematical modelling, many such systems reduce to a finite degrees-of-freedom systems having piecewise smooth restoring and dissipative force characteristics. A vast amount of literature exists on mechanical systems with clearances and impacts as well as on the qualitative study of dynamics of general piecewise smooth systems. Nevertheless, complexities associated with these systems are not completely unfolded till date. Research is still going on and the literature is expanding. The available literature is broadly categorised into two parts, namely

(i) Dynamics of mechanical systems with clearances, impacts and piecewise smooth non-linearity.

(ii) Use of clearances and impacts for vibration control: impact dampers.

1.2.1 Dynamics of Mechanical Systems with Clearances, Impacts and Piecewise Smooth Non-linearity.

The dynamics of piecewise smooth systems has been studied mainly through single and multi degree(s)-of-freedom model having bilinear/trilinear restoring and damping force characteristics. Some amount of theoretical results on the free oscillations of piecewise linear systems can be found in the book by Minorsky [1] under the heading of discontinuous theory. Maezawa et al. [2-4] have discussed different types of non-linear resonances of a periodically forced, single degree-of-freedom

oscillator with piecewise linear restoring force characteristics. Watanbe [5] analysed a single degree-of-freedom piecewise linear system having triangular hysteresis loop. Tomlinson et al. [6] have studied the frequency response characteristics of structures with single and multiple clearance type non-linearity. Shaw et al.[7], Natsiavas [8-10] and several other researchers [11-15] have thoroughly investigated different types of non-linear motion including chaos in bilinear forced oscillators. A detail account of the complex motions of offshore structures modelled by piecewise linear oscillators can be found in reference [16]. It has been demonstrated that even a simple system like a bilinear oscillator can show superharmonic and subharmonic resonances and different types of instabilities leading to chaos. Shaw et al.[17] have discussed the dynamic response of a preloaded joint. Choi et al.[18] considered the non-linear response of an articulated loading platform (ALP) tower with the help of a piecewise non-linear, single degree-of-freedom model. The dynamics of a beam with motion limiting elastic constraints has been analysed both theoretically and experimentally by several researchers [19-20].

A good deal of work has been done addressing the frequency response characteristics of two colliding masses known as an impact pair. Comparin et al.[21] have studied the spectral characteristics of an impact pair under harmonic excitation. In this investigation, the impact between two masses has been modelled by a spring-dashpot which eventually gives rise to a single degree-of-freedom system having piecewise linear restoring force characteristics. Bapat et al.[22-23] addressed the same

problem where the impact is modelled by a rule (using the concept of coefficient of restitution) governing the instantaneous change in the velocity after the collision. The dynamics of an impact pair under random excitations has also been investigated [24-26]. The dynamics of an inclined impact pair [27] has shown some fundamental differences from that of a horizontal one. The global dynamics, stability and chaos of an impact pair have been studied by Holmes [28] with the help of a non-linear map. The same problem is also treated by Bapat et al.[29] and others [30].

When one of the masses involved in an impact pair possess finite stiffness and inertia while the other has infinite stiffness and inertia the system is known as an vibroimpacting oscillator. The motivation behind the study of such systems stems from the practical need of designing impacting tools. Senator et al. [31] and Fu et al. [32] investigated the noise stabilization problem of a vibrating hammer. Whiston [33] and Fang et al.[34] considered a single degree-of-freedom impact oscillator under periodic excitation. Nguyen et al.[35-36] have carried out a detail parametric study and discussed some non-dimensional design parameters for the impact behaviour of an oscillator with limiting stops. Whiston [37] has considered the dynamic singularities associated with the global dynamics of an impact oscillator. Experimental investigation on the dynamics of an impacting pendulum system has been carried out by Moore et al. and others [38-39]. Aidanpaa et al. [40] considered a two degrees-of-freedom linear oscillator, impacting against a rigid stop, to investigate the periodic and chaotic responses. Recently a new type of

bifurcation has been detected in an impacting oscillator by Nordmark [41] and others [42]. The chaotic motions of impacting systems have also been addressed by Thompson et al.[43] and Peterka [44]. Hendricks [45] considered the dynamics of an impact print hammer of a dot matrix printer and demonstrated the possibility of the occurrence of chaos impairing high frequency printing. Several investigations have been carried out on the dynamics of impacting beams [46-48] and strings [49]. Jing et al.[50] reported the random dynamics of a single degree-of-freedom vibroimpacting oscillator where the impact has been modelled by a spring having Hertzian type contact stiffness. Palej et al.[51] have taken a different approach for analysing the impact oscillator where the impact force is treated as a sequence of Dirac distribution. Zhuravely [52] used the method of non-smooth transformation for analysing such a problem. Davies [53] investigated the stochastic vibration of an impacting beam. Bapat et al. [54] have recently shown the dynamic similarities among several vibroimpacting systems.

A general treatment of the dynamics of linear multi degrees-of-freedom system with colliding components can be found in a paper by Natsiavas [55]. In this paper, some problems have also been solved with special application to vibration control. Padmanabhan et al. [56] resolved some spectral coupling issues associated with a two degrees-of-freedom system with clearance type non-linearity. The frequency response characteristics of multi degrees-of-freedom system with clearances has been studied by Comparin et al.[57]. The non-linear dynamics of a rotor with

bearing clearance is reported in reference [58]. Kaharaman and Singh [59-60] have studied the non-linear dynamics of geared systems in the presence of time varying mesh stiffness and clearance. The effects of multiple clearances in a geared rotor bearing system have also been investigated by the same authors [61]. A theoretical and experimental study of the dynamics of a four bar chain with bearing clearances is reported by Stammers et al.[62]. The chaotic dynamics of heat exchanger tubes in the presence of support clearance has been investigated by Paidoussis [63-64].

1.2.2 Use of Clearances and Impacts in Vibration Control: Impact Dampers

Analytical and experimental studies have demonstrated that a class of non-linear auxiliary mass dampers, classically known as impact dampers, can be effectively used to neutralise the vibrations of various systems like light poles, turbine blades, antennae, aircraft wings, chimneys, machine tools etc. It is known that a suitable non-linear vibration neutraliser is, in general, more effective than a linear vibration neutraliser. But, in practice, as mentioned earlier, the introduction of a suitable non-linearity in the system may be difficult. In an impact damper, clearance and impact non-linearity is used which is comparatively easier to generate and control. The idea of using impact dampers for vibration control was conceived as early as late forties of this century. Since then, numerous papers have been published discussing its design and performance. Initially, impact dampers

were called acceleration dampers [65]. The first systematic
analytical basis for the design of an impact damper is given by
Grubin [66] and which was later simplified by Warburton [67].
Masri et al.[68-69] developed an efficient methodology for
studying the general motion and stability of an impact damper.
Their methodology in fact has provided a beginning for the deeper
analysis and estimation of the performance of impact dampers.
Impact dampers have been successfully used in attenuating the
vibrations of steam turbine buckets [70], tall flexible structures
[71] and machine tools [72] etc. A good account of the design
methods and constructional features of the impact dampers can be
found in the book by Mallik [73]. The effect of gravity on the
performance of an impact damper has been studied by Sadek et
al.[74]. The stable performance of an impact damper heavily
depends on the suitable choice of the design parameters such as
the clearance, the mass ratio and the coefficient of restitution
of the impact pair etc. Dokinish et al.[75] discussed the optimum
design parameters for an impact damper. Pinotti et al.[76]
provided design procedure and charts. Bapat et al.[77] carried out
a detail parametric study and reported the effects of different
design and system parameters on the performance of a single unit
impact damper towards controlling the forced and and free
vibrations of a single degree-of-freedom linear oscillator.
Mansour [78] considered the effect of friction on the performance
of an impact damper. Yasuda et al.[79] have provided an estimate
of the equivalent damping effect of an impact damper during free
vibration.

All the above mentioned investigations were performed assuming the excitation to be strictly harmonic which does not represent reality. In reality, the excitation is normally random in nature. Masri et al. [80] considered the response of an impact damper under stochastic excitations. Recently Semercigil et al.[81] have also treated the same problem.

Despite several attractive merits viz, simple constructional features, easy tunability and high amplitude reduction capability etc. the impact dampers have got certain limitations. The optimum performance of an impact damper is impaired in the presence of broad band excitations. Several attempts have been made to increase the operational bandwidth of an impact damper. One attractive way is to use a conventional dynamic vibration neutraliser where the auxiliary mass is provided with motion limiting stops [82-83]. Such an arrangement makes use of the good features of both the conventional dynamic neutraliser (larger operational bandwidth) and the impact damper (high attenuation). The use of spring supported secondary mass is another alternative [84]. Recently, Semercigil et al.[85] proposed a new vibration absorber which uses a conventional tuned absorber and an impact damper. Such a device is demonstrated to offer better vibration attenuation characteristics under broad band excitations.

The quest for quieter technologies gave birth to bean bag damper [86-87] where instead of a rigid slug, packaged particles known as bean bag is used as the secondary loose mass. Due to the plastic nature of the bean bag, the noise produced by an impact gets reduced. Recently the concept of migration control using an

impact damper for a non-linear primary system is proposed by Chatterjee et al.[88]. Such a scheme obviates the need of continuous noisy operation of an impact damper.

Another way of enhancing the performance of an impact damper is to use multi-particle single-unit or multi-unit systems. The motion and stability of an impact damper consisting of two-particle single unit container, have been discussed by Masri et al. [89]. Analytical and experimental investigations of multi-unit impact dampers have been reported by several researchers [90-92]. Cempel [93-94] used the continuous force approach and receptance model for analysing the performance of a multi-unit impact damper(MUVIN).

Most of the above investigations were carried out for a single degree-of-freedom model of the primary system which clearly signifies the importance of a single dominant mode of vibration. But such an assumption is true only for a simple system with well separated modes. When several modes are of significance, a multi degrees-of-freedom model of the primary system is necessary. Keeping that in view, the potential use of an impact damper for a multi degrees-of-freedom system has been studied by Nigam et al.[95]. They have questioned certain basic assumptions made by the earlier authors. Recently, Chelmers et al.[96] used two-unit impact dampers, placed at different locations, for controlling the vibrations up to the second mode of a cantilever beam.

The use of motion limiting stops for a centrifugal pendulum vibration absorber has also been reported [97].

Despite several modifications, a passive impact damper is incapable of performing well in a varied dynamic environment. This fact led Masri et al.[98-99] to develop an active parameter control technique for controlling the vibrations of an arbitrary non-linear system under a general kind of loading. One of the strong features of the technique is that no mathematical model of the system is at all necessary to design the control strategy.

It is a well known fact that even a low dimensional model of a non-linear system can very well explain the existence of different kinds of complex instabilities leading to chaos. On one hand the study of chaos gives some explanations of the presence of noise in an otherwise simple system and on the other hand, it gives the indications of potential dangerous components lying hidden in the beneficiary applications of non-linearity. Shaw et al.[100] have studied the nature of chaotic motions of a two degrees-of-freedom impact oscillator. Recently Sung et al.[101] have reported the existence of chaos in the model of an impact damper.

1.3 Objectives and Organization of the Present Work

Very often vibratory systems are modelled as linear systems. The principles and hardware designs of the control methods for such linear vibrations are well documented. A design based on the linear model suffices if the oscillatory movement is small. However, the non-linearity becomes pronounced when the vibration is large and needs to be controlled. Furthermore, there exist real life systems which, due to the presence of clearances and

self-excitation mechanisms, are basically non-linear. The inclusion of a secondary system in the form of a loose mass which undergoes repeated collisions with the primary system is a common method of vibration control. Such a secondary system is known as an impact damper. The major objective of the present thesis is to study the performance and design of an impact damper attached to non-linear primary systems. Three different models of the primary system, viz.,

(i) harmonically excited Duffing's oscillator,

(ii) autonomous van der Pol oscillator

and (iii) harmonically excited van der Pol oscillator

have been investigated. Both elastic and inelastic impacts have been discussed. Besides the design of an impact damper for these systems, the bifurcations and chaotic dynamics of the last two systems have been given special attention. Accordingly, the presentation has been organized as detailed below.

The systems under consideration can be classified as piecewise smooth, non-linear systems. In chapter 2, the equivalent linearization procedure has been extended for such systems and is termed as the equivalent piecewise linearization (EPL) method. The efficacy of the method, as compared simple harmonic balance method (HBM), for piecewise smooth, non-linear systems has been demonstrated by considering a Duffing's oscillator with motion limiting stops (Vibroimpacting oscillator). The stability analysis of the solutions is also presented. All the analytical results are verified by numerically integrating the equations of motion.

In chapter 3, the design and performance of an impact damper for controlling the high-amplitude vibration of a harmonically excited, duffing type primary system are discussed. Again, the results are obtained by HBM, EPL and numerical integration. A detailed parametric study is carried out to demonstrate the effects of various parameters. The procedure for arriving at an optimal design is presented. The question of controlling the subharmonic response has also been addressed to. Finally, the possibility of using the impact damper discontinuously in an active manner has been demonstrated. In this mode, the impact damper is shown to act as a migration controller which changes the initial conditions so as to bring the original system within the basin of attraction of a lower amplitude solution. Thus the feature of multiple stable solutions of a non-linear primary system is put to use.

In chapter 4, the performances of an impact damper towards controlling the autonomous (limit cycle amplitude) and harmonically entrained forced oscillations of self-excited oscillators, are discussed separately. In the latter case, after a detailed parametric study, an empirical relation for the optimum design is established. A sensitivity analysis of the design with reference to the self-excitation and forcing parameters is included.

In chapter 5, a study of bifurcations and chaos in self-excited, autonomous oscillators with an impact damper is presented. Results have been obtained by considering various models of the self-excitation mechanism. The major emphasis is on

the detection of the types of bifurcations which are independent of the exact nature of the model. In this chapter, a numerical technique for analysing the eigen properties of the numerically integrated response has been proposed.

In chapter 6, different routes to chaos for a forced, van der Pol oscillator with an impact damper have been investigated. Some uncommon intermittency routes to chaos have been detected. Finally in chapter 7, the overall conclusions and some suggestions for future works are included.

C H A P T E R - 2

PERIODIC RESPONSE OF PIECEWISE SMOOTH NON-LINEAR

OSCILLATORS UNDER HARMONIC EXCITATION

2.1 Introduction

A harmonically excited non-linear oscillator has been studied extensively in various branches of mathematics, physics and engineering. More commonly, the non-linearity in such oscillators is represented by the restoring and/or damping forces which are smooth non-linear functions of the state variables. Another source of non-linearity is the presence of discontinuity in the stiffness or damping coefficient or in the state variables. There exist a number of real life oscillators whose mathematical models include both the sources of non-linearity mentioned above. Typical examples in this class include mechanical devices with clearance and backlash, non-linear oscillators with motion-limiting stops or impact dampers, beams with cracks etc. Such an oscillator, for which the restoring (and/or damping) force is represented by a number of smooth non-linear functions, each valid for a range of the state variables, is called a piecewise smooth, non-linear oscillator. The harmonic balance method (HBM) is most commonly used for obtaining the periodic solutions of a harmonically excited, non-linear oscillator. It has also been used for piecewise smooth, non-linear oscillators [88]. The HBM, though works quite well for a weakly non-linear system, fails to give satisfactory results if the effective non-linearity

is large due to the sharpness of the change between the adjacent smooth functions. Moreover, the inclusion of higher harmonics in closed form becomes impossible due to the presence of Heaviside step functions in the mathematical model of such an oscillator.

The difficulties encountered in the HBM while tackling a piecewise smooth, non-linear oscillator are taken care of by the incremental harmonic balance method (IHBM) [102]. This method, based on the local linearization in the parameter space, is also capable of including higher harmonics in the solution. Kim et al. [11] have developed an useful method by combining the fast Fourier transform and harmonic balance techniques (FFT-HB). This method has been used to study the dynamics of both piecewise linear and piecewise smooth, non-linear systems [18].

The accuracy of the results obtained by the IHBM and FFT-HB technique depends, like all harmonic balance techniques, on the number of harmonics included. Sometimes, ten to twenty harmonics are to be retained for convergence [18]. Basically both the methods are iterative and hence computationally involved. No uniform convergence criterion can be used in the iterative scheme. These problems become more prominent if the response contains sharp spikes (e.g., due to a sharp change in the restoring force as in the impacting situation) when a large number of harmonics need to be retained. The stability analysis associated with the above methods uses variational technique for non-differentiable systems (which is mathematically heuristic) and gives rise to Hill's equation. Both the IHBM and FFT-HB technique, while having general applicability, may turn out to be computationally

inefficient for some simple non-linear systems undergoing sharp changes in the restoring and/or damping force. Sometimes recasting of a problem to suit the algorithm also becomes complicated.

In the present chapter, we propose to first transform a piecewise smooth, non-linear system to an equivalent piecewise linear (EPL) system and thereafter, use an exact method proposed by Masri el al. [69]. In this method, the form of the solution for each range having different coefficients of equivalent linearity is known. The solution contains a number of unknowns which are subsequently determined by imposing the conditions of periodicity, symmetry (if any) and consistency to be maintained at every junction of adjacent linear ranges. Thus, in the present method, the form of the solution is not based entirely on the harmonic components and the sharp change between the adjacent non-linear ranges are treated as such. Consequently, the sharp spikes in the time series of the responses are predicted much more easily as compared to that by the IHBM or FFT-HB technique. A dual representation of the solution is used to greatly enhance the algebraic simplicity and numerical efficiency. The stability analysis is carried out using the method of error propagation [68] wherein a linearized Poincare' map relating the perturbation vectors at the end and beginning of a period is constructed. The eigenvalues of the Poincare map determine the stability of the obtained solution.

It must, however, be mentioned that an accurate knowledge of the number of junctions to be encountered during one period (of the periodic response) is a pre-requisite for using the proposed

method. The method obviously becomes unwieldy if the number of such junctions becomes too many. Fortunately, for a number of models of practical interest, this number is often small for a wide range of parameter values. Numerical results are included to demonstrate the efficacy of the proposed method for the following two situations:

i)   a harmonically driven Duffing's ossillator having an one-sided elastic constraint and

ii) a harmonically driven Duffing's oscillator having an one sided rigid constraint.

2.2   Harmonically Driven Duffing's Oscillator with One-sided Elastic Constraint.

To demonstrate the efficacy of the proposed method (EPL), let us consider a harmonically excited Duffing's oscillator with one-sided elastic constraint (Figure 2.1). The equation of motion of the system in non-dimensional form is given by

$$\ddot{X} + 2h\,\dot{X} + X + \varepsilon\,X^3 + r_1(X-1)\,U(X-1) = F_0 \cos \Omega\tau \qquad (2.1)$$

where $X = x/x_0$, $\omega_0 = \sqrt{K_1/m}$, $h = C/(2\,m\,\omega_0)$,

$\varepsilon = K_2 x_0^2/(m\,\omega_0^2)$, $r_1 = K_3/(m\,\omega_0^2)$, $\tau = \omega_0 t$,

$\Omega = \omega/\omega_0$, $F_0 = F/(m\,\omega_0^2\,x_0)$

and the dot denotes differentiation with respect to the
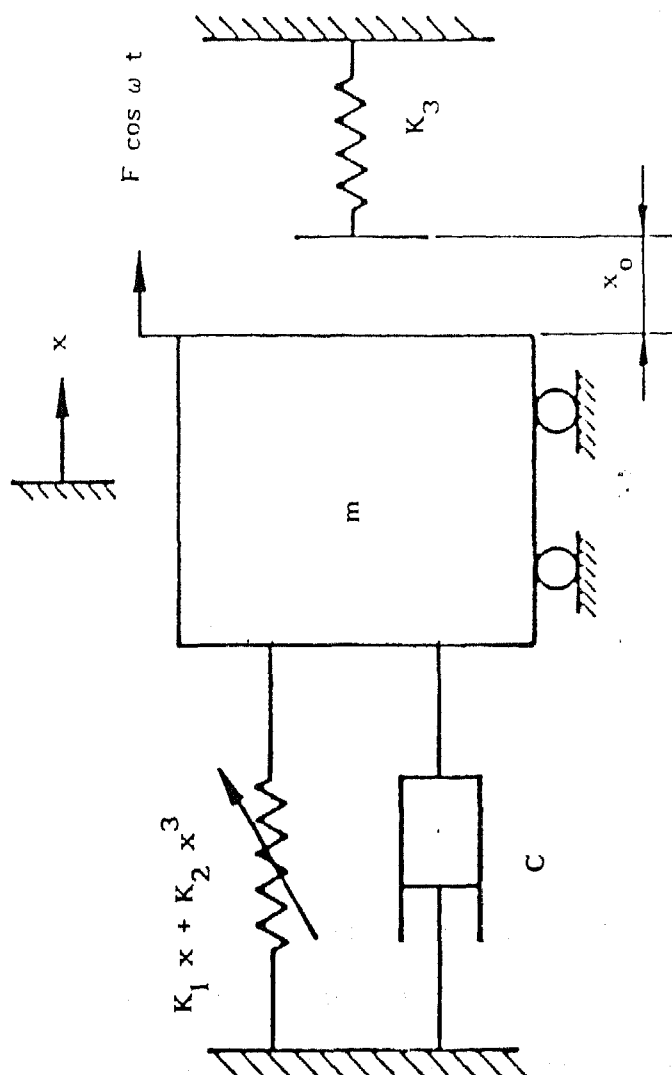
Figure 2.1   Model of a single degree-of-freedom Duffing's oscillator with an one-sided elastic constraint.

non-dimensional time τ. The Heaviside's step function U(.) is defined as

$$U(Z) = 1 \quad Z > 0$$
$$\quad\quad = 0 \quad Z < 0$$

It is desired to suitably transform equation (2.1) into piecewise linear form given by

$$\ddot{X} - 2\,\rho\,\dot{X} + X + \varepsilon\,K_e\,X + r_1\,(X-1)\,U\,(X-1) = F_o \cos \Omega\tau \quad\quad (2.2)$$

With $\rho = - h$ and K_e as an unknown constant. Equation (2.2) can be solved using the method of condition matching [69]. However, the solution so constructed carries the unknown K_e, which can subsequently be calculated as elaborated in the next section.

2.2.1 Periodic Solution

We are interested in constructing a periodic solution of equation (2.2) having a period τ_p, which is an integral multiple of the forcing period $(\tau_f = 2\pi/\Omega)$. To start with, we consider the type of solution depicted in Figure 2.2. Numerical simulation of equation (2.1) suggests that this type of motion of the oscillator does occur for a wide range of parameter values. In Figure 2.2, we have arbitrarily set $\tau = 0$ when the contact with the constraint is first established with positive velocity and the contact is maintained for a time interval τ_c. This arbitrary setting of the time origin requires introduction of an unknown phase ϕ in the forcing function. Thus, a solution of the form shown in Figure 2.2 can be written as
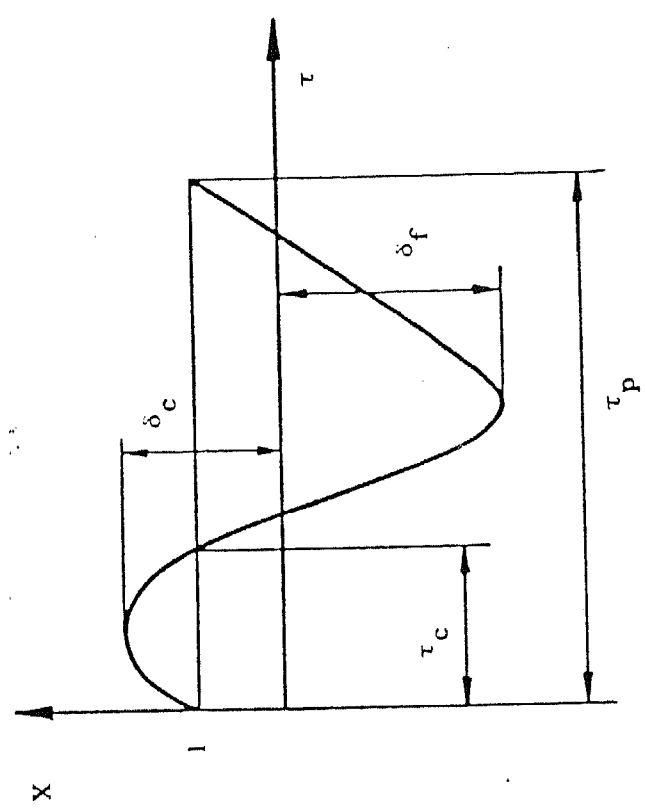
Figure 2.2 A typical periodic solution having a single crossing per cycle.

$$X(\tau) = X_1(\tau) \ U(-T) + X_2(\tau) \ U(T) \qquad (2.3)$$

where $T = \tau - \tau_c$ and X_1 and X_2 are given by (see equation (2.2))

$$\ddot{X}_1 - 2\rho \ \dot{X}_1 + \omega_1^2 \ X_1 = F_o \cos(\Omega\tau + \phi) + r_1 \qquad (2.4)$$

$$\text{with } X_1(\tau) > 1 \ , \quad \forall \ 0 < \tau < \tau_c$$

and

$$\ddot{X}_2 - 2\rho \ \dot{X}_2 + \omega_2^2 \ X_2 = F_o \cos(\Omega\tau + \phi) \qquad (2.5)$$

$$\text{with } X_2(\tau) < 1 \ , \quad \forall \ 0 < \tau_c < \tau < \tau_p$$

with ω_1 and ω_2 defined as

$$\omega_1^2 = 1 + \varepsilon K_e + r_1$$

$$\omega_2^2 = 1 + \varepsilon K_e \ .$$

The solutions of equations (2.4) and (2.5) can be written as

$$X_1(\tau) = e^{\rho\tau} (d_1 \cos(\eta_1\tau) + d_2 \sin(\eta_1\tau)) + M_1\cos(\Omega\tau + \phi + \theta_1)$$

$$+ \frac{r_1}{\omega_1^2} \qquad (2.6)$$

and

$$X_2(\tau) = e^{\rho(\tau-\tau_c)} (d_3\cos \eta_2(\tau-\tau_c) + d_4\sin \eta_2(\tau-\tau_c))$$

$$+ M_2\cos(\Omega\tau + \phi+\theta_2) \qquad (2.7)$$

where

$$\eta_i = \sqrt{\omega_i^2 - \rho^2}$$

$$M_i = F_o / \sqrt{(\omega_i^2 - \Omega^2)^2 + (2\rho\Omega)^2}$$

and $\tan \theta_i = \dfrac{2 \rho \Omega}{\omega_i^2 - \Omega^2}$ with $i = 1,2$.

Satisfying the continuity condition (at $\tau = \tau_c$) and using the periodicity with time-period τ_p one can write

$$X_1(0) = X_1(\tau_c) = X_2(\tau_c) = X_2(\tau_p) = 1$$

$$\dot{X}_1(0) = \dot{X}_2(\tau_p) = \dot{X}_o \text{ (say)}$$

and $\qquad \dot{X}_1(\tau_c) = \dot{X}_2(\tau_c) = \dot{X}_c$ (say). $\hfill (2.8)$

It should be noted that equations (2.6) and (2.7) contain seven unknowns, viz., d_1, d_2, d_3, d_4, ϕ, τ_c and K_e. Using conditions (2.8) we can eliminate d_1, d_2, d_3, d_4 and ϕ to obtain a relation of the form

$$f_1(K_e, \tau_c) = 0 . \hfill (2.9)$$

One may think of several ways of computing K_e from (2.9) with the objective of minimizing the integral

$$I = \int_o^{\tau_p} \Big(\ddot{X}(\tau) - 2\rho \dot{X}(\tau) + X(\tau) + \varepsilon X^3(\tau) +$$

$$r_1(X(\tau) - 1) U(X(\tau) - 1) - F_o \cos(\Omega\tau) \Big)^2 d\tau$$

where $X(\tau)$ is defined by equation (2.3). However, direct substitution of equations (2.6) and (2.7) in the integral I makes the subsequent algebra too formidable. An iterative way would be to start with an initial guess value of K_e. But such a numerical procedure is found to be computationally very inefficient simply because no good initial guess of K_e can be made in a systematic way and the solution of equation (2.9) along with the evaluation of the integral I makes the algorithm very slow.

We, therefore, suggest the following method. First the solution $X(\tau)$ is expanded in its Fourier basis and written as

$$X^*(\tau) = A_o + A_1 \cos (\Omega\tau + \psi_1) + \ldots\ldots \tag{2.10}$$

and K_e is determined as a function of the Fourier coefficients

$$K_e = K_e (A_o, A_1, \ldots\ldots) \tag{2.11}$$

to render

$$\frac{\partial}{\partial K_e} \int_o^{\tau_p} (X^{*^3} - K_e X^*)^2 \, d\tau = 0 \ . \tag{2.12}$$

It should be noted that $X^*(\tau)$ and $X(\tau)$ are two different representations of the solution of the same differential equation. So these should be brought closer by minimizing the least square of their difference, i.e.,

$$\int_{0}^{\tau_p} (X^*(\tau) - X(\tau))^2 \, d\tau \qquad \text{is minimum} \qquad (2.13)$$

According to the theory of Fourier series, this minimization takes place if A_o, A_1..etc. correspond to the Fourier coefficients of $X(\tau)$ given by equation (2.3). This condition generates appropriate number of equations to solve the problem as explained below.

Let us consider

$$X^*(\tau) = A_o + A_1 \cos(\Omega\tau + \psi_1) \qquad (2.14)$$

when equation (2.12) yields

$$K_e = \frac{2f_a A_o + f_b A_1}{2A_o^2 + A_1^2} \qquad (2.15)$$

where $\qquad f_a = A_o^3 + \frac{3}{2} A_o A_1^2$

and $\qquad f_b = 3 A_o^2 A_1 + \frac{3}{4} A_1^3$.

From condition (2.13) we get

$$A_o = \frac{1}{\tau_p} \int_{0}^{\tau_p} X(\tau) \, d\tau \qquad (2.16)$$

and $\qquad A_1^2 = \left(\frac{2}{\tau_p}\right)^2 \left| \int_{0}^{\tau_p} X(\tau) \, e^{i\Omega\tau} \, d\tau \right|^2 \qquad (2.17)$

where the constants appearing in $X(\tau)$ (see equations (2.6) and (2.7)) are also expressed in terms of K_e and τ_c. Equation (2.9) can be rewritten, by using equation (2.15), in the form

$$f_2 \ (A_o, \ A_1, \ \tau_c) = 0 \qquad\qquad (2.18)$$

Now equations (2.16)-(2.18) can be solved to obtain A_o, A_1 and τ_c when all the quantities appearing in equations (2.6) and (2.7) can easily be obtained.

It should be emphasized that in this method one gets dual approximations of the solution; namely $X^*(\tau)$ and $X(\tau)$. So far as the nature of the solution is concerned, $X(\tau)$ gives better approximation as compared to $X^*(\tau)$. However, it will be seen later that sometimes $X^*(\tau)$ can also accurately predict the maximum displacement of the oscillator. We call $X(\tau)$ as the primary solution and $X^*(\tau)$ as the secondary solution.

2.2.2 Stability Analysis

Both stable and unstable solutions are obtained by the proposed EPL method. The method of error propagation explained by Masri et al. [68] has been used to ascertain the stability of the obtained solution. Towards this end, we consider the obtained solution $X(\tau)$ represented by the solid line in Figure 2.3 and its perturbed form $\bar{X}(\bar{\tau})$ represented by the dashed line in the same figure. Referring to Figure 2.3 we can write
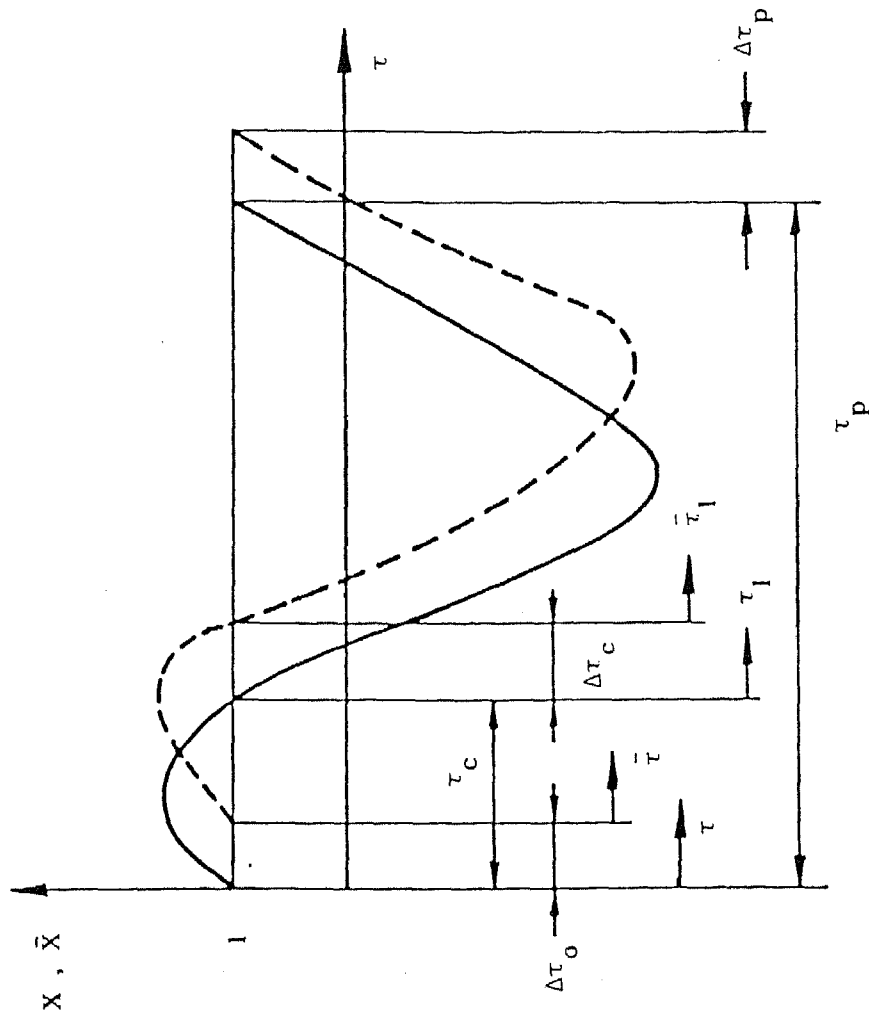
Figure 2.3 A typical periodic solution and its arbitrarily perturbed form. —— solution, - - - perturbed form where $X = X_1$ if $X > 1$, $X = X_2$ if $X < 1$, $\bar{X} = \bar{X}_1$ if $\bar{X} > 1$ and $\bar{X} = \bar{X}_2$ if $\bar{X} < 1$.

$$\bar{X}_1(0) = \bar{X}_1 \ (\tau_c + \Delta T_o) = 1$$

$$\dot{\bar{X}}_1(0) = \dot{X}_o + \Delta \dot{X}_o$$

$$\dot{\bar{X}}_1 \ (\tau_c + \Delta T_o) = \dot{X}_c + \Delta \dot{X}_c \qquad (2.19)$$

(see condition (2.8) for the definitions of $\dot{X}_o$ and $\dot{X}_c$)

where $\Delta T_o = \Delta \tau_c - \Delta \tau_o \qquad (2.20)$

Using the above conditions one obtains the linearized relations between the perturbations in the form

$$\left\{ \begin{array}{c} \Delta \tau_c \\ \Delta \dot{x}_c \end{array} \right\} = [P_1] \left\{ \begin{array}{c} \Delta \tau_o \\ \Delta \dot{x}_o \end{array} \right\} \qquad (2.21)$$

where the elements of the 2x2 matrix $[P_1]$ are functions of the system parameters and the constants appearing in the solution given by equation (2.6). Considering the solution for the interval beyond τ_c(and $\leq \tau_p$) given by equation (2.7) and using the following conditions:

$$\bar{X}_2(0) = \bar{X}_2 \ (\tau_p + \Delta T_1) = 1 \ ,$$

$$\dot{\bar{X}}_2(0) = \dot{X}_c + \Delta \dot{X}_c$$

$$\text{and} \ \dot{\bar{X}}_2 \ (\tau_p + \Delta T_1) = \dot{X}_f + \Delta \dot{X}_f \qquad (2.22)$$

where $\Delta T_1 = \Delta \tau_p - \Delta \tau_c - \tau_c$ and $\dot{X}_f$ is the velocity of the oscillator at the end of the period, one obtains

$$\left\{ \begin{array}{c} \Delta\tau_p \\ \Delta\dot{x}_f \end{array} \right\} = [P_2] \left\{ \begin{array}{c} \Delta\tau_c \\ \Delta\dot{x}_c \end{array} \right\} \tag{2.23}$$

Combining equations (2.22) and (2.23) one gets

$$\left\{ \begin{array}{c} \Delta\tau_p \\ \Delta\dot{x}_f \end{array} \right\} = [P] \left\{ \begin{array}{c} \Delta\tau_o \\ \Delta\dot{x}_o \end{array} \right\} \tag{2.24}$$

where $[P] = [P_2] [P_1]$. A solution is stable if all the eigenvalues of $[P]$ lie inside the unit circle around the origin of the complex plane.

2.2.3 Harmonic Balance Techniques

It is known that the IHBM, FFT-HB and HBM are essentially same in the first approximation. As already stated, while the first two methods can be extended to higher order approximations, the HBM can include only the first term in closed form. To see the efficiency of the proposed EPL method (in the first term approximation only) the HBM has been chosen for comparison. Let the first term solution in the HBM be

$$X (\tau) = B_o + B_1 \cos (\Omega\tau + \theta) \tag{2.25}$$

Substituting equation (2.25) in equation (2.1) the coefficients of equal circular functions are matched. While doing so, the Fourier expansions of the Heaviside's step functions are

used. Finally one gets the following non-linear algebraic equations

$$B_o + \varepsilon B_o^3 + \frac{3\varepsilon}{2} B_o B_1^2 + r_1 Q_o = 0 \tag{2.26}$$

$$B_1 (1 - \Omega^2) + \frac{3\varepsilon}{4} B_1^3 + 3 \varepsilon B_o^2 B_1 + r_1 Q_1 = F_o \cos \theta \tag{2.27}$$

and $\quad -2 h B_1 \Omega = F_o \sin \theta \tag{2.28}$

Where, if the collision occurs, i.e., if $\left| \dfrac{B_o - 1}{B_1} \right| \leq 1$, then

$$Q_o = \frac{B_1}{\pi} \sqrt{1 - \left(\frac{B_o - 1}{B_1} \right)^2} + \left(B_o - 1 \right) \left[\frac{1}{2} + \frac{1}{\pi} \sin^{-1} \left(\frac{B_o - 1}{B_1} \right) \right]$$

and $\quad Q_1 = \dfrac{B_o - 1}{\pi} \sqrt{1 - \left(\dfrac{B_o - 1}{B_1} \right)^2} + B_1 \left[\dfrac{1}{2} + \dfrac{1}{\pi} \sin^{-1} \left(\dfrac{B_o - 1}{B_1} \right) \right]$

otherwise $\quad\quad Q_o = Q_1 = 0.$

The solution $X(\tau)$ is thus obtained by solving B_o and B_1 from equations (2.26)-(2.28).

2.2.4 Numerical Results

The periodic solutions with period $2\pi/\Omega$ have been obtained using both the EPL method and simple HBM. These results are compared with the solutions obtained via direct numerical integration using fourth-order Runge-Kutta-Merson algorithm with

adaptive step size control. A typical frequency response characteristic of the system is shown in Figure 2.4. The branches AB and DE in Figure 2.4 correspond to the non-contacting solution and hence can be produced using several techniques widely discussed in the literature. Even a single term harmonic balance can also produce these branches accurately. The branch DC refers to the unstable solution. So we are interested in obtaining only the branch BC where the elastic constraint is in operation.

The response of the system being asymmetric, the maximum displacements of the mass on either side of the equilibrium position (i.e. both positive and negative) are plotted separately in Figures 2.5(a) - 2.5(d) for two different values of r_1.

The maximum displacement on the free side is represented by δ_f as shown in Figure 2.2 whereas that on the constrained side is δ_c. It may be pointed out that the secondary solution $X^*(\tau)$ gives another measure of the maximum displacement of the mass on the free side by $\delta_f^* = |X^*(\tau)|_{max}$.

From Figures 2.5(a) and 2.5(b) it may be seen that for a low value of the stiffness of the restraining spring (r_1), both the EPL and HBM produce a good estimate of δ_f which is also seen to be higher than δ_c. The EPL method, when compared to the HBM, gives better results so far as the displacement on the constraint side is concerned. This will be of significance especially if the deformation of the restraining spring is an important parameter for its design. From Figures 2.5(a) and 2.5(c) we note that as the displacement on the free side increases, δ_f^* becomes more accurate than δ_f. From Figures 2.5(c) and 2.5(d), we can conclude that with
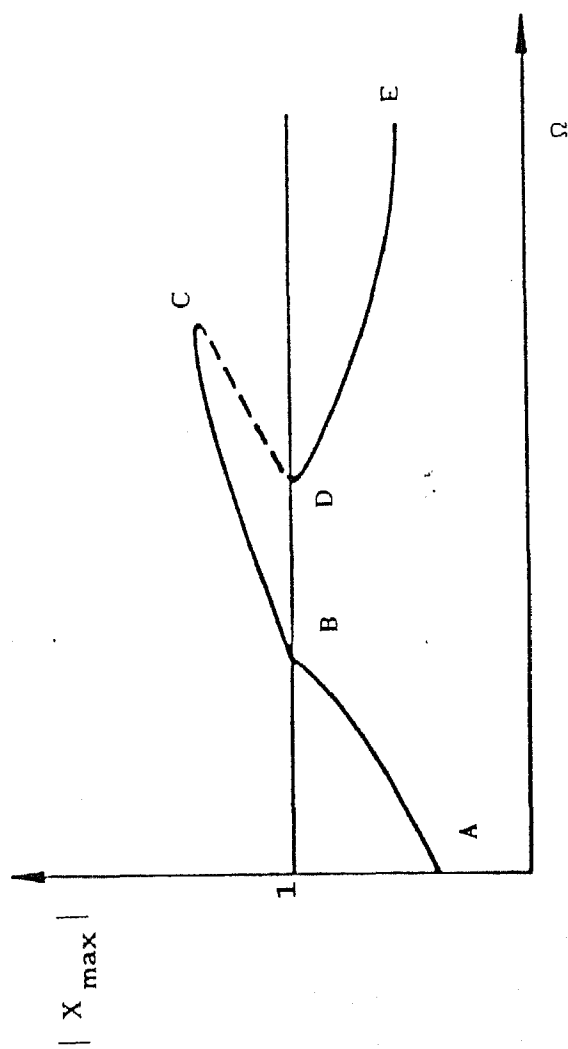
Figure 2.4   Typical frequency response characteristic of a piecewise non-linear system near its fundamental resonance.
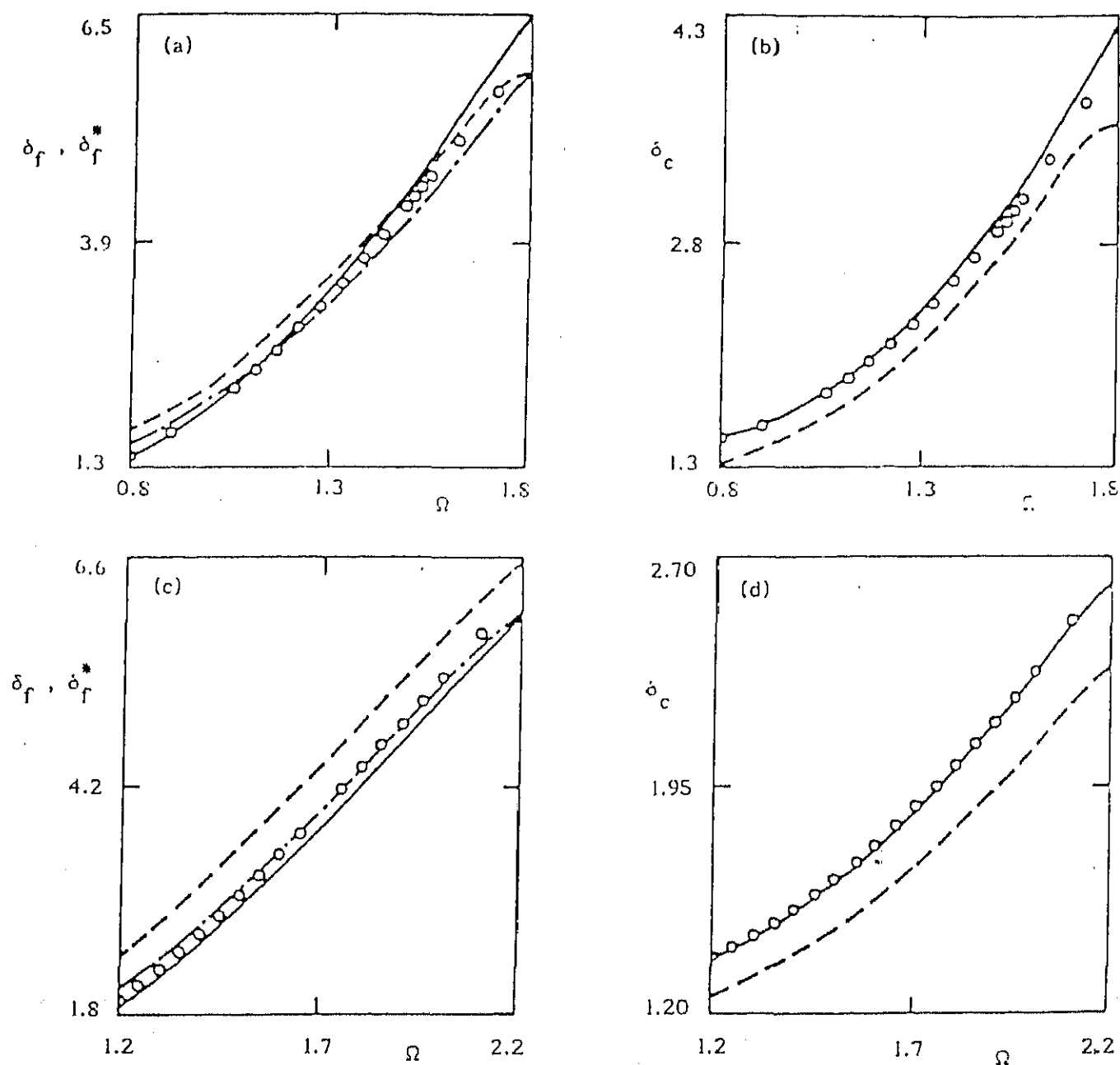
Figure 2.5 Frequency response within the contacting branch near fundamental resonance. $\varepsilon = 0.05$, $F_o = 1$, $h = 0.05$ $r_1 = 5$ in a & b and $r_1 = 25$ in c & d . —— EPL, - - - HBM, - · - · - δ_f^* , o numerical integration.

a stiff restraining spring, the single term EPL solution is much better than that produced by the HBM. The accuracy of the HBM was found to deteriorate drastically with increasing values of r_1.

2.3 Vibroimpacting Duffing's Oscillator

In the previous section we have discussed the efficacy of the EPL method in obtaining the approximate solution of a Duffing's oscillator with one sided elastic constraint. In the present section, the constraint is assumed to be rigid. A rigid constraint can be modelled in various ways. One way would be to assign a very high value (ideally infinity) of r_1. But a very high value of r_1 leads to unavoidable numerical difficulty in solving the algebraic equations (2.16)-(2.18). This difficulty is overcome if the collision of the oscillating mass with the rigid constraint is modelled by assigning a rule governing an instantaneous change in the velocity (using the concept of coefficient of restitution) at the constraint boundary. It should be noted here that such modelling is not amenable to the HBM. However, the EPL method can be used very efficiently as explained below.

2.3.1 Periodic Solution

For the sake of algebraic simplicity, first a single impact per cycle motion having a period τ_p is constructed. The nature of the solution sought is sketched in Figure 2.6 when the displacement of the mass can be written as
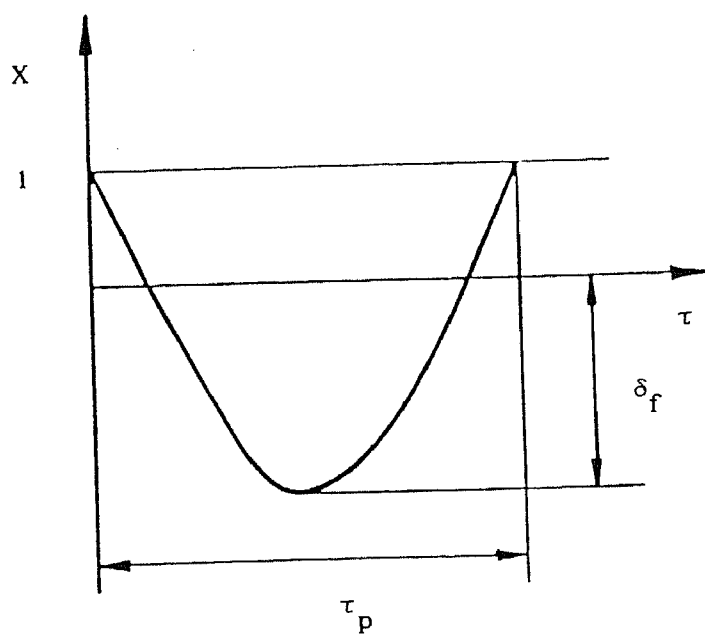
Figure 2.6 A typical periodic solution having single impact per cycle.

$$X(\tau) = e^{\rho\tau} (d_3 \cos(\eta_2\tau) + d_4 \sin(\eta_2\tau)) + M_2 \cos(\Omega\tau + \phi + \theta_2)$$

$$(2.29)$$

Further, we have the following periodicity and impact conditions:

$$X(0) = X(\tau_p) = 1$$

let $\qquad X(0^+) \equiv \dot{X}_a$ and $X(\tau_p^-) \equiv \dot{X}_b \qquad$ (2.30)

with $\qquad \dot{X}_a = -\chi \dot{X}_b$

where χ is the coefficient of restitution.

Using conditions (2.30) we eliminate two unknowns, viz., d_3 and d_4 to obtain a relation of the form

$$f_2(\phi, K_e) = 0 \qquad (2.31)$$

For calculating K_e corresponding to a solution of period $\tau_p = 2\pi/\Omega$, we consider the secondary solution

$$X^*(\tau) = A_o + A_1 \cos(\Omega\tau + \delta_1) + A_2 \cos(2\Omega\tau + \delta_2) \qquad (2.32)$$

when equation (2.12) yields

$$K_e = \frac{2f_a A_o + 2f_b A_1 + f_d A_2 + (A_1 f_c + f_e A_2) \cos(\delta_2 - 2\delta_1)}{2 A_o^2 + A_1^2 + A_2^2}$$

where $\quad f_a = A_o^3 + \dfrac{3}{2} A_1^2 A_o + \dfrac{3}{2} A_2^2 A_o + \dfrac{3}{4} A_2 A_1^2 \cos (\delta_2 - 2\delta_1),$

$$f_b = 3 A_o^2 A_1 + \frac{3}{4} A_1^3 + \frac{3A_2^2 A_1}{2},$$

$$f_c = 3 A_2 A_1 A_o,$$

$$f_d = \frac{3}{4} A_2^3 + 3A_2 \left(A_o^2 + \frac{A_1^2}{2}\right),$$

$$f_e = \frac{3}{2} A_1^2 A_o$$

and equation (2.13) yields

$$A_o = \frac{1}{\tau_p} \int_0^{\tau_p} X(\tau) \, d\tau \quad , \tag{2.33}$$

$$A_n^2 = \left(\frac{2}{\tau_p}\right)^2 \left| \int_0^{\tau_p} X(\tau) \, e^{i\Omega n \tau} \, d\tau \right|^2 \tag{2.34}$$

and $\quad \tan \delta_n = \dfrac{\text{Im } (\lambda_n)}{\text{Re } (\lambda_n)} \quad$ for $n = 1,2$ $\tag{2.35}$

where $\quad \lambda_n = \displaystyle\int_0^{\tau_p} X(\tau) \, e^{i\Omega n \tau} \, d\tau$

and Im (.) and Re(.) represent, respectively, the imaginary and real parts of λ_n.

A similar procedure can be followed for obtaining a solution with higher (than that of the excitation) time-periods. For example, to compute a solution with period $2\tau_f$ the secondary solution is written in the form

$$X^*(\tau) = A_o + A_1 \cos(\Omega\tau + \delta_1) + A_{1/2}\cos(\frac{\Omega}{2}\tau + \delta_{1/2})$$

when finally we obtain

$$K_e = \left\{ f_a A_o + f_b A_1 + f_g A_{1/2} + (A_1 f_c + A_{1/2}f_h) \cos(\delta_1 - 2\delta_{1/2}) \right\} / D$$

where $f_a = A_o^3 + \frac{3}{2} A_o A_1^2 + \frac{3}{2} A_{1/2}^2 A_o + \frac{3}{4} A_{1/2}^2 A_1 \cos(\delta_2 - 2\delta_{1/2})$,

$$f_b = 3 A_o^2 A_1 + \frac{3}{4} A_1^3 + \frac{3}{2} A_{1/2}^2 A_1,$$

$$f_c = \frac{3}{2} A_{1/2}^2 A_o,$$

$$f_g = \frac{3}{4} A_{1/2}^3 + 3A_o^2 A_{1/2} + \frac{3}{2} A_{1/2} A_1^2,$$

$$f_h = 3A_o A_1$$

and

$$D = 2 A_o^2 + A_1^2 + A_{1/2}^2$$

The stability analysis of the solution is carried out using the method of error propagation outlined in section 2.2.2.

2.3.2 Numerical Results

In this section, the numerical results obtained from the EPL method are compared with those obtained from direct numerical integration. Only the stable impacting solutions are plotted. The maximum displacement of the mass on the free side, (δ_f and δ_f^*), obtained with $\tau_p = 2\pi/\Omega$ is plotted against frequency in Figure 2.7. It is seen that the EPL approximation with $A_2 \neq 0$ is better than that with $A_2 = 0$. In fact, the inclusion of more number of harmonics in $X^*(\tau)$ is seen to produce higher accuracy. However, δ_f^* obtained with $A_2 = 0$ gives a reasonably good estimate of the maximum absolute displacement of the oscillation, especially if the value of δ_f^* is high. The impact velocity $(\dot{X}_b)$ is plotted against the forcing frequency in Figure 2.8. It is seen that even the first approximation (i.e. with $A_2 = 0$) gives a very accurate estimate of the impact velocity.

The maximum absolute displacement δ_f for a solution with period $4\pi/\Omega$ is plotted in Figure 2.9. Again it is confirmed that the EPL method can very well account for the subharmonic contributions.

2.4 Conclusions

Simple single term harmonic balance method fails to predict the periodic response of a piecewise smooth, non-linear oscillator, especially if the degree of non-linearity changes sharply at the junction between the adjacent (non-linear) regions. The proposed equivalent piecewise linearization technique works
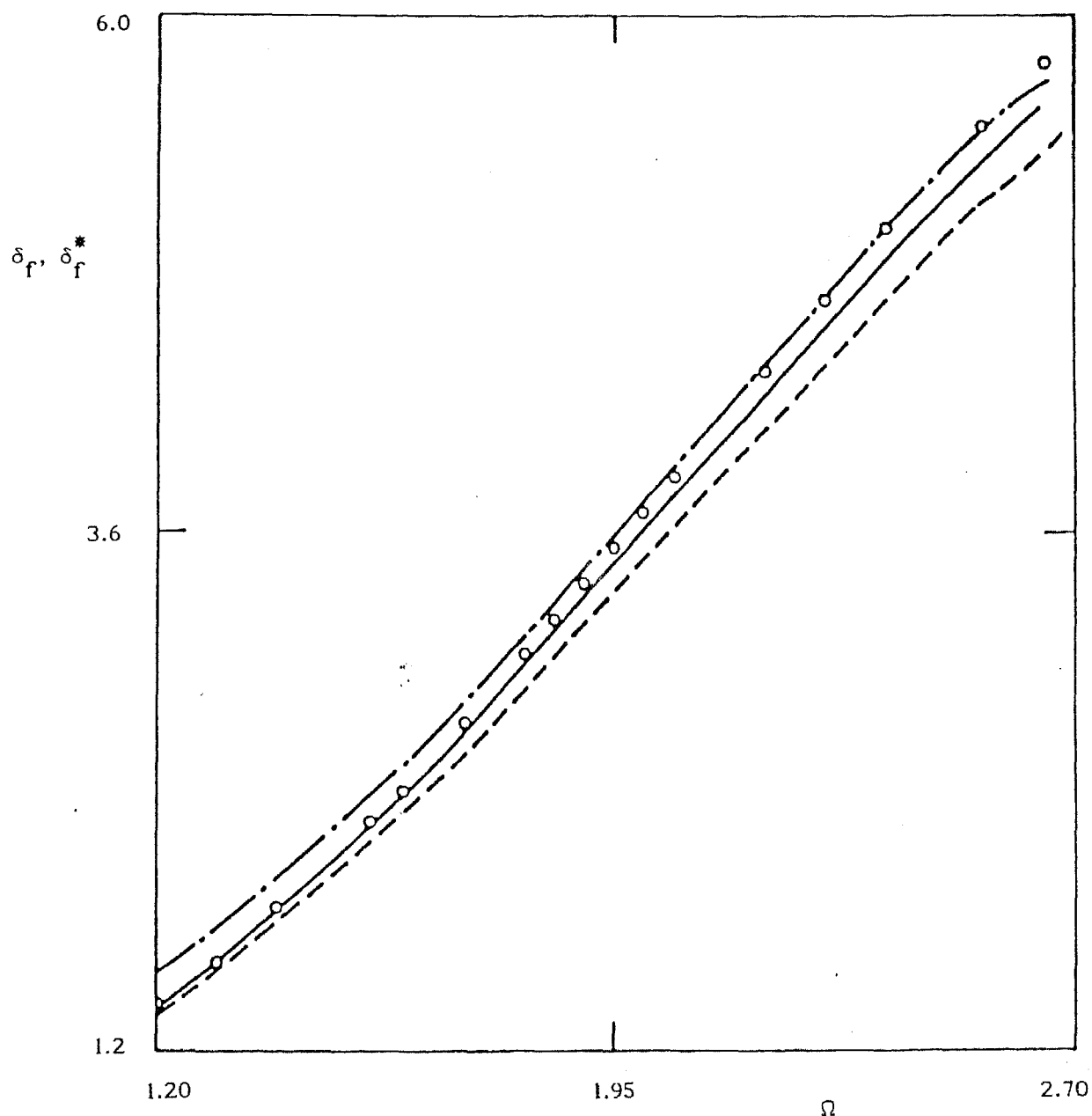
Figure 2.7   Maximum displacement of the vibroimpacting Duffing's
oscillator with $\tau_p = 2\pi/\Omega$. $\chi = 1$ and values of the
parameters h, F_o and ε are specified in Figure 2.5. - -
- - δ_f ($A_2 = 0$), ————— δ_f ($A_2 \neq 0$), - • - • - δ_f^* ($A_2 =$
0), o numerical integration.
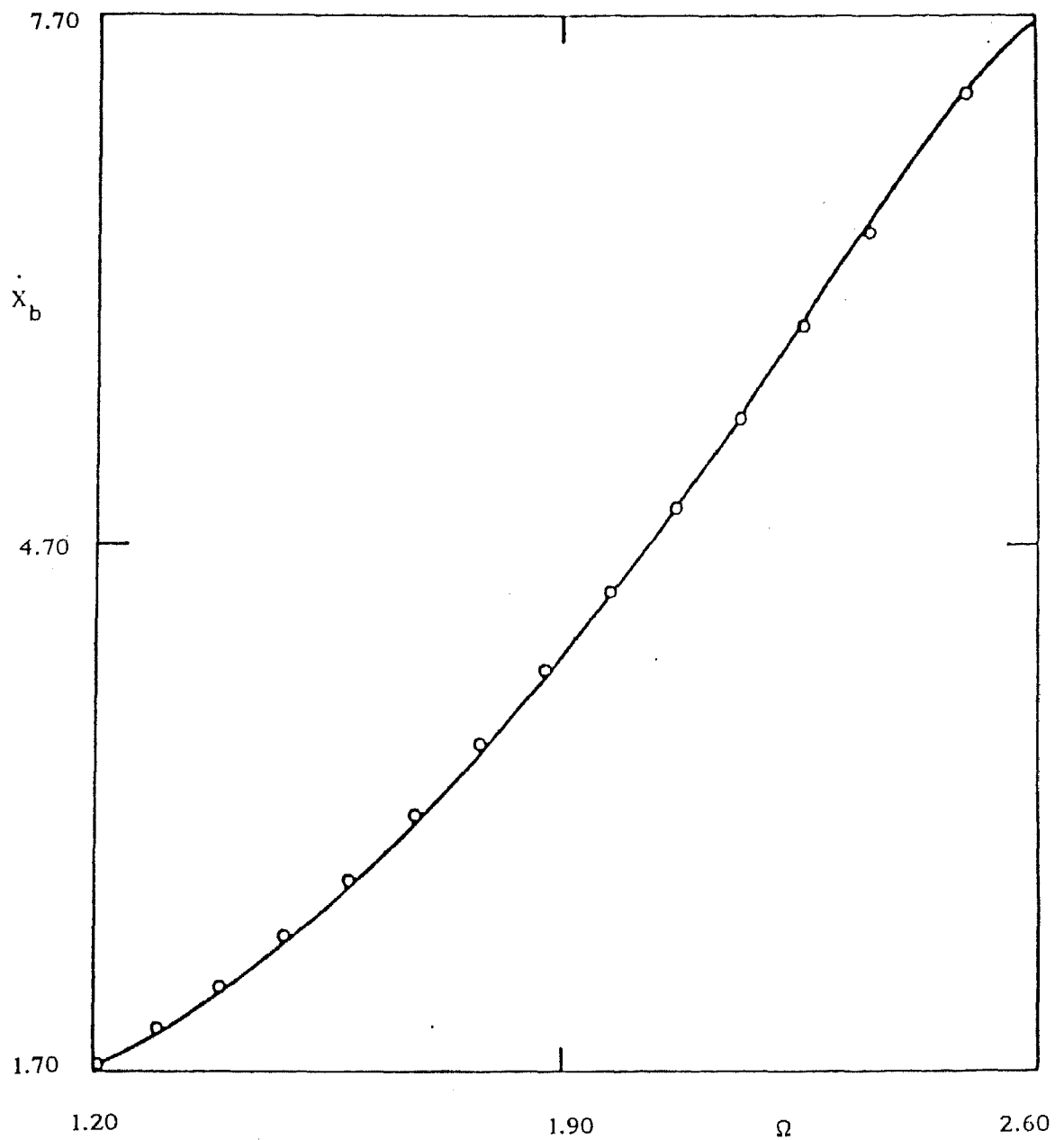
Figure 2.8   Variation of the impact velocity with forcing frequency. Values of h, F_o, ε and χ are specified in Figures 2.5 and 2.7. —— EPL ($A_2 = 0$), o numerical integration.
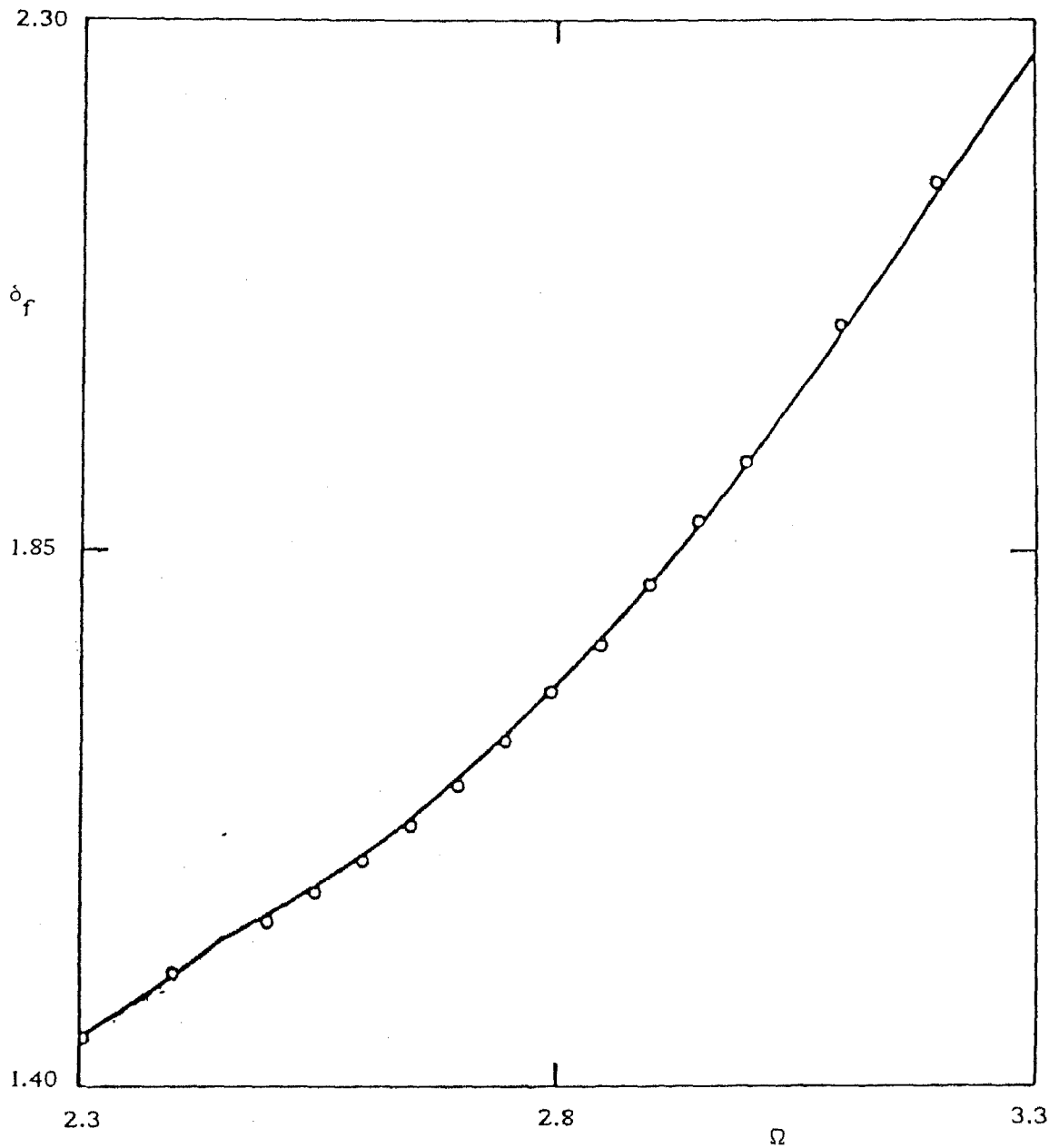
Figure 2.9 Maximum displacement of the vibroimpacting Duffing's oscillator with $\tau_p = 4\pi/\Omega$.. Values of h, χ, F_o and ε are specified in Figures 2.5 and 2.7. —— δ_f, o numerical integration.

much better for such problems. The main reason for this can be explained as follows. The success of the HBM, being basically a frequency domain technique, depends heavily on the inclusion of all the prominent frequencies in the assumed form of the solution. However, for the present problem this is not possible while using the simple HBM. We may add that there may be situations when the simple HBM may provide a good estimate of the maximum response while completely failing to predict the time response. Such an example will be discussed in the next chapter. The proposed EPL method, on the other hand, simultaneously utilizes both the time domain and frequency domain information. This method not only gives better results than that obtained from the simple harmonic balance method but is also capable of including super and subharmonics in the solution. A dual representation of the solution greatly simplifies the algebra involved in the proposed EPL method. The method is not iterative hence computationally less intensive for simpler systems. The EPL method becomes algebraically unwieldy only if the number of smooth non-linear regimes increases. The stability analysis of the obtained solution can be carried out by the method of error propagation.

CHAPTER 3

IMPACT DAMPERS FOR NON-LINEAR VIBRATING SYSTEMS

3.1 Introduction

In this chapter, the performance and design of an impact damper for controlling the high-amplitude vibration of a non-linear oscillator is discussed. Specifically, the primary system is taken as a harmonically excited, viscously damped, Duffing's oscillator. Two different approaches are considered. First, the secondary mass is used in a passive manner to generate a stable low-amplitude solution for the primary system. Towards this end, an initial design, obtained by the single term harmonic balance method, is improved upon using the EPL technique and numerically integrated results. In the second approach, the multistability feature of the non-linear oscillator is utilized. A guided "on-off" control strategy is followed to use the secondary mass for changing the initial state of the primary oscillator. This change of state brings the primary oscillator within the basin of attraction of the non-resonance (low amplitude) branch from the resonance branch. This procedure has been referred to as the guided branch transition. Numerical results are presented to verify the solutions, their stability and thereby the feasibility of the proposed approaches.

3.2 Theoretical Analysis

3.2.1 Harmonic Balance Method

The model under consideration is shown in Figure 3.1. For a linear primary system, it has been shown in previous works [69,77] that an impact damper undergoing elastic collisions performs better than the one having inelastic collisions. Accordingly, here also first we consider elastic impacts between the primary mass m_1 and the secondary mass m_2. The elastic impacts are modelled by two linear contact springs, each of stiffness K_2. Later on, we shall include the impact damping to simulate inelastic collisions having a coefficient of restitution $\chi < 1$. The value of χ is known to control the frequency bandwidth of the effectiveness of the impact damper [69]. The friction force between m_1 and m_2 is neglected.

The equations of motion for m_1 and m_2 are

$$m_1 x_1'' + c_1 x_1' + K_\ell x_1 + K_1 x_1^3 + K_2[(y - \tfrac{d}{2})\ U\ (y - \tfrac{d}{2})$$

$$+ (y + \tfrac{d}{2})\ U(-y - \tfrac{d}{2})] = F \cos \omega t \qquad (3.1)$$

and

$$m_2 y'' + K_2[(y - \tfrac{d}{2})\ U\ (y - \tfrac{d}{2})$$

$$+ (y + \tfrac{d}{2})\ U(-y - \tfrac{d}{2})] = m_2 x_1'' \qquad (3.2)$$

where the prime denotes differentiation with respect to time t, $y = x_1 - x_2$. All other symbols are explained in Figure 3.1. In
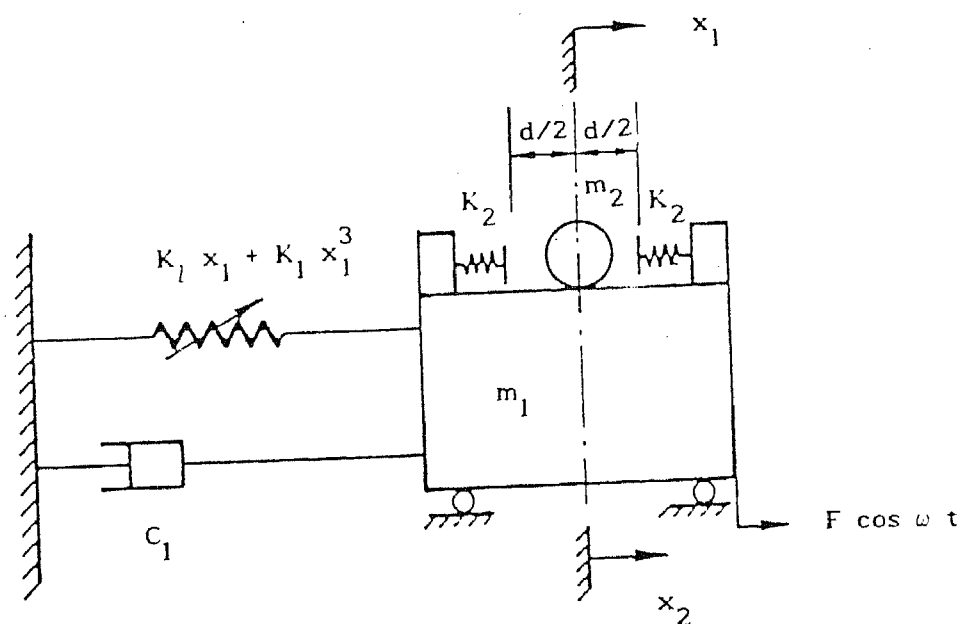
Figure 3.1 Model of an elastic impact damper.

equations (3.1) and (3.2), $U(.)$ is the Heaviside step function defined as

$$U(\xi) = 0 \quad \text{if } \xi < 0 \quad \text{and}$$

$$= 1 \quad \text{if } \xi > 0.$$

Substituting the following non-dimensional parameters

$$Z_1 = x_1/x_o, \quad Z_2 = y/x_o, \quad \omega_o t = \tau, \quad \omega_o = \sqrt{K_1 \, x_o^2/m_1} \quad , \quad r_1 = K_2/(m_1\omega_o^2),$$

$$r_m = m_2/m_1, \quad d_o = d/2x_o, \quad h = C_1/(m_1\omega_o), \quad \Omega = \omega/\omega_o, \quad \omega = K_\ell \,/(m_1\omega_o^2 \,)$$

and $x_o = (F/K_1)^{1/3}$ in equations (3.1) and (3.2) we get

$$\ddot{Z}_1 + h \, \dot{Z}_1 + \omega_\ell^2 \, Z_1 + Z_1^3 + r_1\phi(Z_2) = \cos \Omega\tau \tag{3.3}$$

and

$$\ddot{Z}_2 + (r_1/r_m) \, \phi(Z_2) = \ddot{Z}_1 \tag{3.4}$$

where $\phi(Z_2) = (Z_2 - d_o) \, U \, (Z_2 - d_o) + (Z_2 + d_o) \, U(-Z_2 - d_o)$ and the dot denotes differentiation with respect to τ.

Let us seek solutions of equations (3.3) and (3.4) in the form

$$Z_1 = a \cos (\Omega\tau + \theta_1)$$

and

$$Z_2 = b \cos (\Omega\tau + \theta_2) . \tag{3.5}$$

Substituting the above solutions in equations (3.3) and (3.4) we expand $\phi(Z_2)$ in a Fourier series retaining only the first harmonic. Thereafter, equating, respectively, the coefficients of

$\sin (\Omega\tau+\theta_1)$, $\sin (\Omega\tau+\theta_2)$, $\cos(\Omega\tau+\theta_1)$ and $\cos(\Omega\tau+\theta_2)$ from both sides we get the following set of non-linear algebraic equations:

$$a\omega_\ell^2 - a\Omega^2 + 3 \, a^3/4 + r_1 \, B(b) \cos (\theta_2-\theta_1) = \cos \theta_1, \qquad (3.6a)$$

$$-h \, a \, \Omega - r_1 \, B(b) \sin (\theta_2-\theta_1) = \sin \theta_1, \qquad (3.6b)$$

$$- \, b \, \Omega^2 + (r_1/r_m) \, B(b) = - \, a \, \Omega^2 \cos (\theta_1-\theta_2) \qquad (3.6c)$$

$$\sin (\theta_1-\theta_2) = 0, \qquad (3.6d)$$

where $B(b) = b \left[1 - \dfrac{2}{\pi} \left\{ \dfrac{d_o}{b} \sqrt{1 - (\dfrac{d_o}{b})^2} + \sin^{-1}(\dfrac{d_o}{b}) \right\} \right]$

$$\text{if } |\dfrac{d_o}{b}| < 1$$

$$\qquad (3.6e)$$

$$= 0 \qquad\qquad \text{if } |\dfrac{d_o}{b}| \geq 1.$$

Equation (3.6d) implies $\theta_1- \theta_2 = n\pi$, $n = 0,1,2,\ldots$.
If $\theta_1 - \theta_2 = 0$, 2π, $4\pi\ldots$, then equations (3.6a), (3.6b) and (3.6c) yield

$$a\omega_\ell^2 - a \, \Omega^2 + 3 \, a^3/4 + r_1 B(b) = \cos \theta_1, \qquad (3.7a)$$

$$- \, h \, a \, \Omega = F_o \sin \theta_1 \qquad (3.7b)$$

and $\qquad - \, b \, \Omega^2 + (r_1/r_m) \, B(b) = -a \, \Omega^2 . \qquad (3.7c)$

Similarly, with $\theta_1 - \theta_2 = \pi, 3\pi, 5\pi...,$ we get

$$a\omega_\ell^2 - a \Omega^2 + 3 a^3/4 - r_1 B(b) = - \cos \theta_2, \qquad (3.8a)$$

$$h a \Omega = \sin \theta_2 \qquad (3.8b)$$

and $\qquad - b \Omega^2 + (r_1/r_m) B(b) = a \Omega^2 \qquad (3.8c)$

which, with $a = -a^*$, can be rewritten as

$$a^* \omega_\ell^2 - a^* \Omega^2 + 3 a^{*3}/4 + r_1 B(b) = \cos \theta_2 , \qquad (3.9a)$$

$$- h a^* \Omega = \sin \theta_2 \qquad (3.9b)$$

and $\qquad - b \Omega^2 + (r_1/r_m) B(b) = -a^* \Omega^2 \qquad (3.9c)$

Thus, we see that the solution set (a,b,θ_1) obtained from equations (3.7) is same as the solution set (a^*,b, θ_2) obtained from equations (3.9). Therefore, we use only equations (3.7) to get all the solutions.

In all real life situations, the value of r_1 is very high implying

$$b = d_o + \varepsilon, \quad \text{where } 0 < \varepsilon \ll 1 . \qquad (3.10)$$

Using equation (3.10) in equation (3.6e), we obtain

$$B(b) = -\frac{2}{\pi} \sqrt{2d_o \varepsilon} + o(\varepsilon) \qquad \text{for } d_o > |b| \tag{3.11}$$

where ε is obtained from equation (3.7c) as

$$\sqrt{\varepsilon} = \frac{r_m \pi \, (a - d_o) \, \Omega^2}{2\sqrt{2} \, d_o \, r_1} \tag{3.12}$$

Using relations (3.11) and (3.12) in equations (3.7a) and (3.7b) we finally obtain

$$a\omega_\ell^2 - a\,\Omega^2 + 3a^3/4 - r_m\,\Omega^2\,(a-d_o) = \cos\theta_1 \tag{3.13a}$$

and

$$-h\,a\,\Omega = \sin\theta_1 . \tag{3.13b}$$

Substituting $\Delta = \tan(\theta_1/2)$ in equations (3.13a) and (3.13b) and eliminating the variable a, the following equation in Δ is obtained:

$$\Delta^6\,(\nu+1) + \alpha\,\Delta^5 + (3\nu+1)\,\Delta^4 + (\beta + 2\alpha)\,\Delta^3 + (3\nu-1)\,\Delta^2$$
$$+ \alpha\,\Delta + (\nu-1) = 0 \tag{3.14}$$

where

$$\alpha = -\frac{2}{h\,\Omega}\,(\omega_\ell^2 - \Omega^2 - r_m\,\Omega^2)$$

$$\beta = -\frac{6}{h^3\,\Omega^3}$$

and

$$\nu = r_m\Omega^2 d_o$$

After solving the polynomial equation (3.14) for Δ, we get the values of the amplitudes (a) from equation (3.13b). Before proceeding on to the stability analysis of these solutions (presented in the next section), it may be worthwhile to note that equations (3.13a) and (3.13b) represent the single term harmonic balance solution of the following differential equation:

$$\ddot{x} + h \dot{x} + \omega_\ell^2 x + x^3 = \cos \Omega\tau - r_m \ddot{x} - r_m \Omega^2 d_o \cos (\Omega\tau+\theta_1).$$

$$(3.15)$$

Equation (3.15) implies that the addition of an impact damper to the primary oscillator is equivalent to the addition of acceleration feedback and force-modification mechanisms. This confirms the use of the term acceleration damper [66,67] as a synonym for an impact damper.

3.2.2 Stability Analysis

To analyse the stability of the solutions obtained in the previous section, we consider

$$Z_1 = a(\tau) \cos (\Omega\tau + \theta_1(\tau)) \qquad (3.16a)$$

and $$Z_2 = b(\tau) \cos (\Omega\tau + \theta_2(\tau)) \qquad (3.16b)$$

with $a(\tau)$, $b(\tau)$, $\theta_1(\tau)$ and $\theta_2(\tau)$ as slowly varying functions of time. Substituting equations (3.16a) and (3.16b) in equations (3.3) and (3.4) and carrying out the harmonic balance after neglecting small terms such as $\ddot{a}(\tau)$, $\ddot{b}(\tau)$, $\ddot{\theta}_1(\tau)$, $\ddot{\theta}_2(\tau)$, $h\dot{a}$, $h\dot{b}$ etc, we get the following four autonomous differential equations:

$$\dot{a} = -\frac{1}{2\Omega}\left\{ h\ a\ \Omega + r_1\ B(b)\ \sin\ (\theta_2-\theta_1) + \sin\theta_1 \right\} \ , \qquad (3.17a)$$

$$\dot{\theta}_1 = -\frac{1}{2a\Omega}\left\{ \cos\ \theta_1 - r_1\ B(b)\ \cos\ (\theta_2-\theta_1) - a\omega_\ell^2 - \frac{3}{4}\ a^3 + a\ \Omega^2 \right\} \ , \qquad (3.17b)$$

$$\dot{b} = -\frac{1}{2\ \Omega}\left\{ \sin\ \theta_2 + h\ a\ \Omega\ \cos\ (\theta_1-\theta_2) \right.$$

$$\left. + (a\omega_\ell^2 + \frac{3}{4}\ a^3)\ \sin\ (\theta_1-\theta_2) \right\} \qquad (3.17c)$$

and

$$\dot{\theta}_2 = -\frac{1}{2\Omega b}\left\{ b\ \Omega^2 - r_1\ B(b)\ (1+\frac{1}{r_m}) + h\ a\ \Omega\ \sin\ (\theta_1-\theta_2) \right.$$

$$\left. - (a\omega_\ell^2 + \frac{3}{4}\ a^3\ )\cos\ (\theta_2-\theta_1) + \cos\ \theta_2 \right\} \ . \qquad (3.17d)$$

While deriving equations (3.17a)-(3.17d), the Fourier series of the function $\phi(Z_2)$, with $Z_2 = b(\tau)\ \cos\ (\Omega\tau + \theta_2(\tau))$ had to be carried out. However, the Fourier coefficients of $\phi(Z_2)$ can not be obtained in a closed form. Hence, the following approximation is made. Since r_1 is very high, the contact time during an impact is very small. Consequently, $\phi(Z_2)$ is zero for most of the time during the period $2\pi/\Omega$ and assumes nonzero value only for a very small interval of time during which the slowly varying functions $b(\tau)$ and $\theta_2(\tau)$ can effectively be considered as constants. This

approximation makes the closed form evaluation of the Fourier coefficients possible. The stability of the solutions can thus be judged from the signs of the real part of the eigenvalues of the Jacobian of the right-hand-side of equations (3.17) evaluated at $(a, b, \theta_1, \theta_2)$. The details of the Jacobian are given in the Appendix A. If the real part of all the eigenvalues are negative, the solution is stable and otherwise unstable.

3.3 Design of an Elastic Impact Damper

By design of the impact damper, we mean the determination of the values of the parameters r_m and d_o for which the response of the primary system, i.e. the value of the amplitude (a), is rendered small. Before going into the details of this design, the following points should be mentioned:

(i) The variation of the amplitude of the primary system with the forcing frequency, in the absence of the impact absorber, has the general trend shown in Figure 3.2 (for not too high values of h and ω_ℓ). The frequency corresponding to the maximum value of the amplitude is defined as the peak frequency Ω_p.

(ii) The relative amount of non-linear contribution in the restoring force of the primary system can be controlled by the parameter ω_ℓ. A higher value of ω_ℓ implies a lower relative non-linearity and vice versa.

(iii) To numerically integrate the equations of motion, the fourth order Runge-Kutta-Merson algorithm of NAG with adaptive step-size control was used. We have randomly selected a large number of initial conditions within a ball of radius 2 around the origin of
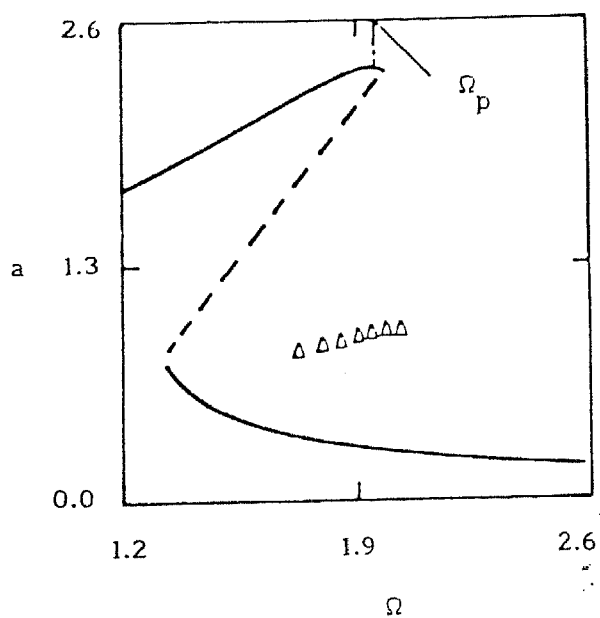
Figure 3.2 Typical frequency response curve of a sinusoidally driven Duffing's oscillator. —— stable branch, - - - - unstable branch, Δ - one-third subharmonic. $\omega_\ell = 0$, $h = 0.215$

the phase-space. All these initial conditions resulted in motions where collisions occurred. There may exist certain special combinations of initial conditions (depending on the values of other parameters) where no collision occurs. In this work, no further attention has been given to such non-colliding motions.

(iv) The steady state of the motion has been ascertained by considering the Poincare section (stroboscopic map with $2\pi/\Omega$ as the strobe period) of the phase trajectories. When the iterates of the Poincare map reach a fixed point, the corresponding motion obviously has a period $2\pi/\Omega$. Similarly, the existence of n fixed points in the iterates implies a motion having a period $2\pi n/\Omega$. This fact is used to locate the subharmonic solutions.

From the approximate solution given by equation (3.14), it is easy to see that if r_m and d_o are chosen to satisfy the relation

$$r_m \, \Omega^2 \, d_o = 1 \,, \tag{3.18}$$

then one of the values for the amplitude (a) turns out to be zero. Of course under such a situation i.e., when equation (3.18) holds good, the solution of equations (3.7) does not give the amplitude as exactly zero, but does reveal a very small amplitude of the primary system. By following the stability analysis presented in section 3.2.2, this small amplitude solution is found to be stable. The existence of such a stable, small amplitude solution is also confirmed by obtaining it through direct numerical integration. It was also observed that the other impacting solutions, different from this small amplitude solution, obtained from equations (3.14), (3.7) and numerical integration match very

closely.

Selecting the design frequency as Ω_p, the parameters r_m and d_o are chosen satisfying the relation

$$r_m \, d_o = 1/ \, \Omega_p^2 \ .$$

The frequency responses obtained from equation (3.7) for a fixed value of r_m with d_0 given by equation (3.19) are shown in Figures 3.3(a) - 3.3(c) for various value of ω_ℓ. With the impact damper in operation, only the stable solutions are shown. It is seen that, a stable, small amplitude solution is always present around the peak frequency Ω_p irrespective of the value of ω_ℓ. Apart from this low amplitude solution, a high-amplitude stable solution is also present. However, there is always a region around Ω_p where only the low amplitude solution exists. We define the frequency-range around Ω_p, where the impact damper introduces a single, low amplitude solution in place of the resonance branch of the primary system, as the suppression band ($\Delta\Omega_s$). These suppression bands, indicated in Figures 3.3(a) - 3.3(c), widen with increasing ω_ℓ (i.e., decreasing relative non-linearity). However, within the suppression band, the percentage reduction in the amplitude is relatively insensitive to the degree of non-linearity. A decrease in ω_ℓ reduces the value of Ω_p. Consequently, for a given value of r_m, the optimum value of d_0 obviously increases with decreasing ω_ℓ (see equation (3.19)) as can also be noted from Figures 3.3(a) - 3.3(c). It is known from previous works [77] on linear systems, that near the resonance frequency, the loose mass undergoes two
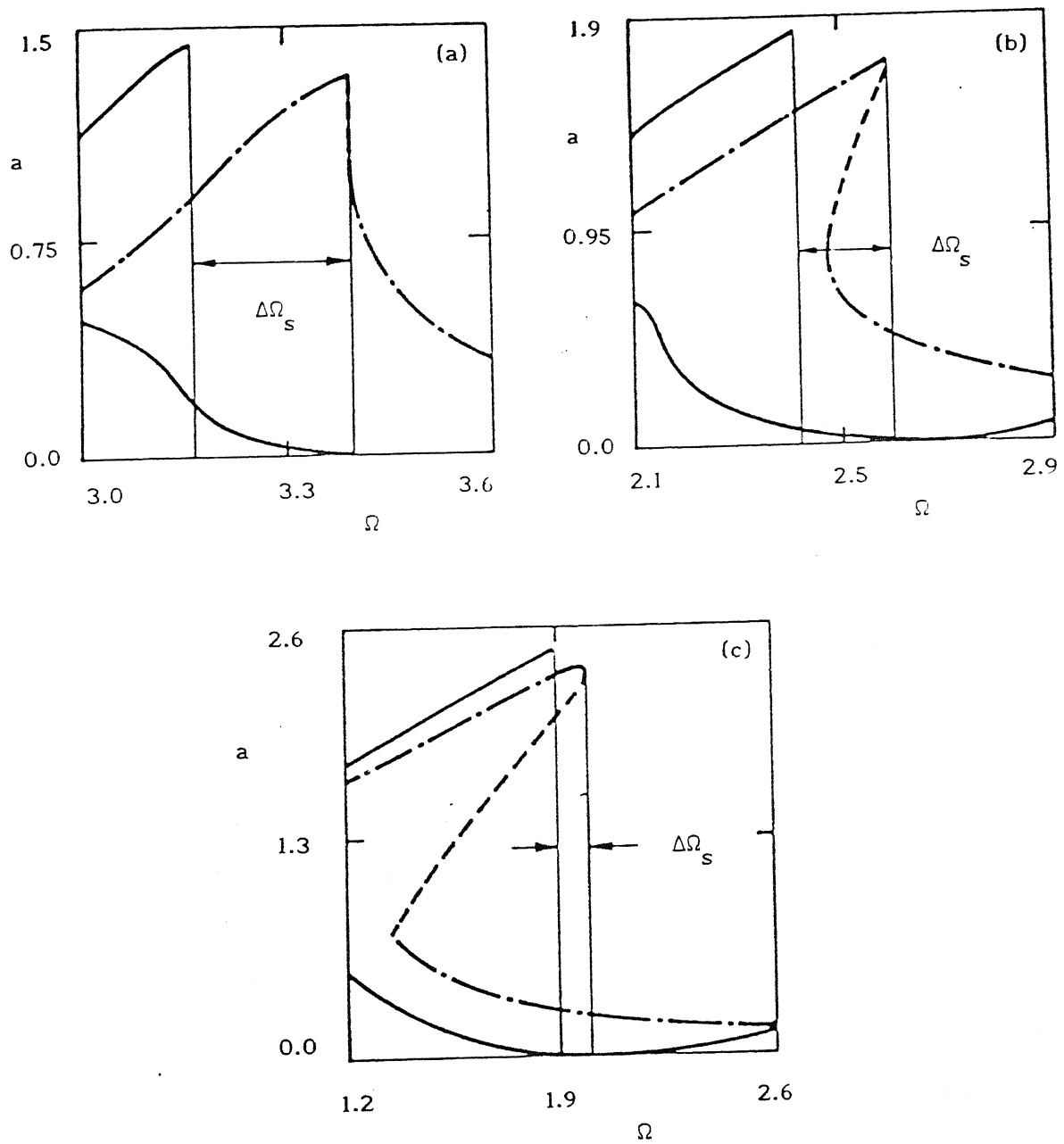
Figure 3.3 Frequency response of primary system with and without the impact damper. ——— stable branch (harmonic balance) with damper, —— . —— stable branch without damper,- - - unstable branch without damper. h = 0.215 ,rl = 2000 ,r_m = 0.12. a) ω_ℓ= 1.5, d_0 =0.69, b) ω_ℓ = 1, d_0= 1.2 , c) ω_ℓ = 0 ,d_0= 2.

symmetric collisions per cycle. To examine what happens in the presence of a non-linear restoring force, the phase diagrams of the primary system were also studied. A representative diagram is shown in Figure 3.4 which clearly reveals the existence of two symmetric impacts/cycle.

From here until section 3.5, the primary system will be considered to have only a cubic restoring force, i.e., $\omega_\ell = 0$. The frequency responses of the system obtained from equation (3.7) for different combinations of r_m and d_o satisfying equation (3.19) are shown in Figures 3.5(a) - 3.5(c). The results obtained by the direct numerical integration are also shown in the same figures. The small amplitude motion is vindicated by the direct numerical integration (revealing two symmetric impacts per cycle). However, the high-amplitude solution, obtained by integrating the equation of motion, revealed more than two impacts per cycle. The frequency regions having different number of impacts per cycle were also seen to be separated by narrow chaotic regimes.

The number of impacts per cycle is not an important issue in the method of harmonic balance. For a single term approximation to yield meaningful results, only the energy content in the fundamental frequency is of primary importance. Of course the stability analysis carried out in this work is approximate and therefore, is not able to capture all the delicate instability regions. However, both the amplitude and the width of the suppression band are estimated accurately by the harmonic balance method which goes a long way to provide an initial design. Both the harmonic balance and numerically integrated results showed
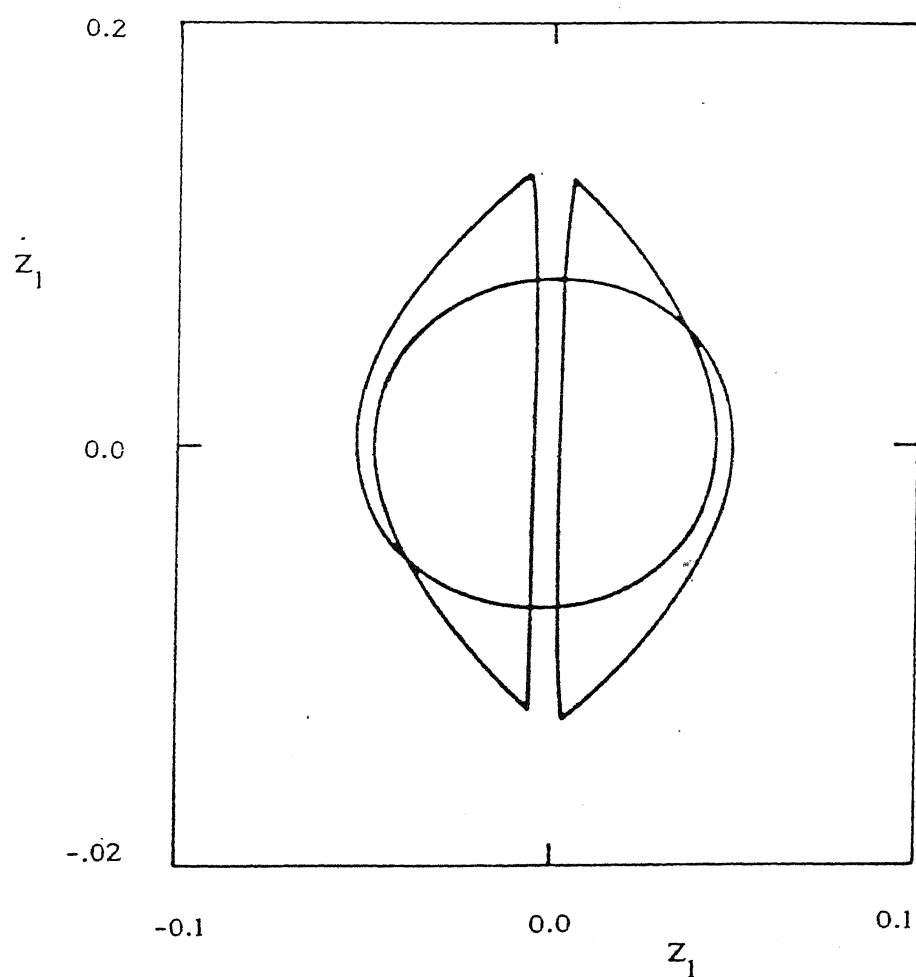
Figure 3.4 Phase plot of the low amplitude motion of the primary system $.r_m = 0.12$, $d_o = 2$, $\Omega = 2$,$h = 0.215$, $\omega_\ell = 0$,$r_1 = 2000$. Initial conditions (1, 0,0.1, 0)
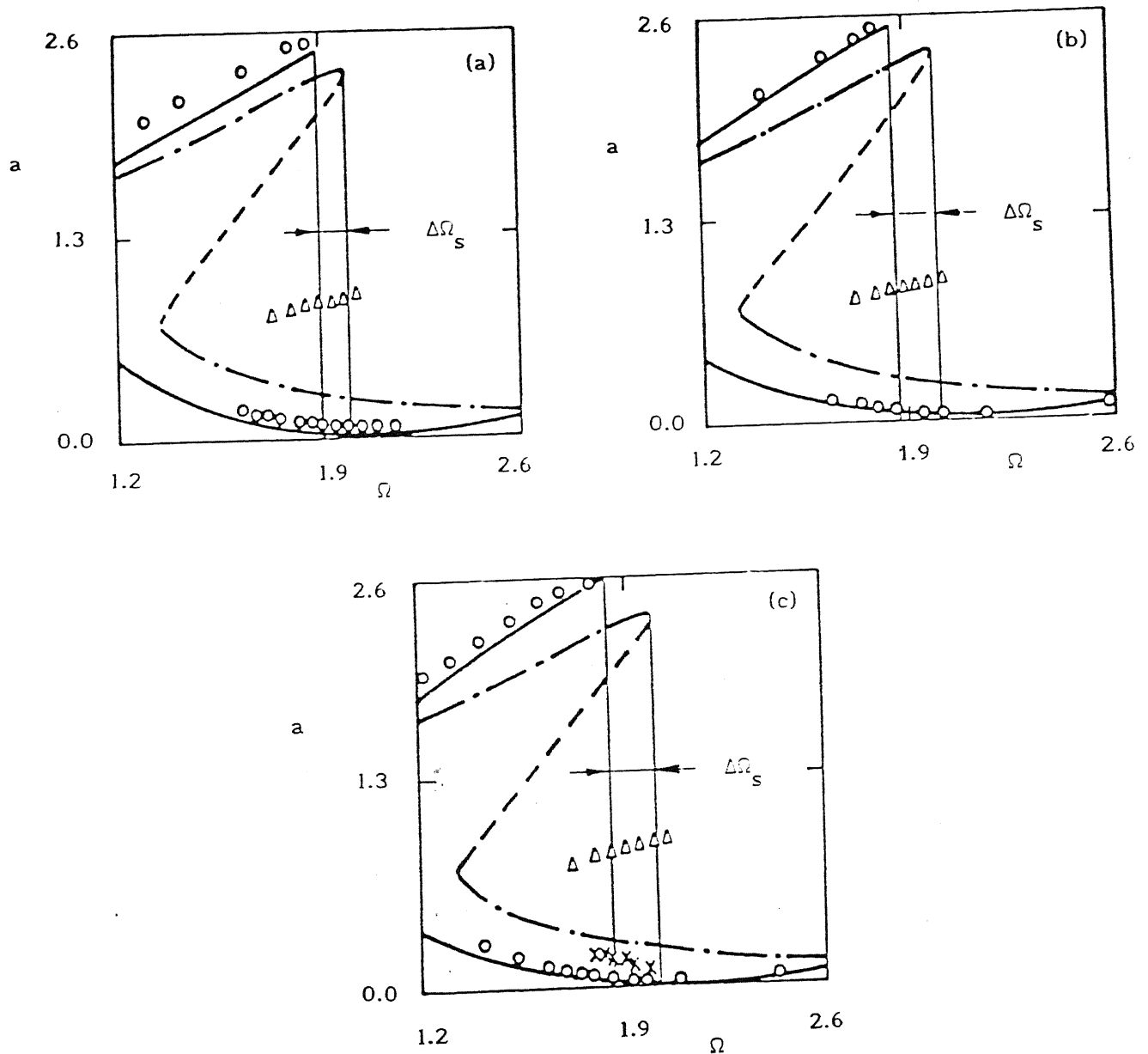
Figure 3.5 Frequency response of the primary system with and without the impact damper. —— stable branch (harmonic balance) , o-numerical integration, —•— stable branch without damper, - - - unstable branch without damper, Δ - one-third subharmonic without damper, x one-third subharmonic with damper. h = 0.215, ω_ℓ= 0, r1 = 2000.(a) r_m= 0.12, d_o= 2; (b) r_m= 0.25, d_o= 1 ; (c) r_m = 0.4, d_o= 0.625.

that the motions of the primary and the loose mass are almost in anti-phase for $\Omega < \Omega_p$ and almost in phase for $\Omega > \Omega_p$.

Let us define the set of values of the pair (r_m, d_o) satisfying equation (3.19) as the optimum set. In the following discussion we vary (r_m, d_o) only in that set. A comparison of Figure 3.5(a) with Figure 3.5(b) reveals that the suppression band widens with increasing values of r_m. Thus, a high value of r_m is to be preferred for a wider suppression band. Moreover, higher the value of r_m, lower is the value of the oscillation amplitude in the suppression band. But too high a value of r_m makes the system more prone to subharmonic oscillations (within the suppression band) as indicated in Figure 3.5(c).

To determine the optimum values of r_m and d_o, we compute the response of the primary system at the design frequency for three different values of r_m with varying values of d_o. The maximum displacement of the primary mass is obtained both from equations (3.7) and numerical integration. These results are shown in Figure 3.6. The numerically integrated results are seen to yield a little higher value of the optimum d_o as compared to that obtained from the harmonic balance method. However, the motion of the primary mass at Ω_p is seen to be rather insensitive to the value of r_m if the optimum value of d_o is used. Thus, depending on the required suppression bandwidth and available space, a value of r_m can be chosen and the first estimate of d_o should be obtained from equation (3.19). Around these values of r_m and d_o, the exact optimum values can then be obtained from the numerically integrated results. The insensitivity of the primary response near
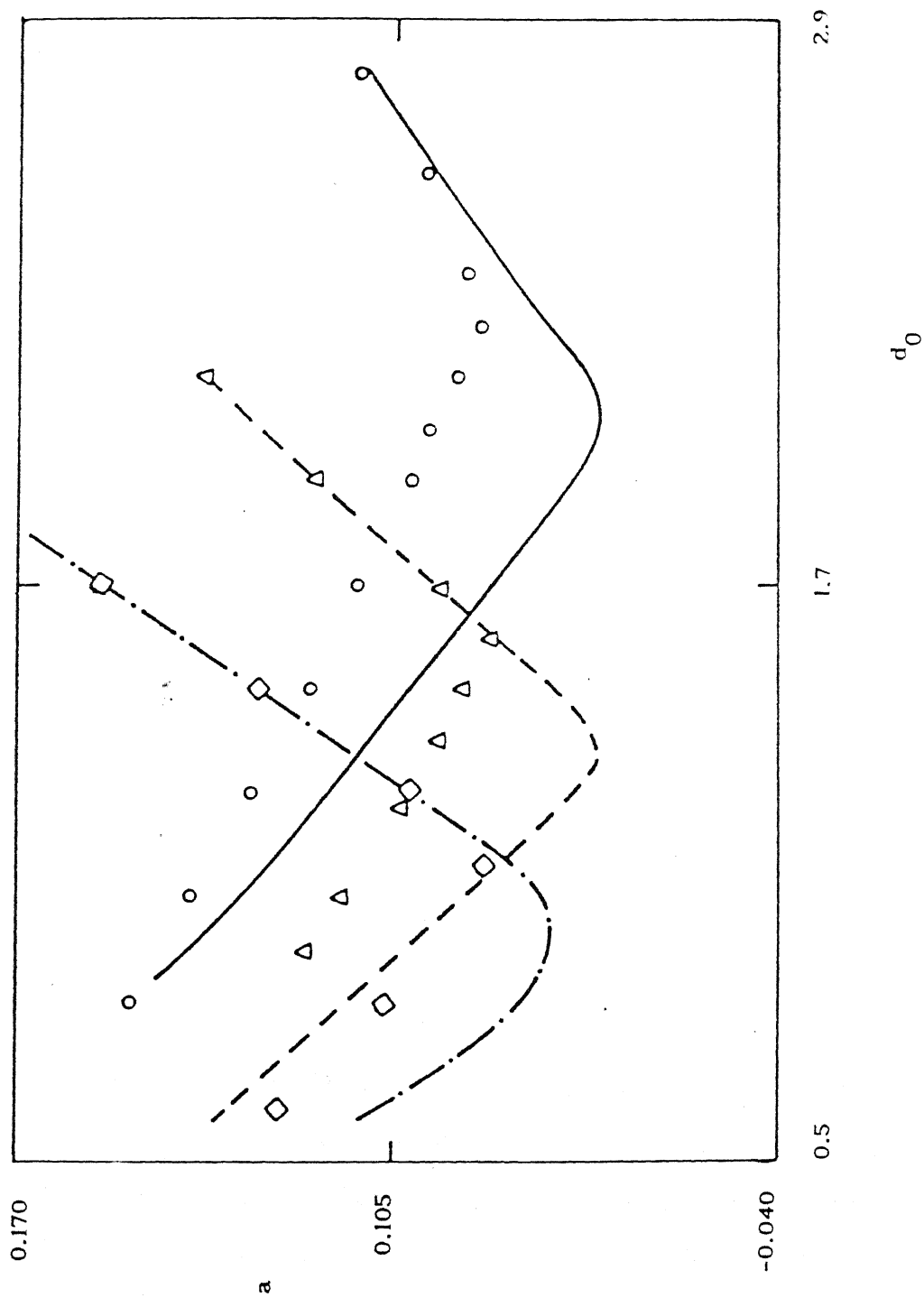
Figure 3.6 Comparative study of analytical and numerical optimum design values, h = 0.215, Ω = 2. r_m = 0.25 ——• analytical,◇ numerical; r_m = 0.18, – – – analytical, △ numerical; r_m = 0.12, —·—·— analytical, o numerical.

the optimum design ensures satisfactory performance of the impact damper, even if the actual parameters are a little away from the theoretical optimum values. These observations remain valid for different values of the parameter h as can be seen from Figure 3.7. Furthermore, one can conclude that the HBM overestimates the optimum performance.

Another important feature of the impact damper for a non-linear primary system is the suppression of the one-third subharmonic response. Figure 3.2 reveals that the primary system without the damper can have one-third subharmonic oscillation near the design frequency. Figures 3.5(a) and 3.5(b) clearly show that the one-third subharmonic motion can even be completely suppressed by a properly designed impact damper. With higher values of r_m, the one-third subharmonic motion may appear but with considerably lower amplitude. Such control of the one-third subharmonic response is prominently displayed with a low value of h as indicated in Figure 3.3.

3.4 Inelastic Impact Damper

A mathematical model of an impact damper undergoing inelastic collisions is shown in Figure 3.9, where the impact is modelled by a linear spring with stiffness K_2 and a dashpot with viscous damping coefficient C_2. The non-dimensionalized equations of motion can be written as
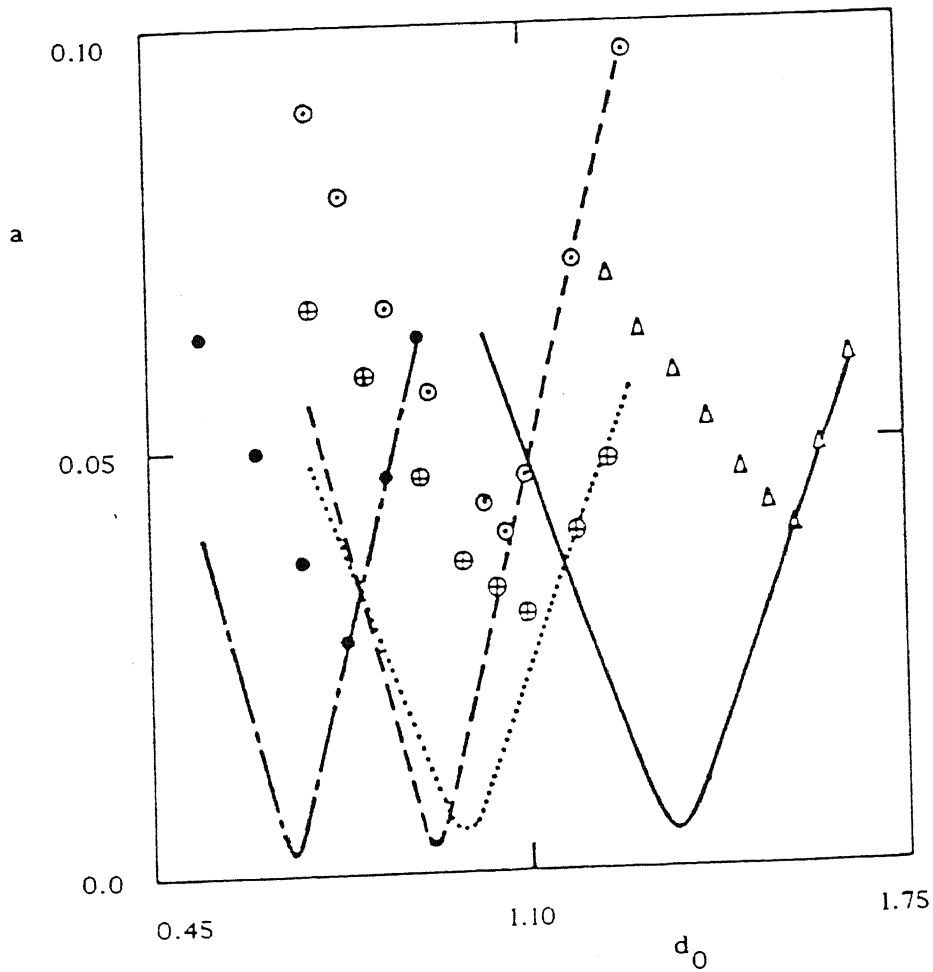
Figure 3.7 Comparative study of analytical and numerical optimum design for various values of the parameter h. h = 0.107, $\Omega = \Omega_p(= 2.8)$, $r_m= 0.18$, $- \cdot - \cdot$ -analytical, ● numerical; r_m = .12, ... analytical, ⊕ numerical. h = 0.15, $\Omega = \Omega_p(= 2.37)$, $r_m= 0.18$, $- - - -$ analytical, ⊙ numerical; r_m = 0.12, —— analytical, Δ numerical.
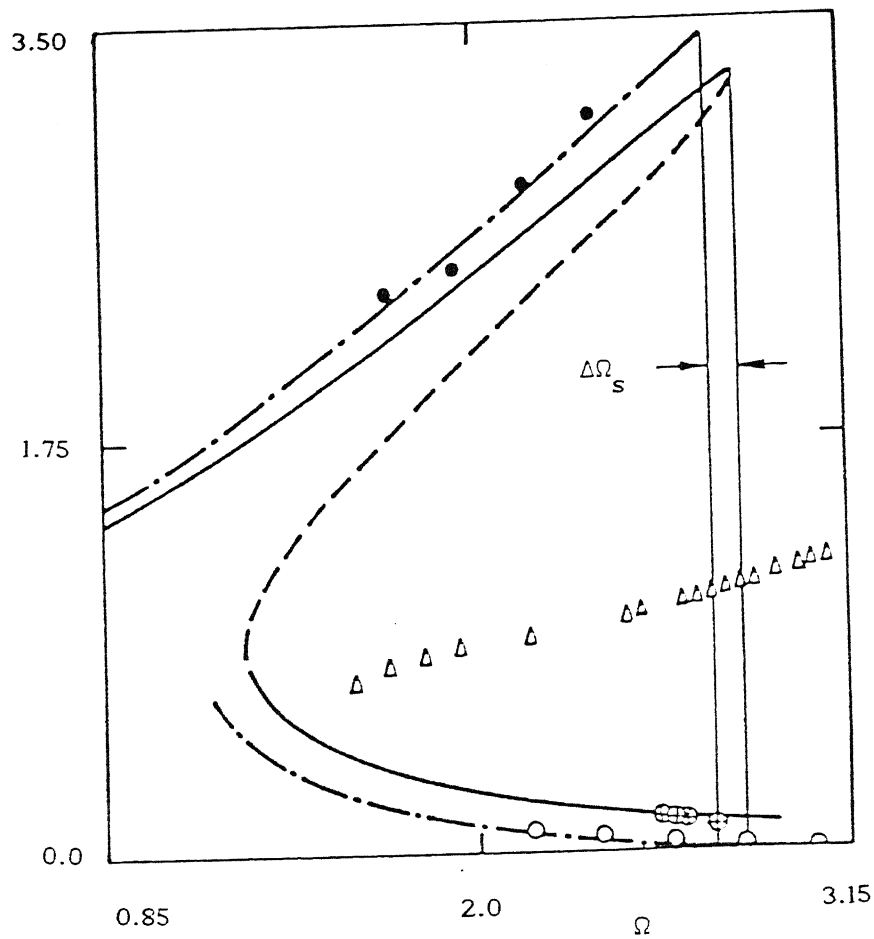
Figure 3.8 Frequency response of the primary system with and without the impact damper. $h = 0.107$, $r_1 = 2000$, $r_m = 0.12$. —— stable solution without damper, - - - unstable solution without damper, - • - analytical stable solution with damper, o numerical low amplitude solution with damper, • numerical high amplitude solution with damper, Δ one-third subharmonic solution without damper, ⊚ one-third subharmonic solution with damper.
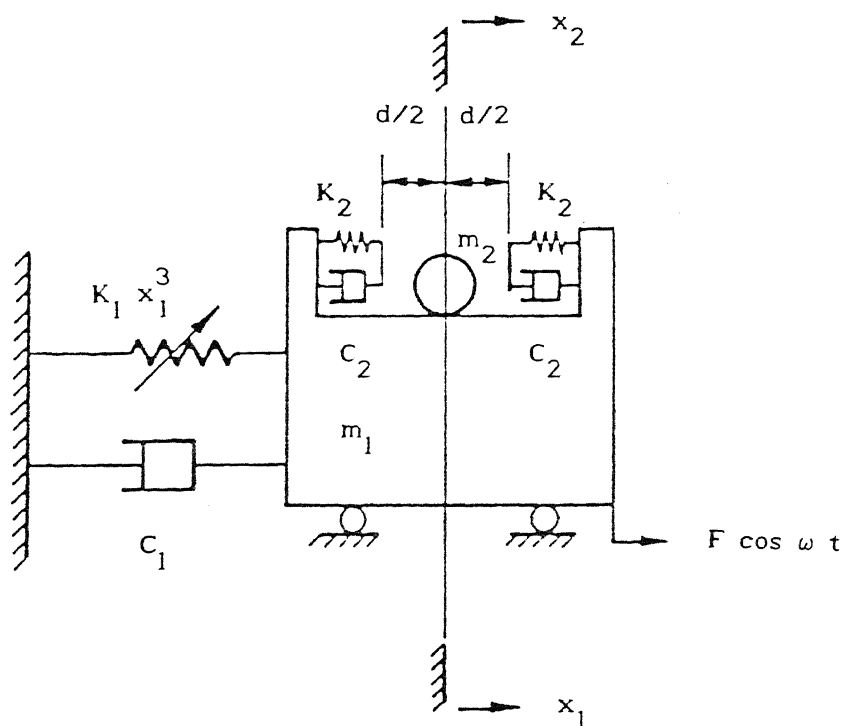
Figure 3.9 Model of an inelastic impact damper.

$$\ddot{z}_1 + h\, \dot{z}_1 + z_1^3 + \psi_1(Z_2, \dot{Z}_2) = \cos \Omega \tau \tag{3.20}$$

$$\text{and} \quad \ddot{z}_2 + \psi_2(Z_2, \dot{Z}_2) = \ddot{z}_1 \tag{3.21}$$

with

$$\psi_1(Z_2, \dot{Z}_2) = r_1 \phi(Z_2) + 2\xi_c \sqrt{r_1 r_m}\; \tilde{M}(Z_2)\, \dot{Z}_2, \tag{3.22}$$

$$\psi_2(Z_2, \dot{Z}_2) = (r_1/r_m)\, \phi(Z_2) + 2\xi_c \sqrt{r_1/r_m}\; \tilde{M}(Z_2)\, \dot{Z}_2 \tag{3.23}$$

$$\text{and} \quad \tilde{M}(Z_2) = U(Z_2 - d_o) + U(-Z_2 - d_o). \tag{3.24}$$

As shown in the Appendix B, the damping ratio ξ_c is obtained in terms of the coefficient of restitution (χ) as

$$\xi_c = -\frac{\ln(\chi)}{\sqrt{(1 + r_m)[\pi^2 + (\ln(\chi))^2]}} \tag{3.25}$$

To study the effects of the coefficient of restitution on the performance of the impact damper, equations (3.20) and (3.21) are numerically integrated to obtain the primary response. The frequency response of the primary system is plotted in Figure 3.10 for $\chi = 0.75$. We observe from this figure that the suppression band with $\chi < 1$ is wider than that with $\chi = 1$. However, the response amplitude with inelastic collisions is marginally higher than that with elastic collisions. In general, higher the impact damping (i.e. lower the value of χ) wider is the
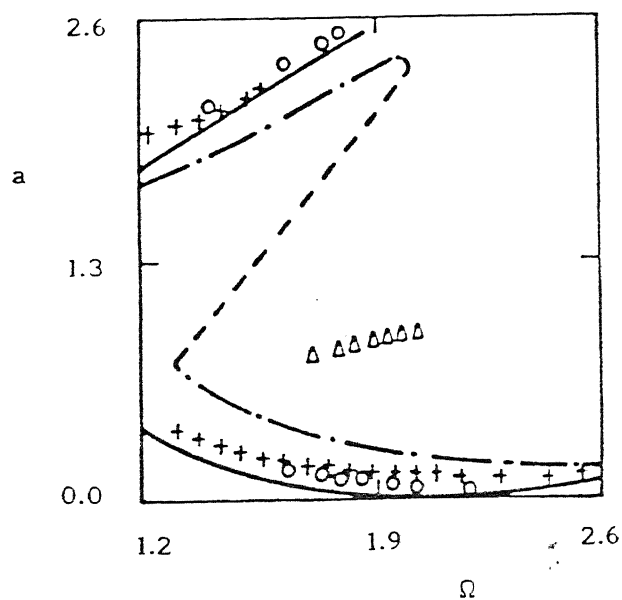
Figure 3.10 Frequency response of an inelastic impact damper. χ = 0.75, r_m = 0.25, d_o =1, h = 0.215.- • - • - stable branch without damper, - - - unstable branch without damper, —— stable branch with elastic damper [analytical], o numerical with elastic damper, Δ one-third subharmonic without damper, + numerical with inelastic damper.

suppression band, but larger is the response amplitude (in the suppression band). A similar behaviour was also seen for a linear primary system [69]. Thus, a high value of χ, signifying almost elastic collisions, is preferable for optimum performance in case of a synchronous operation.

The variations of the amplitude of the primary system with d_o for various values of r_m and χ are shown in Figure 3.11. From this figure, it may be concluded that higher the impact damping, lower is the required value of d_o for optimum performance. Moreover, as the impact damping increases, the primary response becomes more insensitive to the variation in d_o (for a near optimal design).

3.5 Improvement of the Design Using the EPL Technique

In the previous sections the harmonic balance method (HBM) was used for designing and analysing the performance of an impact damper. In case of a perfectly elastic damper, a simple approximate relation for the optimum design was established. However, this optimum design had to be improved upon using numerical simulations. Further, for an inelastic damper only the numerical integration could produce meaningful results. The results obtained using the HBM were found to be quite inaccurate and are not presented here. Considering the difficulty and the amount of time involved in numerical simulations, in this section, we make use of the powerful EPL analysis (discussed in the previous chapter) for obtaining a good initial design. It has been
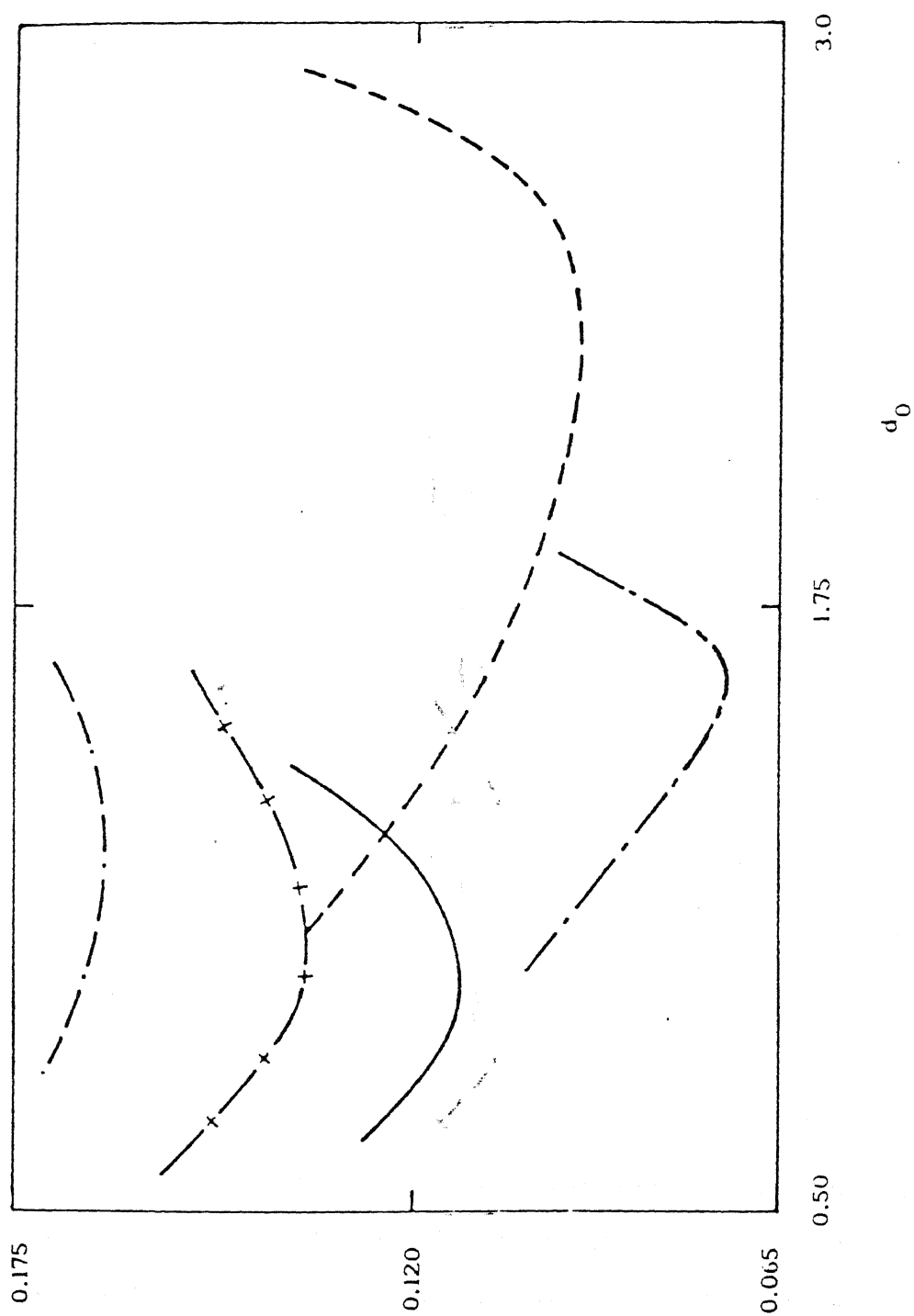
Figure 3.11   Numerical   optimum   design   values   of   inelastic
damper.— • — $r_m = 0.12$, — + — $r_m = 0.18$, —— $r_m = 0.25$; all for $\chi = 0.75$. — — $r_m = 0.12$, —•— $r_m = 0.18$ all for $\chi = 0.9$.

mentioned earlier that the optimum performance of an impact damper corresponds to a periodic motion having two symmetric impacts per cycle. In the HBM analysis one really does not require any information regarding the number of impacts. However, in the EPL analysis a periodic solution is constructed considering the number of impacts per cycle (two for the present problem). It is also to be mentioned that for the present analysis, a spring-dashpot model of an impact is not really necessary. Rather, the concept of coefficient of restitution is used in the subsequent analysis to relate the velocities before and after an impact.

3.5.1 Periodic Solution

The equations of motion of the oscillator between two consecutive impacts can be written in the following non-dimensional form

$$\ddot{Z}_1 + h \, \dot{Z}_1 + \omega_\ell^2 \, Z_1 + Z_1^3 = \cos(\Omega\tau), \tag{3.26a}$$

$$\dot{Z}_p = \text{constant} \tag{3.26b}$$

and the impacts occur at $\quad Z_1 - Z_p = \pm d_o$

where $\quad Z_p = x_2 / x_o$

For analysing the motion with two symmetric impacts per cycle, we set $\tau = 0$ at the instant of an impact occurring with the right side of the container when the next impact occurs at $\tau = (\pi/\Omega)$ with the left side of the container. In the subsequent analysis a

+ sign denotes the instant just after an impact and a − sign denotes the instant just before an impact. We concentrate only on the motion occurring between $0^+ < \tau < (\frac{\pi}{\Omega})^-$. By the equivalent linearization procedure, equations (3.26) are rewritten as

$$\ddot{Z}_1 - 2\rho\, \dot{Z}_1 + \omega_\ell^2\, Z_1 + K_e\, Z = \cos(\Omega\tau) \tag{3.27a}$$

$$\dot{Z}_p = -v \qquad\qquad \forall\, 0^+ < \tau < (\frac{\pi}{\Omega})^- \tag{3.27b}$$

where $\rho = - h/2$ and v is the constant velocity of the loose mass between two successive impacts. The solution of equation (3.27a) is written as

$$Z_1(\tau) = e^{\rho\tau}(B_1 \cos \eta\tau + B_2 \sin \eta\tau) + M \cos(\Omega\tau + \phi + \hat{\theta})$$

$$\forall\, 0^+ < \tau < (\frac{\pi}{\Omega})^- \tag{3.28}$$

where $\qquad \eta = \sqrt{\omega_1^2 - \rho^2},$

$$\tan \hat{\theta} = \frac{2\,\rho\,\Omega}{\omega_1^2 - \Omega^2}$$

and $\qquad M = \dfrac{1}{\sqrt{(\omega_1^2 - \Omega^2)^2 + (2\rho\Omega)^2}}$

with $\qquad \omega_1^2 = \omega_\ell^2 + K_e \, .$

The symmetry of the motion implies

$$Z_1(0) = -Z_1(\frac{\pi}{\Omega}) \equiv Z^O \text{ (say)}$$

$$\dot{Z}_1(0^+) = -\dot{Z}_1(\frac{\pi}{\Omega}^+) \equiv \dot{Z}^1 \text{ (say)} \qquad (3.29)$$

and $$\dot{Z}_1(\frac{\pi}{\Omega}^-) = -\dot{Z}_1(0^-) \equiv \dot{Z}^O \text{ (say)}$$

The conservation of momentum during the impact and the definition of the coefficient of restitution imply :

$$\chi = (v + \dot{Z}^1)/(v - \dot{Z}^O) \qquad (3.30)$$

$$2 d_O + 2 Z^O = \frac{v\pi}{\Omega} \qquad (3.31)$$

and $$2 r_m v = \dot{Z}^1 - \dot{Z}^O \qquad (3.32)$$

where χ is the coefficient of restitution and $r_m = m_2/m_1$ is the mass ratio. Using the above conditions we eliminate other constants to obtain

$$f_3(K_e, v) = 0 \qquad (3.33)$$

To determine K_e we assume the secondary solution as

$$z_1^*(\tau) = A_1 \cos(\Omega\tau + \theta_1)$$

when from equation (2.12) we get

$$K_e = \frac{3}{4} A_1^2 \qquad (3.34)$$

and the condition (2.13) gives

$$A_1^2 = \left(\frac{2\Omega}{\pi} \right)^2 \left| \int_0^{\pi/\Omega} Z_1(\tau) \ e^{i\Omega\tau} . \ d\tau \right|^2 \tag{3.35}$$

Thus, using equations (3.33) - (3.35) both the primary $(Z_1(\tau))$ and secondary $(Z_1^*(\tau))$ solutions for the displacement of the main mass are obtained. We may recall (mentioned in section 2.4) that the EPL provides the time response $Z_1(\tau)$ (equation (3.28)) accurately whereas the single term HBM given by equation (3.5) may fail. An example substantiating this statement, in the context of the system under consideration, is elaborated in the Appendix C.

3.5.2 Stability Analysis

The stability analysis of the solutions discussed in Section 3.5.1 is carried out using the method of error propagation described in Section 2.2.2. However, the system under discussion, in contrast to those discussed in Sections 2.2 and 2.3, has two degrees-of-freedom. Consequently the required perturbation vector whose change over a cycle is correlated by the matrix [P] (see equation (2.24)) has four components and the matrix [P] becomes a 4x4 matrix. The four components of the perturbation vector are taken as $(\Delta Z_1, \ \Delta \dot{Z}_1, \ \Delta v, \ \Delta \psi)$ where $\Delta \psi$ is the perturbation in the forcing phase. As usual, if all the eigenvalues of [P] lie within the unit circle around the origin of the complex plane then the solution is stable.

3.5.3 Results and Discussions

The optimum values of d_0 obtained for a given design frequency via different methods are plotted in Figures 3.12(a) and 3.12(b). The Stable regions for the motion (with symmetric, two impacts per cycle) are also delineated in the same figures. The following conclusions can be drawn from Figures 3.12(a) and 3.12(b):

(i) The optimal values of d_0 obtained using the EPL technique are in perfect agreement with the numerical results.

(ii) For a perfectly elastic damper, the optimum values may be unstable for some choices of r_m as seen from Figure 3.12(a).

(iii) As shown in Figure 3.12(b), a slight impact damping stabilizes the motion corresponding to the optimum design in the entire range of the r_m considered in this work.

(iv) A relation like

$$r_m \, d_0 = \text{constant}$$

is valid only for an elastic damper. However, the value of the constant is different from $1/\Omega_p^2$ which was obtained using the HBM. For an inelastic damper such a relation is not uniformly valid, the discrepancy being more pronounced for low values of r_m.

3.6 Overall Suggestions for the Design of an Elastic Impact Damper

So far we have presented three different methods, viz., HBM, EPL and direct numerical integration for arriving at the design of an impact damper for controlling the high-amplitude vibration of a harmonically excited Duffing's oscillator. Each of these methods
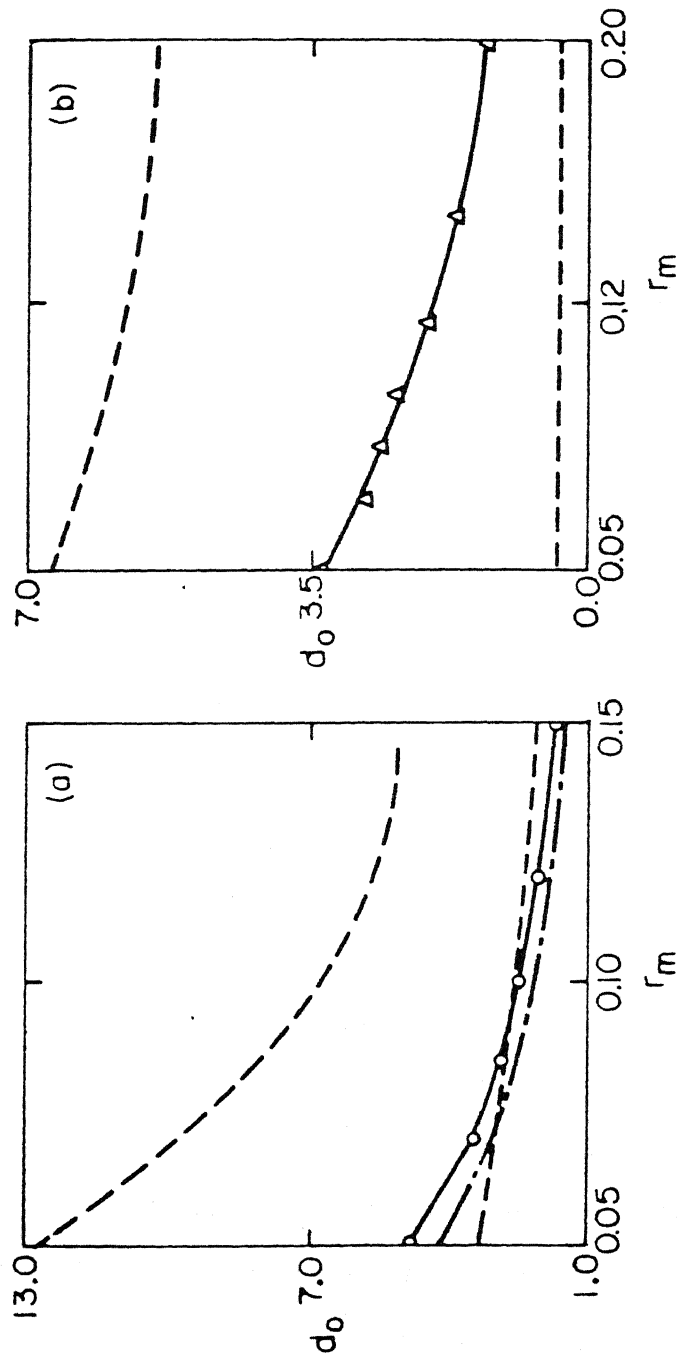
Figure 3.12 Optimum design curves. $\Omega = 2.2$, $h = 0.2$, $\omega_\ell = 1$. a) $\chi = 1$, b) $\chi = 0.9$. —— EPL, —— • —— HBM, o and Δ numerical integration. The zone enclosed between the dashed lines corresponds to stable, symmetric motion with two impacts per cycle.

has certain advantages and disadvantages as discussed below.

The HBM not only provides a good initial design of an elastic impact damper with minimum effort but also gives the overall frequency response without bringing in the actual number of impacts occurring per cycle. However, The initial design needs refinement to arrive at the optimal design. The EPL technique provides the most accurate optimal values. This method is also capable of tackling an inelastic damper. But this method requires prior knowledge of the actual number of impacts per cycle. With increasing number of impacts, the algebra involved in this method becomes unwieldy. Numerical integration being costly in terms of computation time should be done to check the final design.

Considering the merits and demerits of various methods, it can be suggested that an initial design should be made (for a given Ω_p) following equation (3.19). First the optimum value of d_o should be obtained with a low value of r_m. This optimum value should then be refined using the EPL technique. The frequency response of the system with these optimum values should be obtained using the HBM. If the suppression band needs to be widened, a higher r_m has to be tried. Once the final design is decided, direct numerical integration of the equations of motion has to be carried out to ensure the non-existence of any high-amplitude solution (not covered by the HBM, e.g., subharmonics.) in the frequency range of interest.

3.7 Use of an Impact Damper for Guided Branch Transition

The concept of a guided branch transition, or migration control as it is called, is recent in the literature [103,104]. Non-linear systems generally have multiple, steady-state, periodic or strange (chaotic) attractors for fixed parameter values and all such attractors coexist with their respective basins of attraction. The role of a migration controller is to lead the system to a pre- assigned attractor from any initial condition. If the initial condition falls within the basin of an undesirable attractor, then the migration controller operates and guides the system to the basin of attraction of the desired attractor. Once this is achieved, the controller is released. The whole concept can be recast mathematically as follows:

A forced non-linear oscillator can be described by an autonomous first order vector differential equation as follows:

$$\dot{Z} = f\ (Z,\ p(\theta))$$
$$\dot{\theta} = \hat{\alpha} \tag{3.36}$$

where $Z \in \mathbb{R}^n$ and $\theta \in S^1$;

$f\ :\ \mathbb{R}^n \times S^1 \rightarrow \mathbb{R}^n$,

$p\ :\ S^1 \rightarrow \mathbb{R}^\ell$ with $\ell \leq n$,

the dot represents differentiation with respect to time τ and $\hat{\alpha}$ is a constant. With control variables Z_c and the control force $f_c(Z_c)$, the system equations take the following form:

$$\dot{Z} = f(Z, p(\theta)) + f_c(Z_c),$$

$$\dot{Z_c} = f_c^* (\theta, Z, Z_c) \tag{3.37}$$

and $\quad \dot{\theta} = \hat{\alpha}$

where $\quad Z_c \in \mathbb{R}^m$

$\quad\quad f_c : \mathbb{R}^m \to \mathbb{R}^n$

and $\quad f_c^* : \mathbb{R}^n \times \mathbb{R}^m \times S^1 \to \mathbb{R}^m.$

We represent the basin of attraction of the undesirable attractor A_{ud} of equations (3.36) by the set $B_{A_{ud}}$ and that of the attractor A_c of equations (3.37) by B_{A_c}. Let the basin of attraction of the goal attractor A_d of equations (3.36) be represented by B_{A_d}. Thus,

$$B_{A_{ud}} \subseteq \mathbb{R}^n \times S^1$$

$$B_{A_d} \subseteq \mathbb{R}^n \times S^1$$

and $\quad\quad B_{A_c} \subseteq \mathbb{R}^{n+m} \times S^1 .$

We define the flow represented by equations (3.36) and (3.37) by Γ_{wc}^τ and Γ_c^τ, respectively. Let the initial conditions be represented by a point $P_1^r (Z_0, \theta_0) \in B_{A_{ud}}$ such that

$$\lim_{\tau \to \infty} \Gamma_{wc}^\tau (P_1^r(Z_0, \theta_0)) \to A_{ud}.$$

But if the control force is added, P_1^r gets extended to $P_1(Z_0, \theta_0, Z_{co}) \in B_{A_c}$ and

$$\lim_{\tau \to \infty} \Gamma_c^\tau (P_1(Z_0, \theta_0, Z_{co})) \to A_c \leq B_{A_c}.$$

If the control is released when the motion reaches a point $P_2 \in [A_c \cap B_{A_d}]$, then P_2 is restricted to $P_2^r(Z_1, \theta_1)$ $[\in B_{A_d}]$ when

$$\lim_{\tau \to \infty} \Gamma_{wc}^\tau ((P_2^r(Z_1, \theta_1)) \to A_d [\leq B_{A_d}].$$

The whole control action is schematically shown in Figure 3.13.
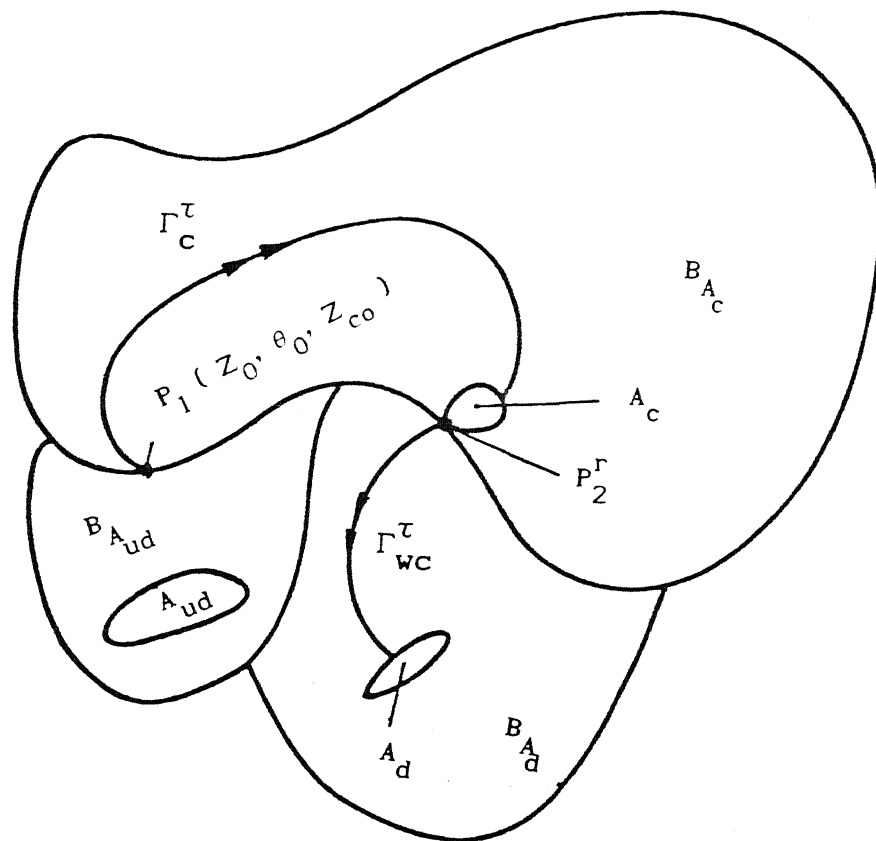
Figure 3.13   Migration control scheme.

In Sections 3.2 and 3.4, we have seen that an impact damper can reduce the response of a harmonically driven, Duffing's oscillator, especially in a frequency-band corresponding to the high-amplitude resonance branch. Using the multiplicity features of the steady-state motion of the Duffing's oscillator, here we use an elastic impact damper as a migration controller. It will be seen how starting from the basin of attraction of the resonance solution, the system goes to the non-resonance branch when an impact damper is used as a controller. It is generally seen that around the higher end of the resonance branch, the probability of finding an initial condition for the non-resonance motion is higher near the trivial initial conditions. Around these trivial (zero) initial conditions, a wide zone exists which forms the subset of the basin of attraction of the non-resonance motion [105]. It has already been seen in sections 3.2 and 3.3 that an impact damper brings the primary system to a near-trivial motion. Thus, the points on the steady-state attractor of the system (including the impact damper) might be completely embedded within the basin of attraction of the non-resonance motion of the primary system (without the impact damper). At the steady-state, the primary motion might choose the initial point suitable for the non-resonance oscillation when the impact damper can be switched off. However, as the system is non-autonomous, the phase of the excitation at the time of withdrawal of the control is very important. The phase should correspond to the desired goal. Thus, using the migration control one can avoid the continuous noisy operation of an impact damper.

A numerical example showing the feasibility of the above scheme is given below:

$$\text{Say} \qquad Z = \left\{ \begin{array}{c} Z_1 \\ \tilde{Z}_1 \end{array} \right\} \quad , \quad \tilde{Z}_1 = \dot{Z}_1 \qquad \text{and}$$

$$f = \left\{ \begin{array}{c} \tilde{Z}_1 \\ f_1(Z_1, \tilde{Z}_1, \theta) \end{array} \right\} \quad , \quad \hat{\alpha} = \Omega$$

where $f_1(Z_1, \tilde{Z}_1, \theta) = -Z_1^3 - h\,\tilde{Z}_1 + \cos\theta$

If an impact damper is used as a controller, then

$$Z_c = \left\{ \begin{array}{c} Z_2 \\ \tilde{Z}_2 \end{array} \right\} \quad , \quad \tilde{Z}_2 = \dot{Z}_2 , \quad f_c(Z_c) = \left\{ \begin{array}{c} 0 \\ f_{c_1}(Z_2) \end{array} \right\}$$

and $f^*_c(\theta, Z, Z_c) = \left\{ (1 + \dfrac{1}{r_m})\, f_{c_1}(Z_2)\ \overset{\tilde{Z}_2}{-}\ f_1(Z_1, \tilde{Z}_1, \theta) \right\}$

where $f_{c_1}(Z_2) = -r_1\left\{ (Z_2 - d_o)\, U(Z_2 - d_o) + (Z_2 + d_o)\, U(-Z_2 - d_o) \right\}$.

Let us take $r_1 = 2000$, $h = 0.215$, $d_o = 2$ and $r_m = 0.12$.
We consider the operation of the impact damper as a migration controller at three different values of the excitation frequency.
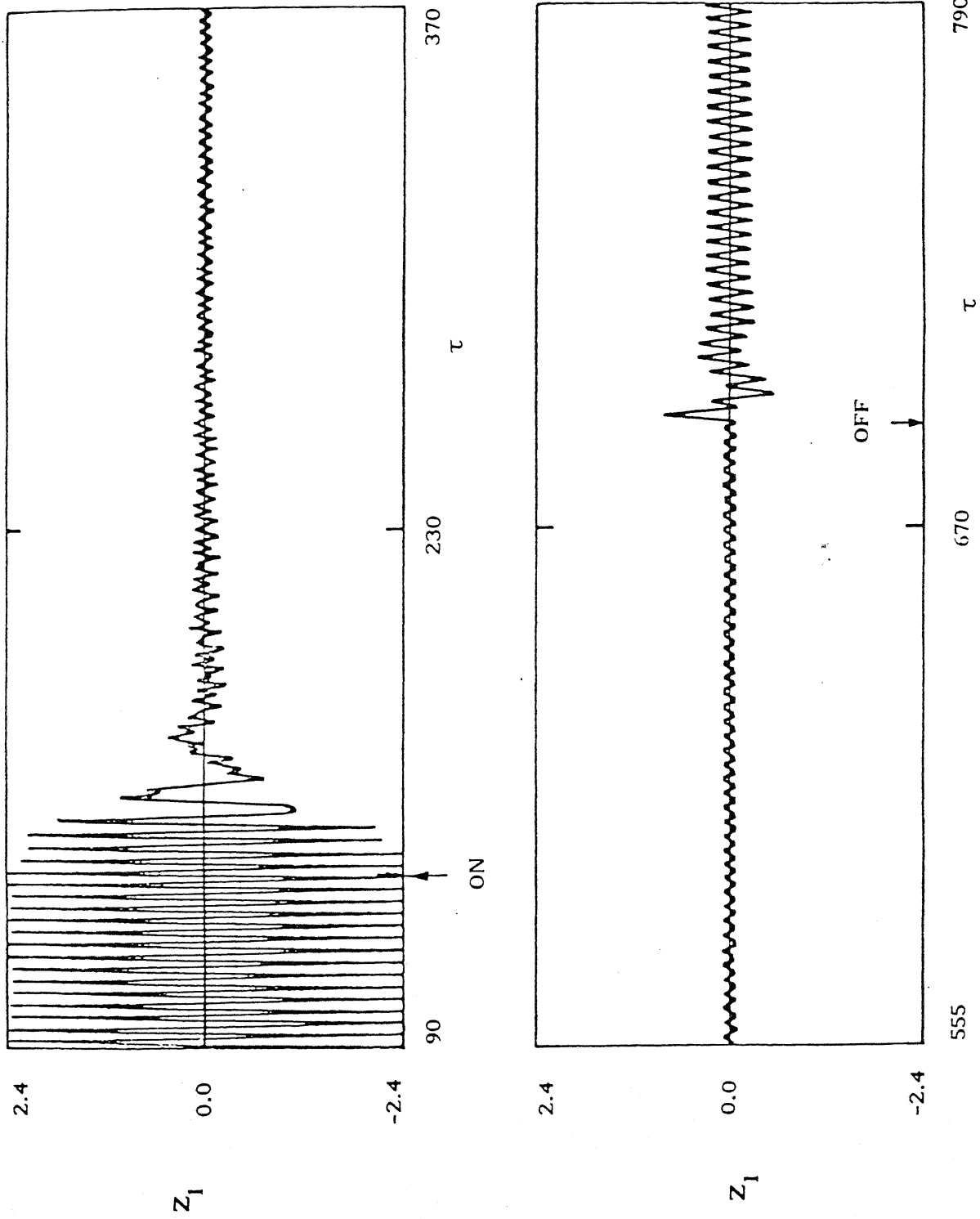
Figure 3.14 Oscillatory signature of the primary system with migration control. $\Omega = 1.95$, $h = 0.215$, $r_m = 0.12$, $d_0 = 2$, $r_1 = 2000$.
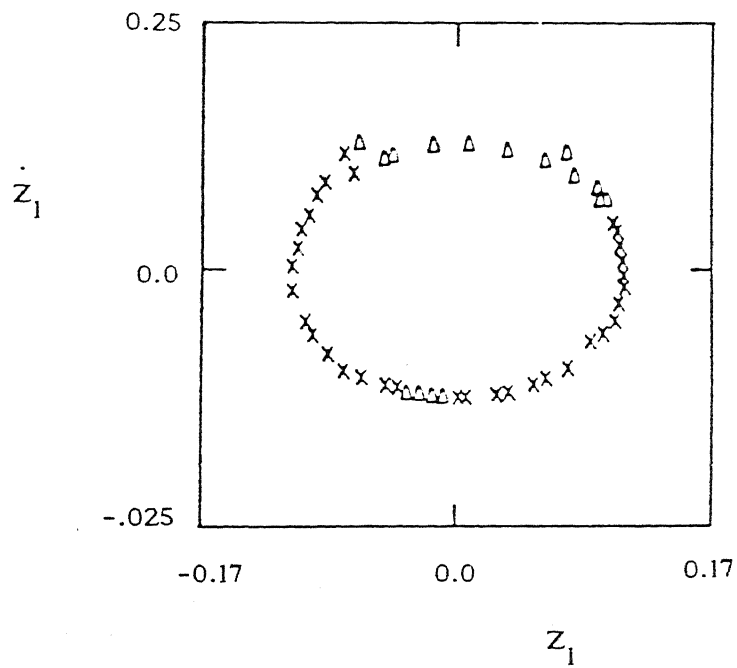
Figure 3.15 Steady-state attractor of the primary system. $\Omega = 1.7$, $r_m = 0.12$, $d_o = 2$, $h = 0.215$. Δ represent the points from which the motion without the impact damper goes to one-third subharmonic oscillation. X represent the points from which the motion without the impact damper goes to the non-resonance motion.
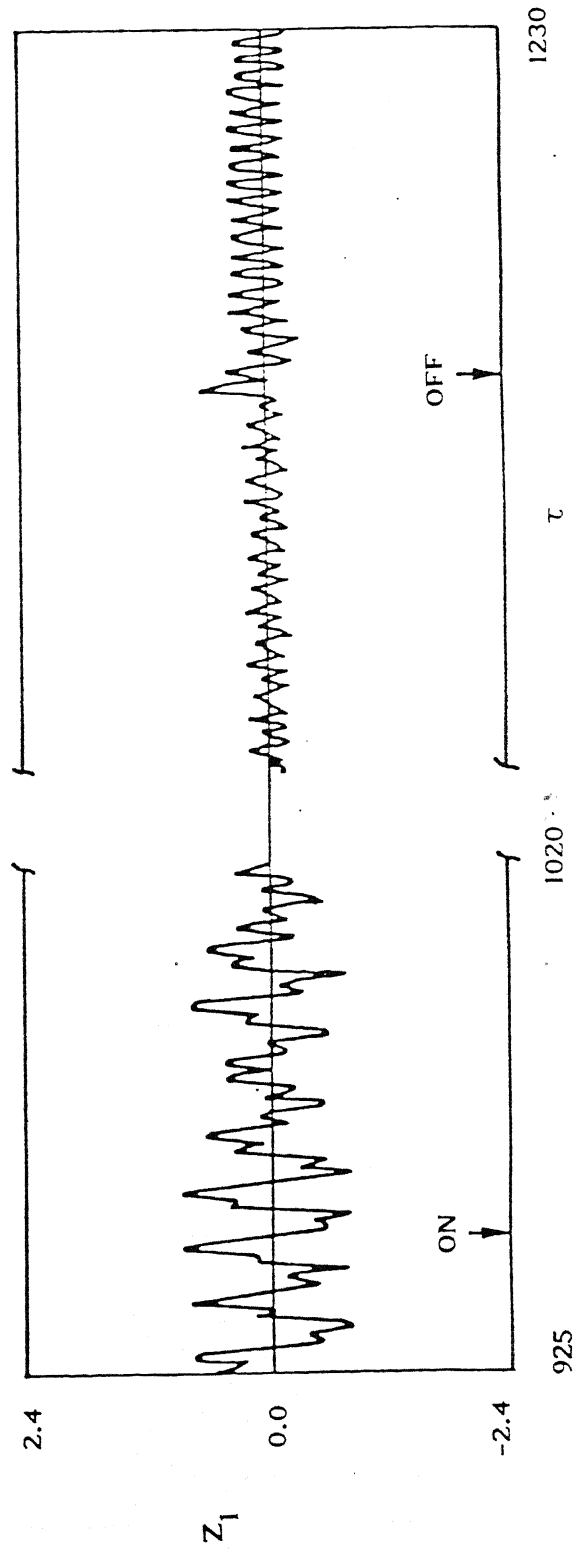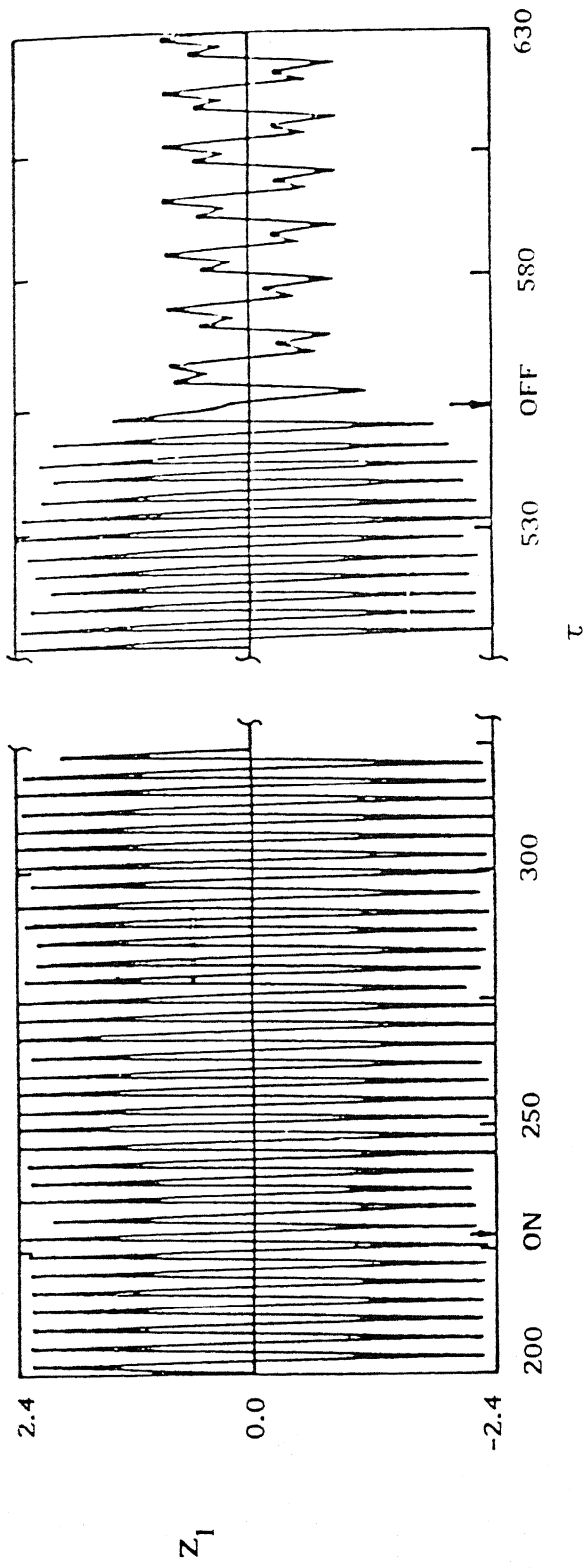
Figure 3.16 Oscillatory signature of the primary with migration control. $\Omega = 1.7$, other parameters are same as in Figure 3.14.
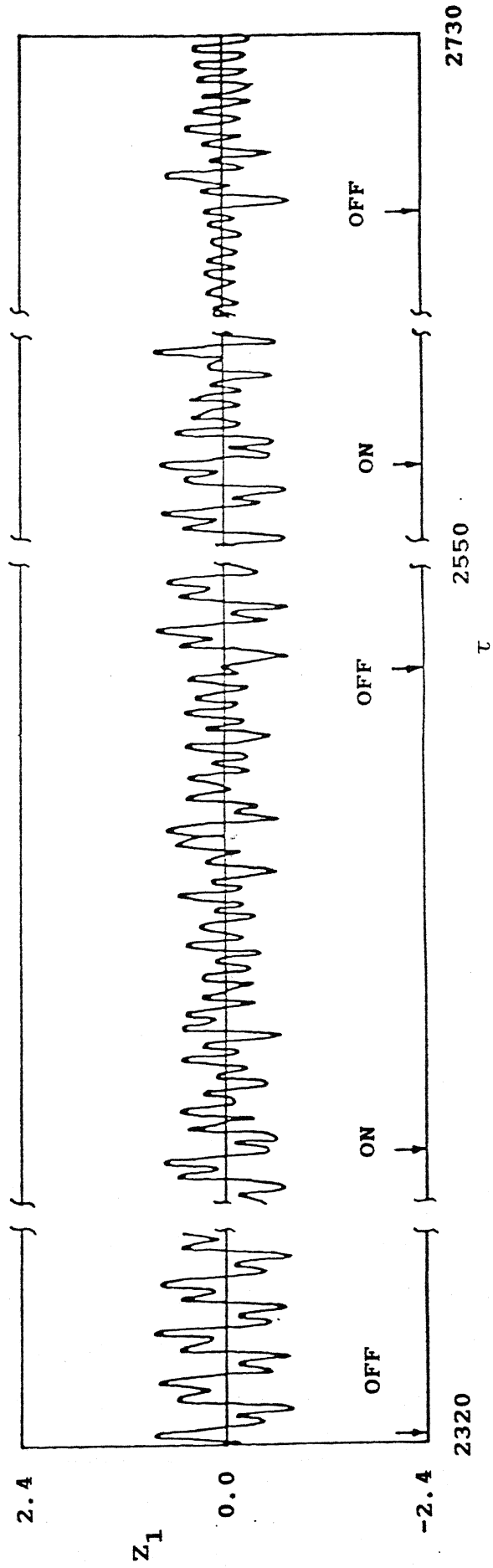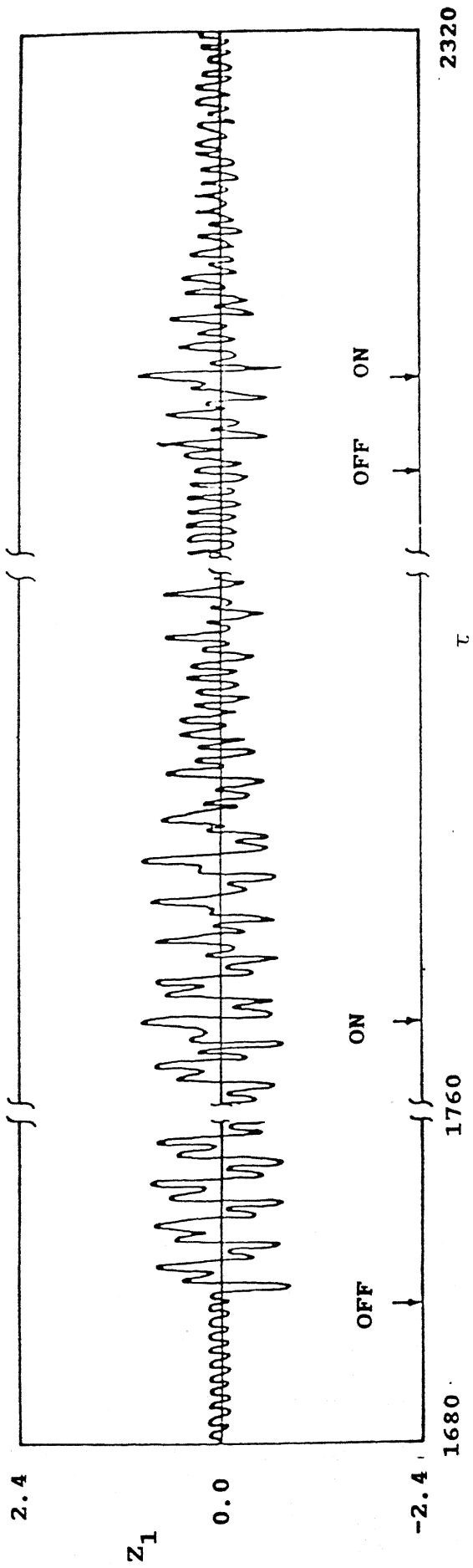
Figure 3.17 Oscillatory signature of the primary with migration control. $\Omega = 1.85$, other parameters are same as in Figure 3.14.

release the control before the steady state is reached. The motion is seen to reach a three-periodic solution. Several switchings of the controller ultimately lead the system to the non-resonance one- periodic motion.

For a number of parameter values tested, it was observed that several on-off switchings spanning, in total, not more than 350 cycles of operation could lead the response to the non-resonance branch. For a safe application of an impact damper as a migration controller, one needs to design the impact damper for its optimum performance. Thereafter, a hit and try control algorithm depicted in Figure 3.18 can be followed for migrating to the desired motion.

3.8 Conclusions

The performance of an impact damper attached to a harmonically excited Duffing's oscillator has been presented. The existence and stability of a low amplitude motion, near the high-frequency, large amplitude resonance branch of the primary system, has been established using the harmonic balance method and the EPL technique. The optimum design predicted by the harmonic balance solution is refined by the EPL technique and numerical integration. For a given mass ratio (r_m), the optimum free space for the loose mass (d_o) is obtained. The primary response is seen to be rather insensitive to the values of both r_m and d_o near this optimal design. With the optimum design, two symmetric collisions per cycle are always seen to occur. The suppression band of the impact damper narrows down with increasing non-linearity in the
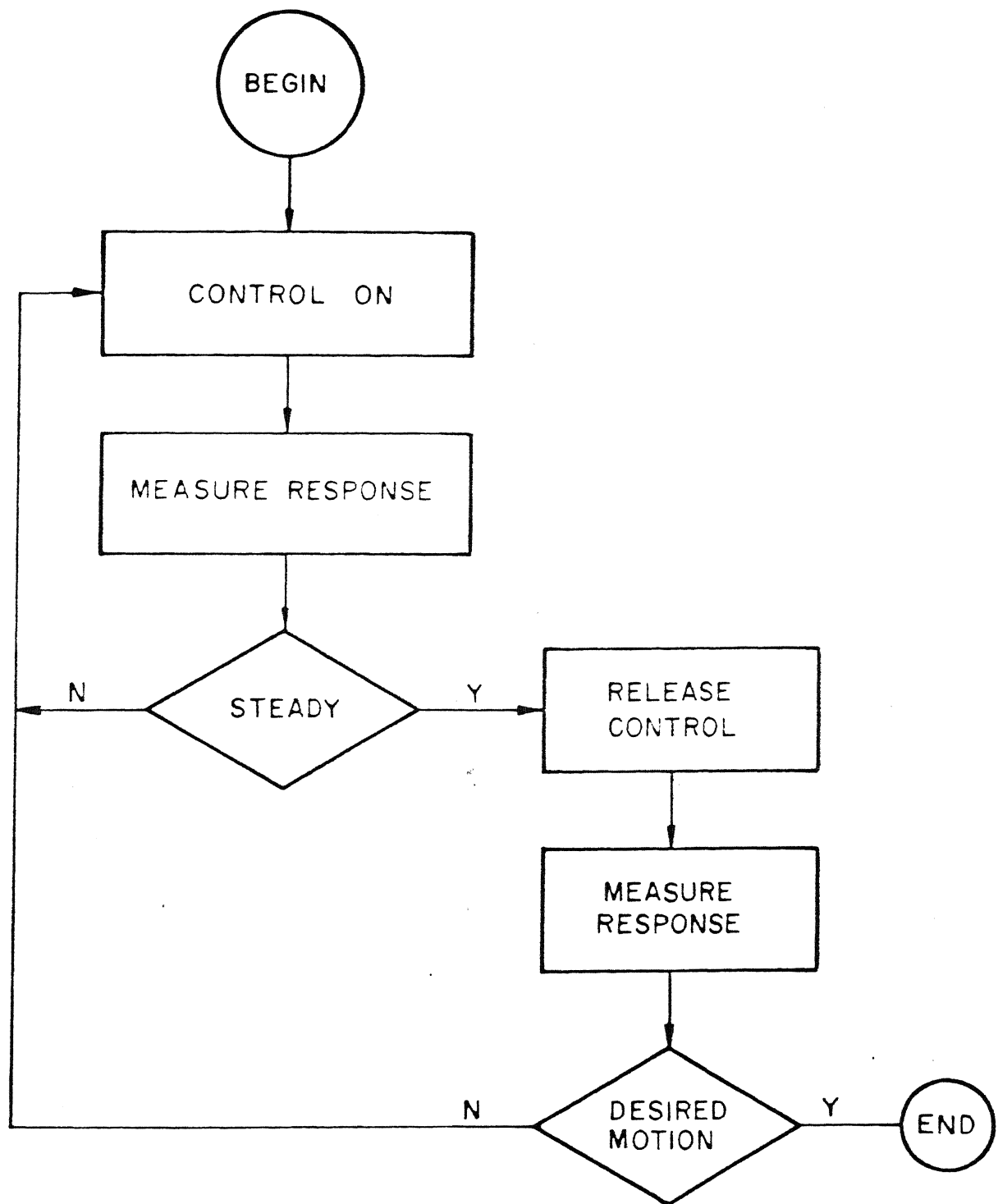
Figure 3.18 Algorithm of migration control.

restoring force, but the percentage reduction of amplitude at the design frequency is seen to be insensitive to the degree of non-linearity. An impact damper is very effective for reducing (or even eliminating) the one-third subharmonic response. An inelastic damper widens the suppression band at the cost of higher primary response. An "on-off" migration control strategy, using an impact damper, for a guided transition from one solution branch to the other is proposed. The feasibility of the proposed scheme is verified through numerical examples. This scheme, applicable to other non-linear primary systems having multistable solutions, obviates the need of continuous, noisy operation of an impact damper.

C H A P T E R - 4
IMPACT DAMPERS FOR CONTROLLING SELF-EXCITED OSCILLATION

4.1 Introduction

If the vibration of a system is excited by a force which depends on the state variables representing the motion, then it is called self-excited vibration. Self-excitation is a common source of vibration in various physical systems, such as (galloping of) transmission lines, (chatter in) metal cutting machine tools, a rotor bearing combination and a number of dry friction driven oscillators. The mechanism of self-excitation is identified with the presence of a non-linear function of state-variables in the mathematical model of the system. The most widely used form of this function is van der Pol type damping which has a negative linear part destabilizing the equilibrium position of the system and a non-linear part limiting the growth of the instability. As a result, a new dynamic equilibrium (the so called limit cycle) is approached and the system continues to vibrate autonomously. Of course, a self-excited system can also be simultaneously subjected to some other external forces when the system is termed non-autonomous or forced.

Several attempts have been made to quench the self-excited vibrations in physical systems. Mansour[106] has investigated the role of a conventional dynamic vibration absorber(DVA) in suppressing the self-excited oscillations. He investigated the possibility of using a linear DVA for stabilizing the self-excitation of a van der Pol oscillator and found the results

not very promising. Tondl [107] extended the analysis of Mansour for the same system and concluded that the absorber can be effective only if the mass ratio (ratio of the absorber mass to that of the main system) is very high. Tondl [108] has also studied the performance of a resilient foundation mounting towards suppressing the self-excited vibration of a rotor system. He investigated the role of dry friction [109] in controlling the self-excited vibration and found that dry friction may be effective in stabilizing the equilibrium position of a van der Pol type oscillator under soft perturbations. Recently, Asfar [110] has proposed the use of a Lanchester damper for quenching both the autonomous and forced self-excited vibrations of a single degree-of-freedom system. He concluded that the tuning of the damper is not important for its efficient operation.

The major emphasis in all the above mentioned works was on the stability of the equilibrium. For successful design of these devices, an accurate knowledge of the strength of the self-exciting force was necessary so that a proper amount of external damping can be incorporated to compensate the negative damping (which is the source of instability). In this chapter we investigate the performance of an impact damper for controlling both free and forced vibrations of a self-excited oscillator. Complete quenching (equivalent to the stabilization of the equilibrium) is obviously not possible by an impact damper, since an impact damper is operative only when there is oscillation. A van der Pol oscillator is analysed and numerical results are presented to show the effects of various parameters.

4.2 Equations of Motion

A mathematical model of a single degree-of-freedom van der Pol oscillator with an impact damper is shown in Figure 4.1(a). The differential equations describing the motion of the system between two consecutive impacts can be written in the following non-dimensional form

$$\ddot{z}_1 + \varepsilon \, \dot{z}_1 \, (\, z_1^2 - 1 \,) + z_1 = F_0 \, \cos(\Omega \, \tau) \qquad (4.1a)$$

$$\text{and} \qquad \ddot{z}_p = 0 \qquad\qquad (4.1b)$$

$$\forall \, | \, z_1 - z_p \, | \, < d_0$$

with $\omega_0 = (K_1/m_1)^{1/2}$, $x_0 = \sqrt{g_1}$, $\Omega = \omega/\omega_0$, $F_0 = F/(m_1 x_0 \omega_0^2)$

$\varepsilon = e_1 x_0^2 / (m_1 \omega_0)$, $z_1 = x_1/x_0$, $z_p = x_2/x_0$, $d_0 = d/2x_0$, $\tau = \omega_0 t$

and the dot denotes differentiation with respect to τ.

When $| \, z_1 - z_p \, | = d_0$, a collision occurs satisfying the following conditions:

$$\dot{z}_1^- = \alpha_1 \, \dot{z}_p^- + \alpha_2 \, \dot{z}_p^+$$

$$\dot{z}_1^+ = \alpha_3 \, \dot{z}_p^- + \alpha_4 \, \dot{z}_p^+$$

where the superscripts + and - denote, respectively, the conditions after and before impacts. Using the conservation of total linear momentum and the definition of the coefficient of
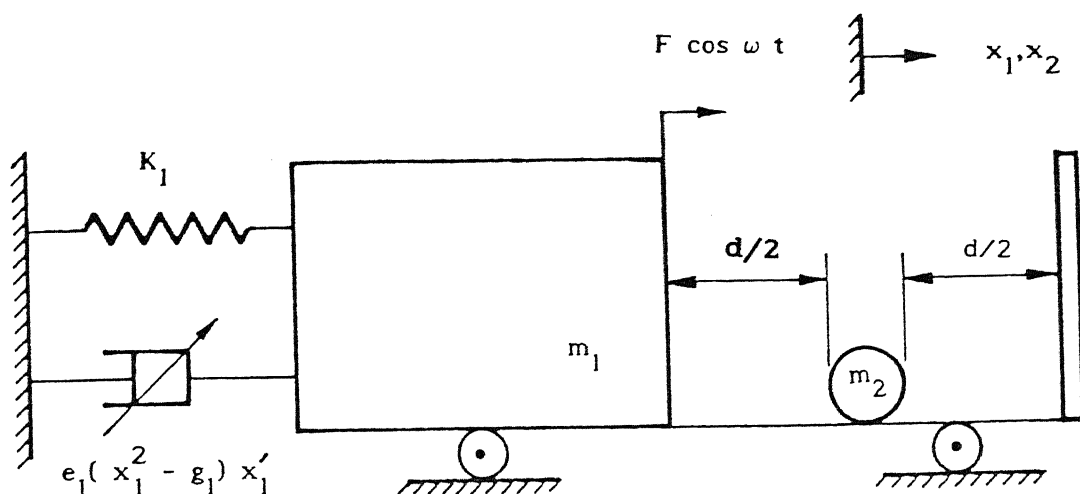
(a)
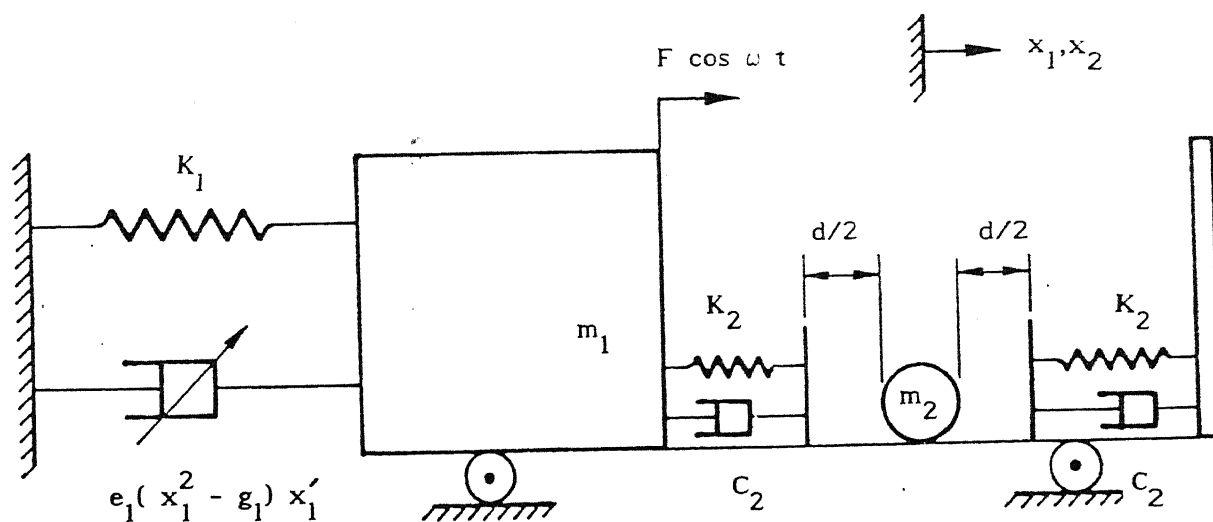
(b)

Figure 4.1 van der Pol oscillator with an impact damper. (a) zero
contact time, (b) finite contact time.

restitution it is easy to obtain α_i' s as follows:

$$\alpha_1 = (\chi - r_m)/(1 + \chi)$$

$$\alpha_2 = (1 + r_m)/(1 + \chi)$$

$$\alpha_3 = \chi (1 + r_m)/(1 + \chi)$$

$$\alpha_4 = (1 - r_m \chi)/(1 + \chi)$$

where χ is the coefficient of restitution and $r_m = m_2/m_1$, is the mass ratio.

An alternative way of modelling an impact damper would be through the introduction of a spring and a dashpot as shown in Figure 4.1(b). The differential equations describing the motion of such a system are written in the following non-dimensional form:

$$\ddot{Z}_1 + \varepsilon(Z_1^2 - 1)\dot{Z}_1 + Z_1 + r_1 \Phi_1(Z_2) + 2\xi_c\sqrt{r_1 r_m}\ \Phi_2(Z_2)\dot{Z}_2 = F_0 \cos \Omega\tau$$

and

$$\ddot{Z}_2 + r_1\Phi_1(Z_2)/r_m + 2\xi_c\sqrt{r_1/r_m}\ \Phi_2(Z_2)\dot{Z}_2 = \ddot{Z}_1 \tag{4.2b}$$

(4.2a)

where

$$\Phi_1(Z_2) = (Z_2 - d_0)U(Z_2 - d_0) + (Z_2 + d_0)U(-Z_2 - d_0)$$

$$\Phi_2(Z_2) = U(Z_2 - d_0) + U(-Z_2 - d_0)$$

when $U(.)$ is Heaviside's step function defined as

$$U(\zeta) = 1 \quad \forall\ \zeta > 0$$

$$= 0 \quad \forall\ \zeta < 0$$

and $r_1 = K_2/K_1$, $Z_2 = (x_1 - x_2)/x_0$ and the damping ratio ξ_c is obtained in terms of the coefficient of restitution χ used in the

first model as (see Appendix B)

$$\xi_c = c_2 / 2\sqrt{K_2 m_2} = - \frac{\ln(\chi)}{\{(1 + r_m)(\pi^2 + (\ln(\chi))^2)\}^{1/2}} \qquad (4.3)$$

This expression is valid except in a small neighbourhood of $\chi = 0$.

With a very high numerical value of r_1 ($\sim o(10^5)$) in equations (4.2), the results obtained from both the models described above are found to be quite close. However, it has been seen that the second model described by equations (4.2) offers special advantages over equations (4.1) during numerical integration.

It may be mentioned here that an impact damper (shown in Figure 4.1(b)) is a special form of a non-linear dynamic vibration absorber (DVA) where the non-linearity is introduced through the clearance. It can be easily seen that the equations of motion reduce to those of a linear DVA if d_0 in equations (4.2) is set to zero.

4.3 Autonomous vibration

For the analysis of autonomous vibration, we put $F_0 = 0$ in equations (4.1) and (4.2). It is a well known fact that an impact damper, used to suppress the vibration of forced linear/non-linear oscillators [77,88], operates efficiently with two symmetric impacts occurring in a forcing cycle. Assuming the same to be true during one cycle of a self-excited oscillator, we shall construct a periodic solution with two symmetric impacts per cycle and analyse its stability.

4.3.1 Periodic Solution

In this section we present a symmetric periodic solution with two impacts per cycle. One half of such a cycle is depicted in Figure 4.2. Without any loss of generality, let us arbitrarily set the time origin ($\tau = 0$) at the instant of an impact with the right hand side wall of the container. Now from the symmetry condition, it is known that the next impact will occur at $\tau = \pi/\Omega_\ell$ where Ω_ℓ is the unknown frequency of the limit cycle. First we transform equations (4.1) into equivalent linear forms given by

$$\ddot{z}_1 + 2 \rho \dot{z}_1 + z_1 = 0 \qquad (4.4a)$$

and
$$\dot{z}_p = - v \qquad (4.4b)$$

$$\nleftrightarrow \quad \left| z_1 - z_p \right| < d_0 \text{ and } 0^+ < \tau < (\pi/\Omega_1)^-$$

where ρ is an unknown constant to be determined later and v is the velocity of the loose mass. From the symmetry of the motion we have the following conditions:

$$z_1(0) = - z_1(\pi/\Omega_\ell) = z^0 \text{ (say)}$$

$$\dot{z}_1(0^+) = - \dot{z}_1(\pi/\Omega_\ell)^+ = \dot{z}^1 \text{ (say)}$$

$$\text{and } \dot{z}_1(\pi/\Omega_\ell)^- = - \dot{z}_1(0^-) = - \dot{z}^0 \text{ (say)} \qquad (4.5)$$

The definition of the coefficient of restitution, equation (4.4b) and the conservation of total linear momentum yield
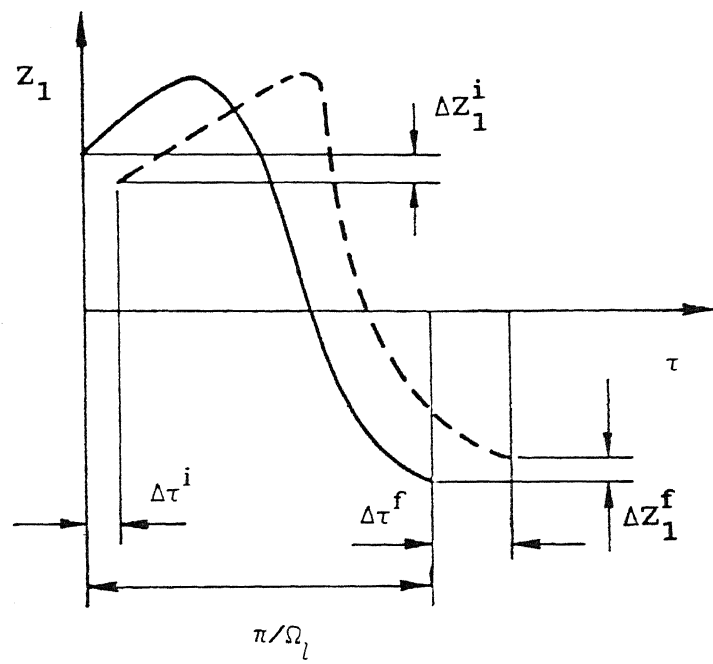
Figure 4.2 Half-cycle of a typical periodic solution having two symmetric impacts per cycle (solid line) and its arbitrarily perturbed form (dashed line).

$$\chi = (v + \dot{z}^1) / (v - \dot{z}^0) ,$$

$$2 d_0 + 2 z^0 = v \pi / \Omega_\ell$$

and
$$2 r_m v = \dot{z}^1 - \dot{z}^0 . \tag{4.6}$$

Solving equation (4.4a) one can write the motion between two consecutive impacts as

$$Z_1(\tau) = \exp(-\rho \tau) (d_1 \cos (\eta \tau) + d_2 \sin (\eta \tau)) \tag{4.7}$$

where $\eta = \sqrt{1 - \rho^2}$

Now using conditions (4.5) and (4.6) one can eliminate other unknowns viz., d_1, d_2, v, $\dot{z}^1$, $\dot{z}^0$ to get an equation of the form

$$f_1(\rho , \Omega_\ell) = 0 \tag{4.8}$$

For determining ρ let us consider a single term Fourier series approximation of $Z_1(\tau)$ given by

$$z_1^*(\tau) = a \cos (\Omega_\ell \tau) \tag{4.9}$$

satisfying the equation

$$\frac{\partial}{\partial \rho} \int_0^{2\pi/\Omega_\ell} \left\{ \varepsilon \, \dot{z}_1^* (z_1^{*^2} - 1) - 2 \rho \, \dot{z}_1^* \right\}^2 d\tau = 0 \tag{4.10}$$

Following this procedure ρ turns out to be

$$\rho = \varepsilon (a^2/4 - 1)/2 \tag{4.11}$$

It is to be noted that equations (4.7) and (4.9) are two different representations of the same solution. Thus, these two should be equal in some least square sense which implies that the first Fourier component of (4.7) should be given by (4.9) i.e.,

$$\left| \frac{\pi}{\Omega_\ell} \int_0^{2\pi/\Omega_\ell} Z_1(\tau) \, e^{i\Omega_\ell\tau} \right| = a \qquad (4.12)$$

It may be mentioned that d_1 and d_2 can be written as explicit functions of the unknown a. Thus, $Z_1(\tau)$ is also an explicit function of a and Ω_ℓ. So equation (4.12) is finally transformed to the form

$$f_2(\, a, \, \Omega_\ell \,) = 0 \qquad (4.13)$$

Now using equations (4.8) ,(4.11) and (4.13) one can find out a and Ω_ℓ when the other unknowns can also be easily determined. In fact, periodic solutions having any number of impacts can be constructed in a similar fashion.

4.3.2 Stability Analysis

For analysing the stability of the solution obtained in the previous section, the method of error propagation explained in reference [69] has been used. A brief sketch of the method is given below. Referring to Figure 4.2, let the solid line represent

the half-cycle of a constructed solution whereas the dotted line represents its perturbed form. The initial perturbation vector ζ_i is represented by

$$\zeta_i = \left\{ \Delta z_1^i \,,\, \Delta \dot{z}_1^i \,,\, \Delta v^i,\, \Delta \tau^i \right\}^T$$

This perturbation vector at the end of a half-cycle is given by

$$\zeta_f = \left\{ \Delta z_1^f \,,\, \Delta \dot{z}_1^f \,,\, \Delta v^f,\, \Delta \tau^f \right\}^T$$

A linearized relation between these two vectors can be written in the closed form as

$$\zeta_f = [\ P\ ]\ \zeta_i \tag{4.14}$$

where [P] is a 4x4 matrix whose elements are functions of the system parameters. As the solution is symmetric, the propagation rule for the perturbation vector during the next half of the cycle is also given by equation (4.14). Thus, the stability of the solution will be governed by the eigenvalues of the matrix [P]. If all the eigenvalues of the matrix [P] lie within the unit circle around the origin of the complex plane, then the solution is stable.

4.3.3 Results and Discussions

In this section, the role and design of an impact damper for reducing the limit cycle amplitude of a van der Pol oscillator is reported. Before going into the detailed discussions, one should remember that the van der Pol oscillator has a non-dimensional limit cycle amplitude 2 irrespective of the value of ε (<1). So our aim is to reduce this limit cycle amplitude by properly designing the impact damper which is described by the parameters r_m, d_0 and χ. It is obvious that a lower value of χ implying larger amount of dissipation counteracts the negative linear damping and thus helps to reduce the amplitude of the oscillator. Therefore, a very low value of χ (= 0.2) is chosen. A material pair having so low a coefficient of restitution is not very uncommon in practice [77]. To determine the effects of the other parameters, viz., d_0 and r_m, results are obtained both analytically and by direct numerical integration. The integration is carried out using fourth order Runge-Kutta-Merson algorithm with adaptive step size control. As mentioned earlier, integration of equations (4.1) is slightly difficult, since it involves the determination of the exact instant of an impact. However, equations (4.2) are easy to integrate due to the presence of a finite duration impact. In fact, the amplitudes of the limit cycles and their stability characteristics obtained from both the models (with a suitable choice of r_1) are found to be quite close.

The variation of the stable limit cycle amplitudes, $|z_1|_{max}$ with d_0, corresponding to the symmetric motion with two impacts per cycle, is plotted in Figures 4.3(a) and 4.3(b). It is seen
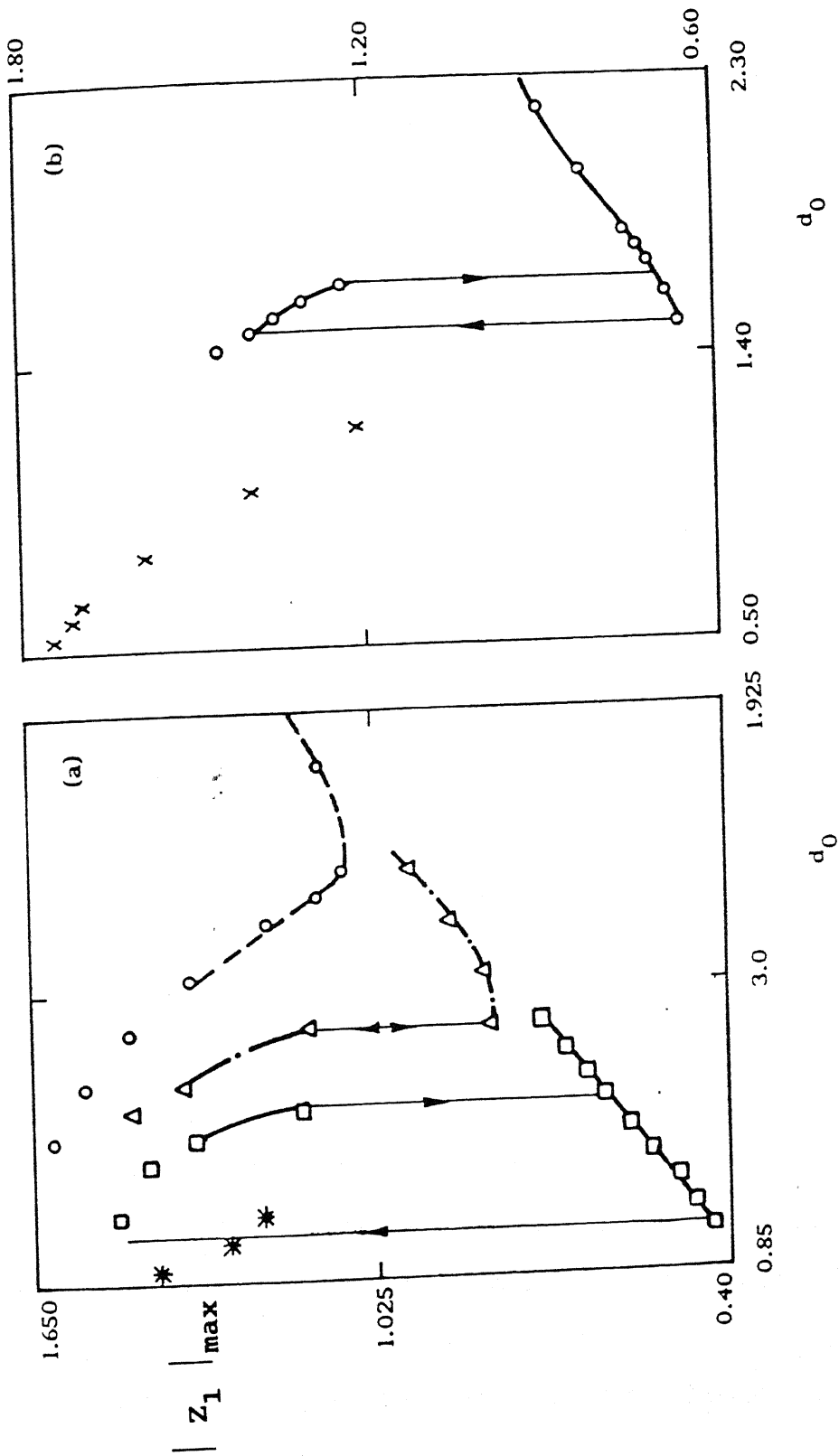
Figure 4.3 Variation of the limit cycle amplitude with d_0. χ = 0.2. (a) ε = 0.25. - - - (analytical), o (numerical) for r_m = 0.1; - • - • - (analytical), $\triangle$ (numerical) for r_m = 0.12 ; ———(analytical), $\square$ (numerical) for r_m = 0.14; * (numerical) for r_m = 0.18. (b) ε = 0.15. ——— (analytical), o (numerical) for r_m = 0.075; x (numerical) for r_m = 0.1.

that a significant reduction of the amplitude is possible with proper choices of r_m and d_0. It may be noticed that for some values of r_m, there is a range of d_0 where two stable limit cycles (both having two symmetric impacts per cycle) may coexist giving rise to a so called 'jump' phenomenon.

The results obtained from direct numerical integration are also plotted in Figures 4.4(a) and 4.4(b). It should be mentioned that, when the numerically integrated results match those predicted by the analysis, the motion is also seen to consist of two symmetric impacts per cycle. The extra results obtained by numerical integration reveal altogether different and complicated types of motion. However, the major objective of this work is to determine suitable values of r_m and d_0 for a good design of the impact damper. Therefore, we shall not discuss in details all these complicated motions which may be one of the following types:

i) stable periodic solution with asymmetric two impacts per cycle and stable periodic solution with more (than two) impacts per cycle,

ii) quasiperiodic,

iii) intermittent and chaotic.

One may conclude from Figures 4.3(a) and 4.3(b) that, for a good design of the impact damper, r_m and d_0 should be chosen so as to minimize the amplitude of the limit cycle. However, if for the design value of r_m, there exists a 'jump' region in the $|z_1|_{max}$ vs d_0 plane, then d_0 should be chosen outside the jump region. This design procedure presumes an exact knowledge of the parameter ε which may not be possible in a real life situation. In fact, the
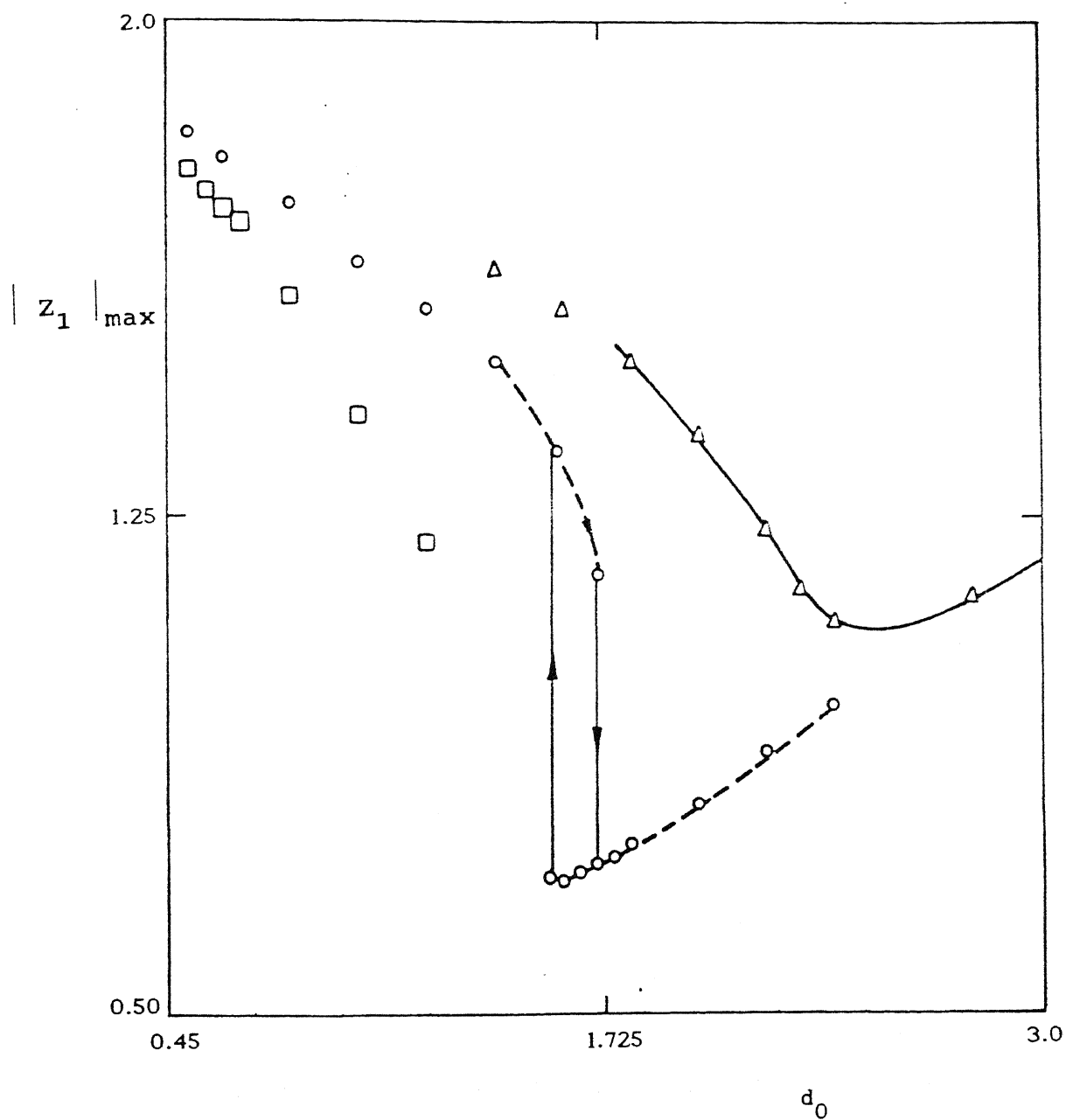
Figure 4.4 Variation of the limit cycle amplitude with d_0 for various levels of self-excitation. χ = 0.2, r_m = 0.1. ——— (analytical), $\triangle$ (numerical) for ε = 0.25; - - - - - (analytical), o (numerical) for ε = 0.2; $\square$ (numerical) for ε =.15.

value of $|Z_1|_{max}$ for a pair of (r_m, d_0) values is highly sensitive to the value of ε as can be explained from Figure 4.4(a). For example with $r_m = 0.1$ the optimum d_0 based on $\varepsilon = 0.2$ is around 1.8. If instead, the actual value of ε is 0.25 then at the same (r_m, d_0) combination, the value of $|Z_1|_{max}$ increases by a factor of 2. On the other hand if the actual value of ε is 0.15, then the desired two symmetric impacts per cycle motion does not exist at all. The variations of $|Z_1|_{max}$ with ε for different (r_m, d_0) combinations are shown in Figure 4.5. Finally we conclude that the design procedure should not be restricted only towards minimizing $|Z_1|_{max}$ but should also take into account its sensitivity to the value of ε.

4.4 Forced Vibration

In this section, the performance of an impact damper for controlling the vibration of a forced, van der Pol oscillator is discussed. A detailed account of the dynamics of a van der Pol oscillator can be found in the literature [111]. It is well known that the phenomenon of frequency entrainment occurs if the external forcing amplitude is greater than a critical value and the forcing frequency is close to an integral or sub multiple of the frequency of the free, limit cycle oscillation. As a result, the oscillator resonates at the forcing frequency. All types of resonances viz, superharmonic, harmonic and subharmonic entrainments are theoretically possible. However, the harmonic entrainment region extends over a large frequency band-width and in this zone the oscillator vibrates with a large amplitude.
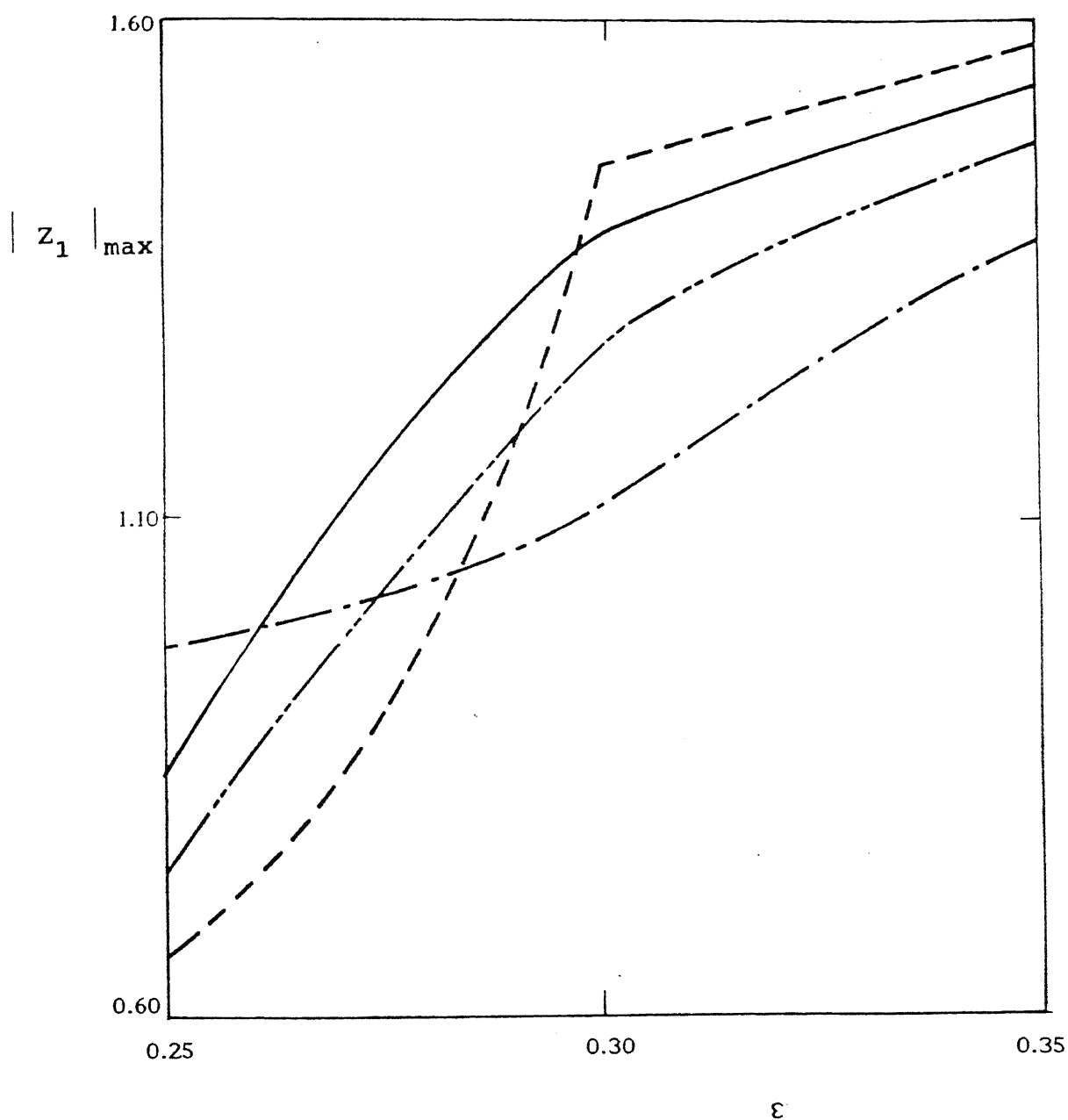
Figure 4.5 Variation of the limit cycle amplitude with ε. χ = 0.2. ———— (r_m= 0.12, d_0= 2); - - - (r_m= 0.14, d_0= 1.6), - · - · - (r_m= 0.12, d_0= 2.4); -··—··—··—··- (r_m= 0.14, d_0= 1.8).

Therefore, the discussion is limited to the control of the forced vibration in the harmonic entrainment zone. As before, we assume that the motion with two symmetric impacts per cycle offers the best mode of operation and proceed to construct the periodic solution corresponding to this mode. A stability analysis is also carried out.

4.4.1 Periodic Solution

For the construction of a symmetric motion with two impacts per cycle we refer back to Figure 4.2. The time origin $\tau = 0$ is set arbitrarily at the instant of an impact with the right hand side wall of the container. Consequently an unknown phase ϕ is introduced in the forcing function. The motion of the oscillator between $\tau = 0^+$ and $\tau = (\pi/\Omega)^-$ is described by the following equivalent linear differential equations

$$\ddot{Z}_1 + 2\,\rho\,\dot{Z}_1 + Z_1 = F_0 \cos(\Omega\,\tau + \phi) \qquad (4.15a)$$

and
$$\dot{Z}_p = -v \qquad (4.15b)$$

$$\forall \ \left| Z_1 - Z_p \right| < d_0 \text{ and } 0^+ < \tau < (\pi/\Omega)^-$$

The solution of equation (5.15a) can be written as

$$Z_1(\tau) = \exp(-\rho\,\tau)(d_1\cos(\eta\,\tau) + d_2\sin(\eta\,\tau)) + M\cos(\Omega\tau + \phi - \theta)$$

where $\eta = \sqrt{1 - \rho^2}$

$$M = \frac{F_0}{\sqrt{(1 - \Omega^2)^2 + (2\rho\Omega)^2}}$$

and $\theta = \tan^{-1}(2\rho\Omega/(1 - \Omega^2))$.

Conditions (4.5) and (4.6) expressing symmetry, momentum conservation and the coefficient of restitution still hold good with $\Omega_\ell = \Omega$. Eliminating d_1, d_2, ϕ, $\dot{z}^1$, $\dot{z}^0$ we get an equation of the form

$$f_2 (v, \rho) = 0 \qquad\qquad (4.16)$$

As before, we consider

$$z_1^*(\tau) = a \cos (\Omega \tau + \theta_1)$$

to obtain

$$\rho = \varepsilon (a^2/4 - 1)/2 \qquad\qquad (4.17)$$

Moreover, equation (4.12) remains valid and we finally have a relation like

$$f_3(v , a) = 0 \qquad\qquad (4.18)$$

Now using equations (4.16) - (4.18) one can determine a and v. Thereafter, the other unknowns are obtained easily.

The stability analysis of the solutions so constructed is carried out by the method of error propagation explained in section 4.3.2

4.4.2 Results and Discussions

For the non-dimensional van der Pol oscillator under discussion, the limit cycle frequency is approximately unity. Thus, the fundamental entrainment takes place at and near $\Omega = 1$. So we set our design frequency at $\Omega = 1$. For most real life applications $r_m < 1$. It is well known, in the context of the impact damper for a forced passive oscillator, that the maximum attenuation is possible for perfectly elastic impacts ($\chi = 1$). However, in the present case, the motion with two impacts per cycle is found to be unstable for perfectly elastic impacts. Therefore, we set χ to be less than unity such that the motion with two impacts per cycle becomes stable. A parametric study showing the effects of the design variables, viz, χ, d_0 and r_m on the amplitude of the forced vibration and the frequency band of suppression is reported. The results are obtained both analytically and by numerical integration.

The variations of the amplitude of vibration, with d_0 for various combinations of r_m and χ, are shown in Figure 4.6 at $\Omega =1$. At this frequency, the oscillator without the impact damper under the same level of excitation showed an amplitude greater than 3 which clearly demonstrates the usefulness of the impact damper. From Figure 4.6 it is obvious that an optimum d_0 exists, the value of which depends on the values of r_m and χ. The two impacts per cycle motion remains stable over a range of d_0 around this optimum value. The graphs also suggest that just as in the case of an impact damper for a passive linear or non-linear oscillator [88], the value of χ should be as high as possible. The
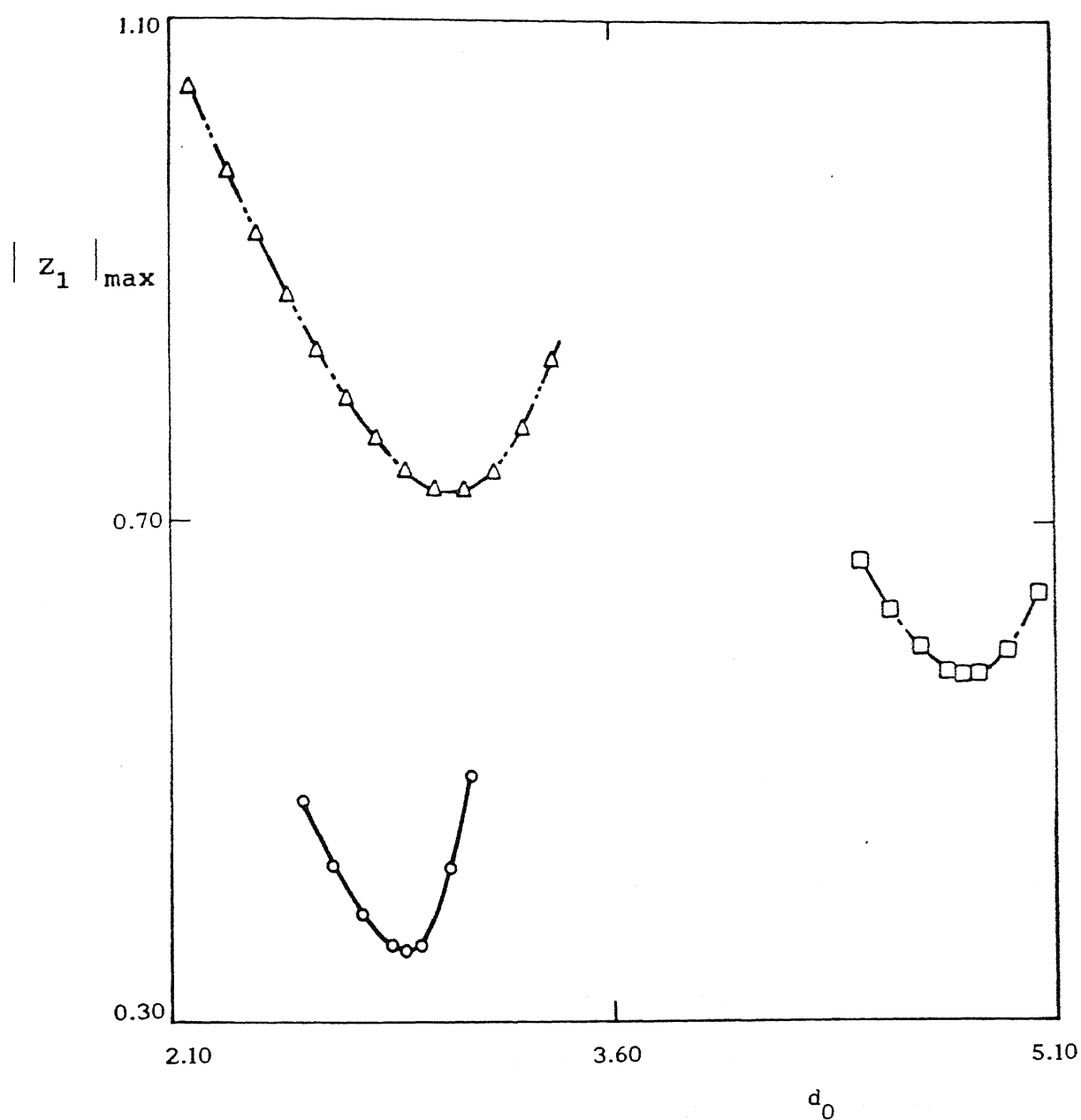
Figure 4.6 Variation of the amplitude of forced vibration with d_0. $F_0 = 0.5$, $\Omega = 1.0$, $\varepsilon = 0.1$. $-\cdots-$ (analytical), Δ (numerical) for ($r_m = 0.25, \chi = 0.5$), $\underline{\hspace{1.5cm}}$ (analytical), o (numerical) for ($r_m = 0.25, \chi = 0.7$). $-\cdot-$ $-\cdot-$ (analytical), □ (numerical) for ($r_m = 0.15, \chi = 0.7$).

variation of optimum d_0 with r_m for given values of the other parameters is shown in Figure 4.7. The limits on the parameter values maintaining the stability of the motion with two impacts per cycle are also indicated in the same figure by the dashed lines. The graph of Figure 4.7 fits the relation

$$r_m (\ d_0)_{opt} = constant$$

quite accurately. It has been found that at $\Omega = 1$, the following approximate relation can be written

$$r_m (\ d_0)_{opt}(\chi)^\beta = \lambda \ F_0^\gamma \ \varepsilon^\delta \qquad (4.19)$$

where $\beta \sim 0.06$, $\lambda \sim 1.85$, $\gamma \sim 1$, $\delta \sim 0.12$.

The frequency response characteristics of the oscillator around $\Omega = 1$, without and with an optimally designed impact damper are shown in Figure 4.8. The design of the impact damper may be optimized either at $\Omega = 1$ or at the operating frequency (around $\Omega = 1$). In the latter case, of course, the value of d_0 has to be actively controlled by sensing the excitation frequency. The frequency range over which the motion of the oscillator (with two impacts per cycle) remains stable is also indicated in Figure 4.8. This range of frequency ($\Delta \Omega_s$) is known as the suppression band. As expected, the actively controlled impact damper performs better (than the one passively tuned at $\Omega = 1$) both in terms of amplitude reduction and suppression band.

Numerical results for the passively tuned (at $\Omega = 1$) impact damper suggested that higher the value of r_m (of course, satisfying equation (4.19)), not only the reduction in amplitude is more, the suppression band is also wider. On the other hand, if
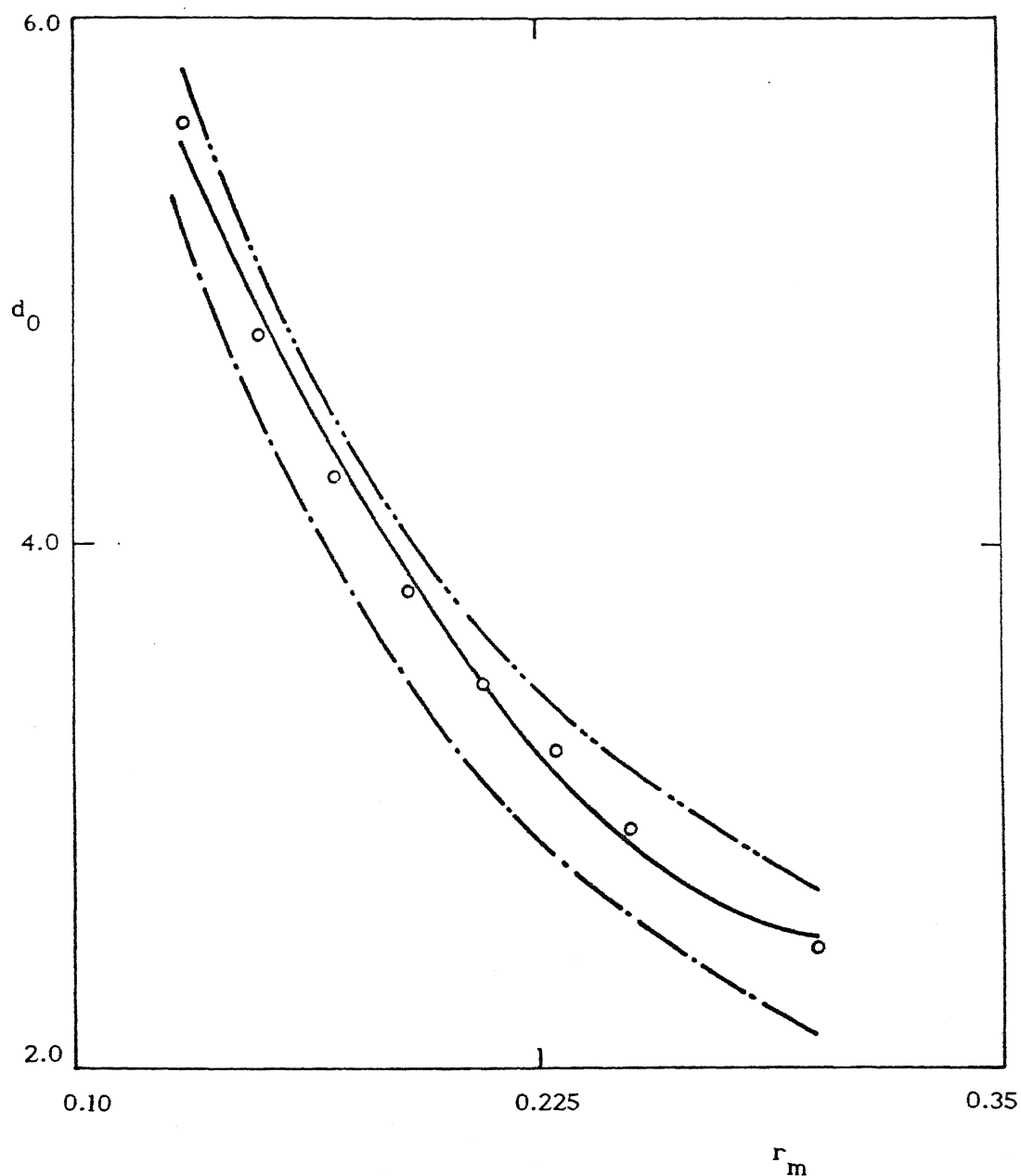
Figure 4.7 Optimum design curve in r_m - d_0 plane. F_0 = 0.5, χ = 0.7, Ω = 1, ε =0.1. ———— (analytical), o (numerical).
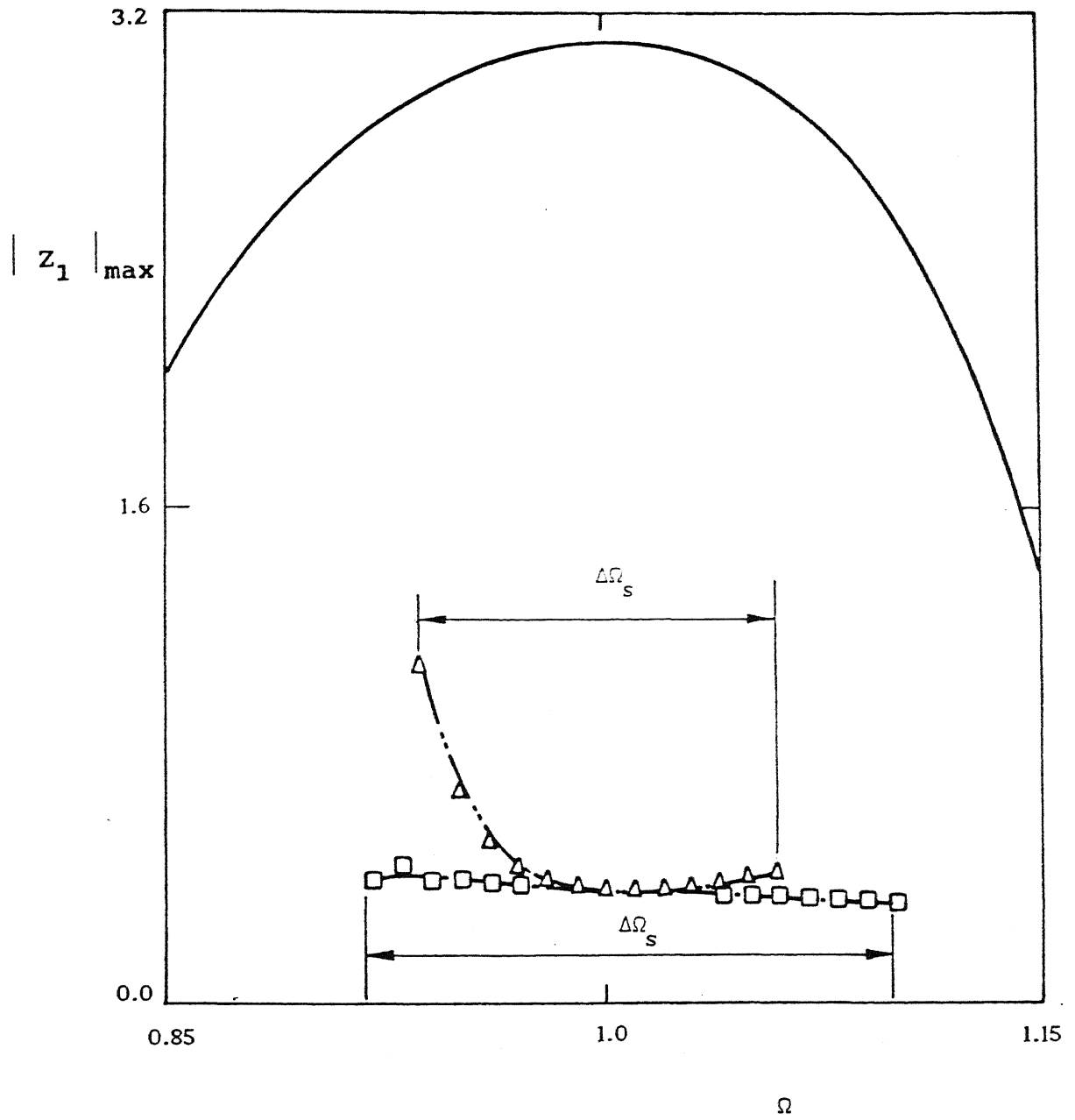
Figure 4.8   Frequency response of the oscillator. F_0 = 0.5, χ = 0.7, ε =0.1, r_m= 0.25, d_0 = 2.9. ————— without impact damper. — · · — · · — with damper (passive, analytical), Δ (passive, numerical). — · · — · · — ▸ — (active, analytical), □ (active, numerical).

the coefficient of restitution is increased, then the reduction in amplitude is more at the cost of narrowing the suppression band. These facts are illustrated in Figure 4.9. The statements made so far regarding the performance of the optimally designed impact damper are true for given values of F_0 and ε. However, the values of F_0 and ε in real life may not be known accurately. The sensitivities of the performance of an optimally designed impact damper (for synchronous operation at $\Omega = 1$) with the variation in F_0 and ε are indicated in Figure 4.10. It is observed that a higher value of r_m takes care of wider variations in the forcing whereas a lower value of χ takes care of wider variations in the value of ε.

4.5 Conclusions

For some combinations of the mass ratio (r_m) and free space (d_0) parameters of the impact damper, an autonomous van der Pol oscillator can have more than one stable limit cycles giving rise to 'jump' phenomenon in the amplitude-d_0 plane. For efficient operation, the impact damper should have a low coefficient of restitution and undergo two impacts per cycle. The parameters should be chosen outside the jump region. For the forced oscillator, a high value of the coefficient of restitution is desirable. An optimum design should attempt at both reducing the amplitude and widening the suppression band. An actively controlled damper performs better than a passively tuned one. The optimum parameters are sensitive to the levels of self and forced excitations.
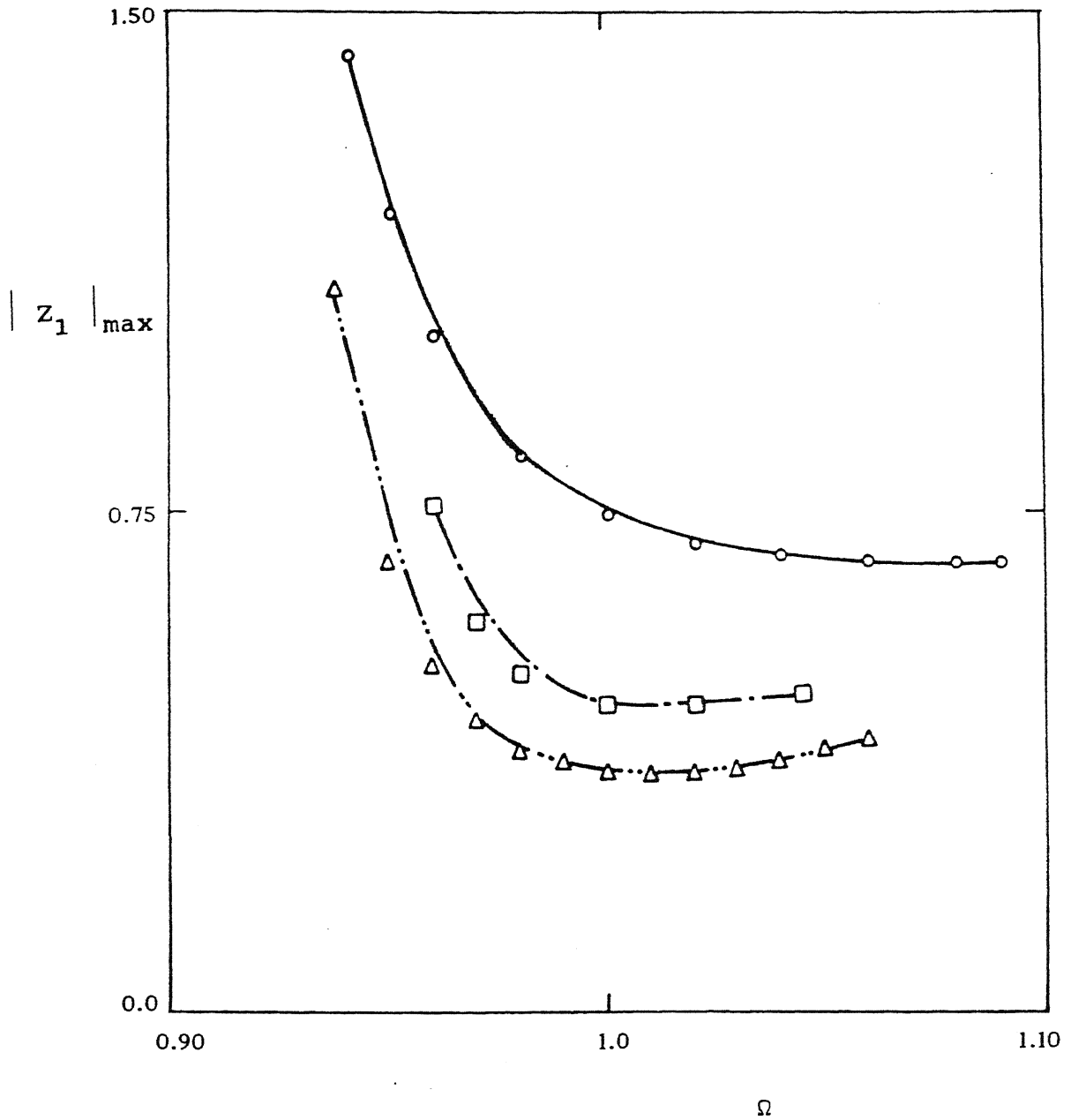
Figure 4.9 Optimum frequency response characteristics for various values of r_m and χ. $F_0 = 0.5$, $\varepsilon = 0.1$. ——— (analytical), o (numerical) for ($r_m = .25$, $\chi = 0.5$, $d_0 = 3.1$) . — · — · — (analytical), □ (numerical) for ($r_m = 0.19$, $\chi = .7$ $d_0 = 3.8$). — · · — · · — (analytical), Δ (numerical) for ($r_m = 0.25$, $\chi = 0.7$, $d_0 = 2.9$).
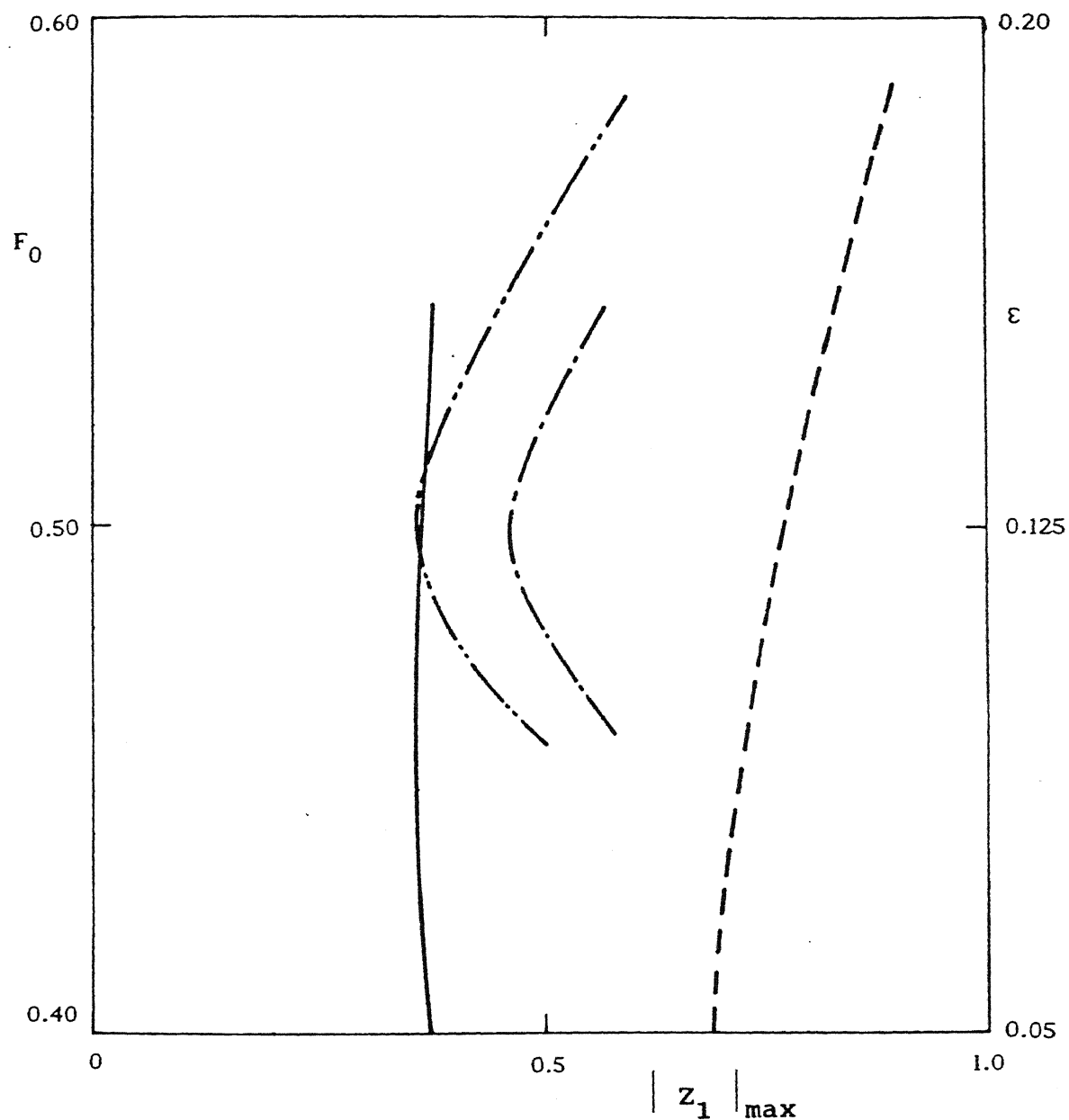
Figure 4.10 Sensitivity of the designed performance to the variations of forcing amplitude F_0 and self-excitation parameter ε. $-\cdot\cdot-\cdot\cdot-$ (r_m = 0.25, ε = 0.1, Ω = 1, χ = 0.7, d_0 = 2.9) and $-\cdot-\cdot-$ (r_m = .19, ε = 0.1, Ω = 1, χ = 0.7, d_0 = 3.8) : sensitivity to the variation of F_0. $\underline{\hspace{1cm}}$ (r_m = 0.25, F_0 = 0.5, Ω = 1, χ = 0.7 d_0 = 2.9) and $---$ (r_m = 0.25, F_0 = 0.5, Ω =1, χ = 0.5, d_0 = 2.9) : sensitivity to the variation of ε.

C H A P T E R - 5

BIFURCATIONS AND CHAOS IN AUTONOMOUS SELF-EXCITED

OSCILLATORS WITH IMPACT DAMPING

5.1 Introduction

Impact dampers in various forms are used to control the response of a vibratory system subjected to either forced or self excitations [70-72]. The response to a forced, harmonic excitation in the presence of an impact damper has been investigated by a number of researchers [67,77,86,91]. Masri [68,69] has constructed a general analytical solution using the piecewise linearity of the equation of motion. A method of analysing the asymptotic stability of the solution was also provided which was later refined by Bapat et al. [23]. A bifurcation study of the same system has recently been reported by Sung et al.[101]. Different kinds of local bifurcations e.g., pitchfork, saddle-node, Hopf etc., and global bifurcation such as homoclinic tangency have been studied. A period-doubling sequence leading to chaos has also been found.

In a self-excited system, the exciting force is dependent on the motion of the system. The most common mathematical model is given by the autonomous van der Pol equation in which the position dependent damping force changes sign once in every cycle and acts as the source of energy for maintaining the vibration. The use of an impact damper for suppressing self-excited vibration is not uncommon. Both the transfer of momentum to the loose mass (from the main system) and the dissipation of energy in every impact provide the mechanism for controlling the vibration. In this

chapter, we present a study on the persistent bifurcation structures and chaotic motions which remain invariant to the exact functional form of the self-exciting force. Both analytical as well as numerical methods have been used. The analytical method is in line with that of Masri et al.[69]. The basic motivation behind undertaking this investigation is explained below.

The first step, towards the understanding and prediction of the dynamical features of any physical system, is to construct a mathematical model. No real life system can be modelled in its entire complexity accounting for every detail. Moreover, idealizations are also necessary for obtaining a meaningful solution. However, certain phenomena predicted by such an idealized model may not be revealed under real life perturbations whereas some unpredicted phenomena may be exhibited by a real life system. Therefore, if possible, it is worthwhile to know which qualitative results of a mathematical model remain invariant under defined perturbations. The study of the qualitative invariance of the bifurcation structure is not very common in vibration modelling. This aspect has been considered in a recent work by Ravindra et al. [113]. It has been shown that the bifurcation set of a forced Duffing's oscillator remains topologically invariant under the possible perturbations of the index of the velocity dependent (i.e. dissipative), non-linear damping force.

In the context of the present problem, it is the self-excitation mechanism which cannot be modelled accurately. No single model can prove to be the best and always represent the reality. Several variations of the model of the self-excitation

mechanism have been attempted. Of course, the self-excitation demands that certain topological conditions be satisfied by the function used to describe it. This topological requirement has been kept invariant in the analysis. The main aim is to detect those bifurcations which persist under defined perturbations, while some others vary with the model.

5.2 Equations of Motion

Let us consider a self-excited mechanical oscillator with a loose mass m_2 (the so called impact damper) as shown in Figure 5.1(a). The collisions between the two masses, in most cases, can be adequately represented by identical, parallel combinations of spring and viscous damper as shown in Figure 5.1(b). This second model, allowing a finite time of contact, eventually smoothens the impact process and facilitates numerical integration of the governing equations of motion which can be written in the following non-dimensional form :

$$\ddot{Z}_1 + \varepsilon\, f(Z_1, \dot{Z}_1)\, \dot{Z}_1 + Z_1 + r_1\, \phi_1(Z_2) + 2\, \xi_c\, \sqrt{r_1 r_m}\, \phi_2(Z_2)\dot{Z}_2 = 0$$

$$(5.1a)$$

$$\ddot{Z}_2 + (r_1 / r_m)\, \phi_1(Z_2) + 2\, \xi_c\, \sqrt{r_1/r_m}\, \phi_2(Z_2)\, \dot{Z}_2 = \ddot{Z}_1 \qquad (5.1b)$$

where the dot at the top indicates differentiation with respect to the non-dimensional time τ ($= \omega_o t$ with t as the time),
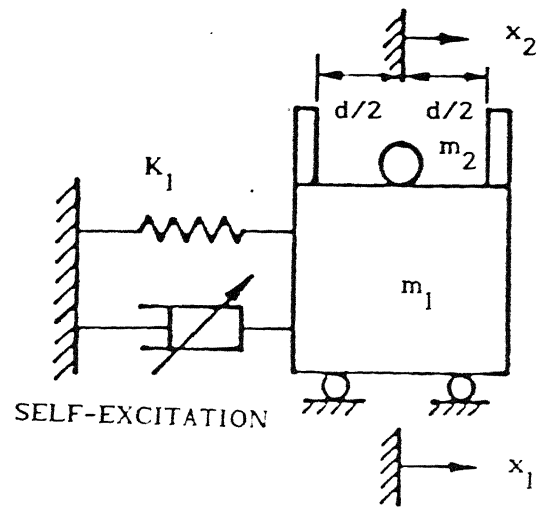
(a)
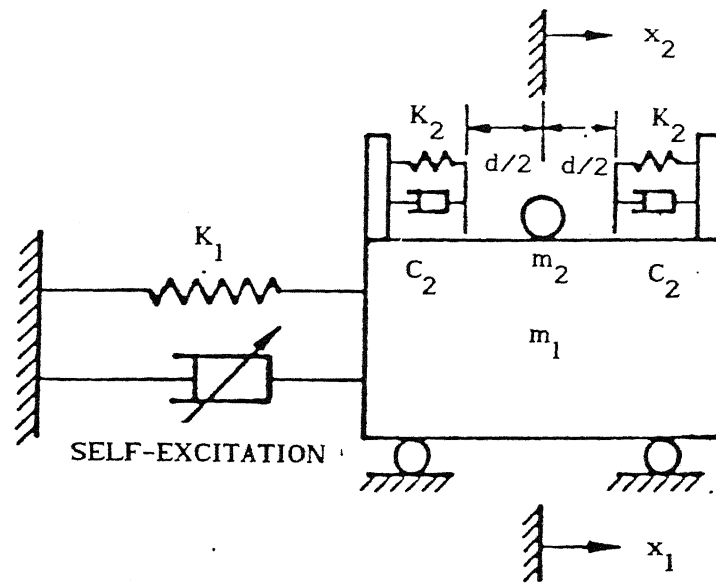
(b)

Figure 5.1   Model of an impact damper. a) with zero contact time.

b) with finite contact time.

$$\phi_1(Z_2) = (Z_2 - d_0) \, U \, (\, Z_2 - d_0 \,) + (Z_2 + d_0) \, U \, (- Z_2 - d_0 \,),$$

$$\phi_2(Z_2) = U \, (\, Z_2 - d_0 \,) + U \, (\, -Z_2 - d_0 \,)$$

and

$$U(\sigma) = 0 \; , \; \sigma < 0$$

$$= 1 \; , \; \sigma > 0$$

with $Z_1 = x_1 / x_0$, $Z_2 = (x_1 - x_2) / x_0$, $\omega_0 = (K_1 / m_1)^{1/2}$, $r_m = m_2 / m_1$,

$$\xi_c = C_2 / (2 \, \sqrt{K_2 m_2} \,), \; r_1 = K_2 / (m_1 \, \omega_0^2) \; , \; d_0 = d / (2 \, x_0) .$$

In the above expressions, x_0 with the dimension of length is suitably chosen depending on the form of the function f. The parameter ξ_c in equations (5.1) is given by [Appendix B]

$$\xi_c = - \frac{\ln(\chi)}{\sqrt{(1 + r_m)(\pi^2 + (\ln(\chi))^2)}} \qquad (5.2)$$

where χ, the coefficient of restitution, is the ratio of the relative velocities of separation and approach during the impact. The self-exciting mechanism is inherent to the form of the function $f(Z_1, \dot{Z}_1)$, which has the topological configuration shown in Figure 5.2(a). A general expression of f, depending on a suitable choice for x_0, can be written as

either $\quad f(Z_1, \dot{Z}_1) = (\alpha \, \dot{Z}_1^2 + Z_1^2 - 1)$,

$$(5.3)$$

or, $\quad f(Z_1, \dot{Z}_1) = (\dot{Z}_1^2 + \beta \, Z_1^2 - 1)$

where α and β are bookkeeping parameters which enable several models of self-excitation to be handled by the form of f with α
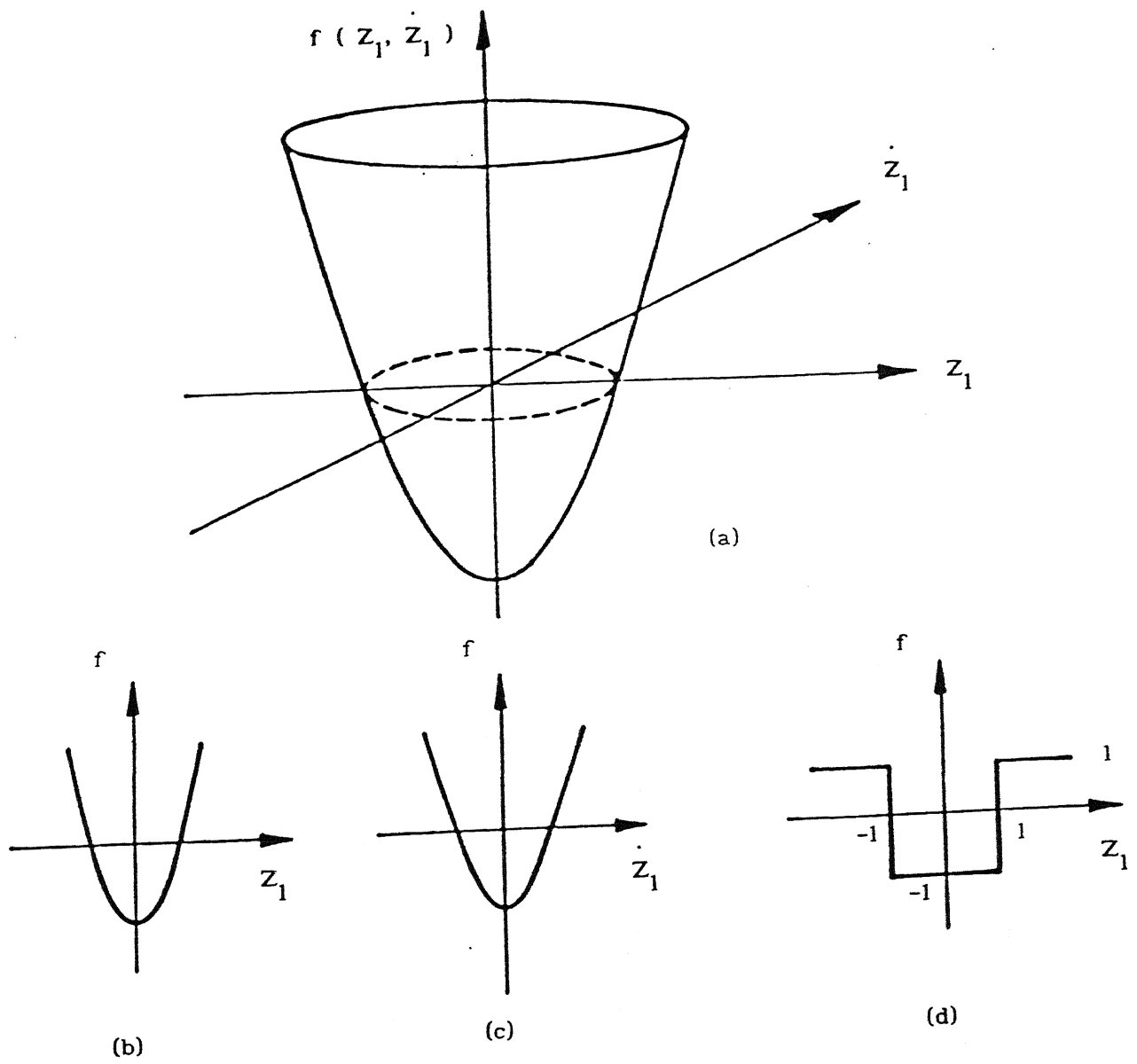
Figure 5.2 Different forms of self-exciting function f.

and β as either zero or unity. The function f represented by Figures 5.2(b) and 5.2(c) can be represented by equation (5.3) with $\alpha = 0$ and $\beta = 0$, respectively. The discontinuous function shown in Figure 5.2(d), also implying self-excitation, is amenable to exact analytical treatment. Moreover, this function also serves as a perturbation of the function shown in Figure 5.2(b) which represents the standard van der Pol form discussed so far in the thesis.

A preliminary numerical simulation (reported in detail in section 5.5) of equations of motion (5.1) reveals the existence of several windows of periodic solutions as the value of the parameter d_0 increases. By a periodic solution, we mean the solution with the minimum possible period which, in the present case, is approximately 6.6. Such a periodic solution is termed as the basic solution. Each window corresponds to a specific number of collisions per cycle. The number of impacts occurring in a period is seen to decrease with increasing d_0. The simplest possible periodic motion observed during the numerical simulation consists of two symmetric impacts per cycle. Other possible periodic solutions correspond to larger (such as 4,6 etc.) number of symmetric impacts per cycle. As the parameter d_0 is varied, the periodic motion within each window undergoes a certain sequence of bifurcations and thereby gives rise to interwindow chaos. In order to determine the route to chaos, the bifurcation structure of the periodic solutions is investigated. In the sections to follow we construct these periodic solutions and analyse their stability.

5.3 Theoretical Analysis

When the self-exciting function f is continuous, an approximate method based on the equivalent linearization can be employed to construct a basic periodic solution. For the sake of algebraic simplicity and relevance to the practical operating mode of an impact damper, the periodic solutions with two symmetric impacts per cycle are constructed, a detailed discussion of which with van der Pol damping has been included in chapter 4. The stability analysis of the solutions is also presented there. However, as stated earlier, an exact analytical treatment is possible for the piecewise constant form of f shown in Figure 5.2(d). In what follows, this method will be briefly outlined for a symmetric periodic solution with four impacts per cycle.

5.3.1 Periodic Solutions and Stability Analysis with Four Impacts per Cycle

For the piecewise constant form of f, the periodic solutions with four symmetric collisions per cycle can be constructed as follows. One-half of a typical solution for Z_1 is shown in Figure 5.3. In this figure, a point is defined as an impact node where an impact occurs. Similarly, a cross node is defined where a sudden change in the value of f takes place . Thus the points a, c and e are impact nodes whereas b and d are cross nodes. Let $(Z_p, \dot{Z}_p)$ be the state of the loose mass. Here onwards, the subscripts + and - are used, respectively, to denote the time instants just after and just before the crossing of a node. The motion of the system is given by
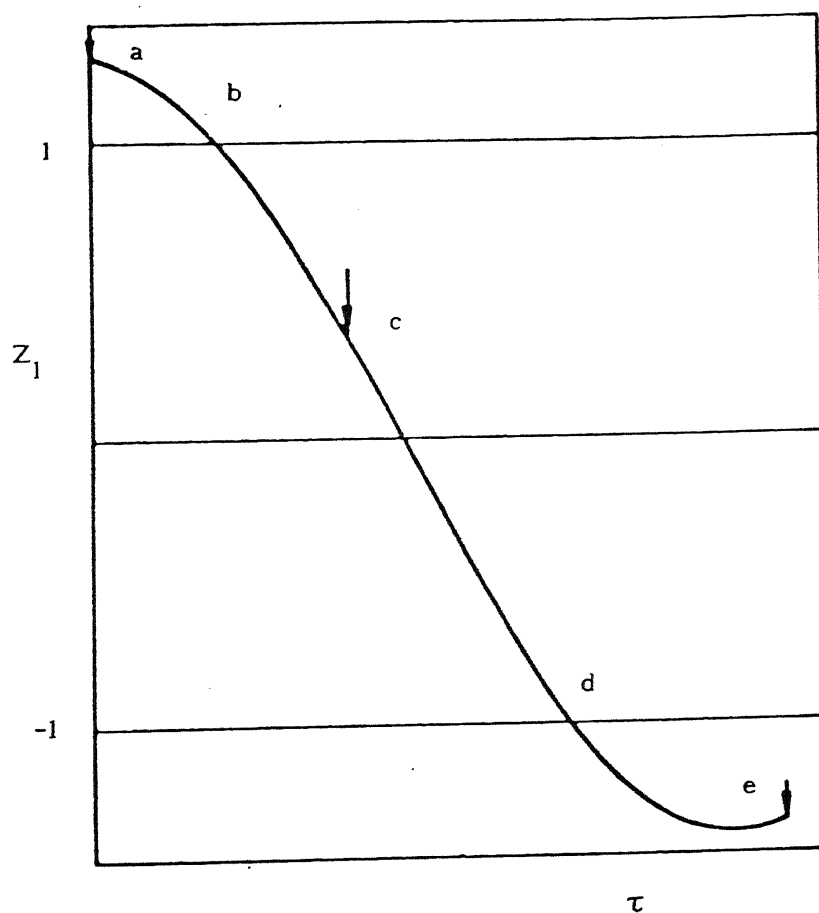
Figure 5.3 Half cycle of a typical four impacts per cycle motion. Arrows indicate the locations of impact.

$$z_{1_i}^{i+1}(\tau) = \exp(-h_{i+1}(\tau-\tau_i))(A_i \cos \eta(\tau-\tau_i) + B_i \sin \eta(\tau-\tau_i))$$

$$(5.4a)$$

and

$$\dot{z}_{p_i}^{i+1}(\tau) = \text{constant} \qquad \text{for } (\tau_i)_+ < \tau < (\tau_{i+1})_-$$

$$(5.4b)$$

where $\eta = \sqrt{1 - h_{i+1}^2}$,

τ_i denotes the instant corresponding to the ith and twice of h_{i+1} is the value of the function $\varepsilon.f$ between the ith and $(i+1)^{th}$ nodes.

If the ith node is an impact node, then

$$\dot{z}_1(\tau_i)_- = \alpha_1 \dot{z}_p(\tau_i)_- + \alpha_2 \dot{z}_p(\tau_i)_+ \qquad\qquad (5.5)$$

$$\dot{z}_1(\tau_i)_+ = \alpha_3 \dot{z}_p(\tau_i)_- + \alpha_4 \dot{z}_p(\tau_i)_+ \qquad\qquad (5.6)$$

where

$$\alpha_1 = (\chi - r_m) / (1 + \chi)$$
$$\alpha_2 = (1 + r_m) / (1 + \chi)$$
$$\alpha_3 = \chi (1 + r_m) / (1 + \chi)$$
$$\alpha_4 = (1 - \chi r_m) / (1 + \chi) .$$

Further, at an impact node,

$$z_1(\tau_i) - z_p(\tau_i) = \pm d_0. \qquad\qquad (5.7)$$

The symmetry of the motion implies

$$\dot{z}_1(\tau_{i+4}) = - \dot{z}_1(\tau_i) \qquad\qquad (5.8)$$

and since the velocity of the loose mass remains unchanged between two successive collisions, we get

$$\dot{Z}_p(\tau_i)_- = - \dot{Z}_p(\tau_{i+2})_+ \qquad (5.9)$$

for the four impacts per cycle motion as depicted in Figure 5.3. If the ith node is a cross-node, then the following conditions hold good :

$$Z_1(\tau_i) = \pm 1 \qquad (5.10)$$

and

$$\dot{Z}_1(\tau_i)_- = \dot{Z}_1(\tau_i)_+ \qquad (5.11)$$

Using the above relations and lengthy algebraic manipulation, we get n number of equations in τ_i 's where n represents the number of nodes per half cycle of the motion. Without loosing any generality, we can set $\tau_1 = 0$ and the remaining $(n-1)$ transcendental equations can be numerically solved for τ_i 's. Thereafter the other unknowns, viz., A_i's, B_i' s and the velocity of the loose mass between two consecutive impacts, can easily be obtained.

The stability of the solution obtained above can be analysed by the method of error propagation [68]. A suitably chosen initial disturbance vector $\vec{\zeta}_1$ having four components is introduced into the analytically constructed solution . Let $\vec{\zeta}_T$ be the disturbance vector measured after a cycle , then $\vec{\zeta}_1$ is related to $\vec{\zeta}_T$ as

$$\vec{\zeta}_T = [P] \, \vec{\zeta}_1 + \text{higher order terms} . \qquad (5.12)$$

The matrix [P] can be estimated in closed form, for a piece-wise linear system, as described below.

Let the ith node be an impact node. In that situation, as revealed by the numerical solution, the $(i+1)^{th}$ node is a cross

node and the $(i+2)^{th}$ node is again an impact node and so on. Between the ith and $(i+1)^{th}$ nodes, the motion of the system is given by equations (5.4). A lengthy algebraic manipulation finally gives

$$Z_1(\tau_{i+2}) = E_i \, Z_1(\tau_i) + D_i \, \dot{Z}_1(\tau_i)_+ \, , \tag{5.13}$$

$$\dot{Z}_1(\tau_{i+2})_- = Q_i \, Z_1(\tau_i) + L_i \, \dot{Z}_1(\tau_i)_+ \, , \tag{5.14}$$

$$\text{and} \quad Z_1(\tau_{i+1}) = G_i \, Z_1(\tau_i) + U_i \, \dot{Z}_1(\tau_i)_+ \tag{5.15}$$

where E_i, D_i, Q_i, L_i, G_i and U_i are functions of τ_i, τ_{i+1} and τ_{i+2} etc. Since in between the impacts the loose mass moves with a constant velocity, we have

$$\dot{Z}_p(\tau_i)_+ = \frac{Z_p(\tau_{i+2}) - Z_p(\tau_i)}{\tau_{i+2} - \tau_i} \, . \tag{5.16}$$

Introducing a perturbation in the ith node given by the vector $\vec{\zeta}_i = (\, \Delta\tau \, , \, \Delta Z \, , \, \Delta\dot{Z}_1^+ \, , \, \Delta\dot{Z}_p^+ \,)_i^T$ and following this perturbation through equations (5.4)-(5.16), the following linearized relation is obtained :

$$\vec{\zeta}_{i+2} = [P]_i^{i+2} \, \vec{\zeta}_i \tag{5.17}$$

Where $[P]_i^{i+2}$ is a 4X4 matrix. Thus, finally we can write

$$\vec{\zeta}_{i+4} = [P]_{i+2}^{i+4} \vec{\zeta}_{i+2} = [P]_{i+2}^{i+4} [P]_{i}^{i+2} \vec{\zeta}_{i} = [P] \vec{\zeta}_{i} . \tag{5.18}$$

So far we have considered only one-half of the cycle, but the motion being symmetric, the other half behaves in a similar fashion and the matrix [P] can be obtained analytically.

If the eigenvalues of [P] lie within the unit circle about the origin of the complex plane, then the corresponding solution is stable. When a control parameter is varied, the eigenvalues may cross the unit circle in different ways leading to different types of bifurcations of co-dimension one.

5.4 Numerical Method of Stability Analysis

The analytical method presented in section 5.3 becomes unwieldy with increasing number of collisions per cycle. Therefore, a numerical method is necessary for obtaining both the solution and its stability analysis. A solution obtained by numerical integration is of course stable. However, nothing is known about the local invariant subspaces (eigen structure) of the solution. In this section, a method for calculating the eigen properties of the fixed point of the Poincare map of a numerically obtained solution is presented.

Let a Poincare section be defined as

$$\Sigma_p = \{ (\tau, \dot{z}_1, z_2, \dot{z}_2) : z_1 = \gamma, \dot{z}_1 > 0 \} \tag{5.19}$$

where γ is a constant. A fixed point W^* in Σ_p corresponds to a

periodic solution and is defined as

$$W^* = \tilde{P}\ (\ W^*\ ) \quad .$$

(5.20)

Neither $\tilde{P}$, nor W^* can be calculated analytically. For ascertaining the local nature of the fixed point,

$$D\tilde{P} = \left[\ \frac{\delta\tilde{P}}{\delta W}\ \right]$$

(5.21)

with

$$W = \{\ \tau\ ,\ \dot{Z}_1,\ Z_2,\ \dot{Z}_2\}^T$$

needs to be computed. As the system under consideration is autonomous, $D\tilde{P}$ can be written in the following partitioned form:

$$D\tilde{P} = \left[\begin{array}{c|ccc} 1 & a_1 & a_2 & a_3 \\ \hline 0 & & & \\ 0 & & [B] & \\ 0 & & & \end{array}\right]$$

(5.22)

where [B] is a 3x3 matrix and is defined as

$$[B] = [\ b_{ij}\ ]\ ;\ i,j = 1\ ,2\ \text{and}\ 3$$

(5.23)

Let us assume that $\tilde{P}$ can be expanded in a Taylor series around the fixed point W^*. In what follows, we explain how [B] can be constructed. Introducing a series of perturbations,

$$\left\{\begin{array}{c} \Delta\dot{Z}_1 \\ \Delta Z_2 \\ \Delta\dot{Z}_2 \end{array}\right\} = \Delta_s \left\{\begin{array}{c} 1 \\ 0 \\ 0 \end{array}\right\}$$

(5.24)

where $s = 1,\ .\ .\ .\ N$, with N representing the number of

perturbations used, in the numerically obtained (integrating equations (5.1)) fixed point, their new values are obtained after the first return on Σ_p as $\{\Delta \dot{z}_1', \Delta \dot{z}_2', \Delta \dot{z}_2'\}_s^T$. One can write

$$\Delta \dot{z}_{1_s}' = \Delta_s b_{11} + \sum_{n=1}^{N-1} \lambda_n (\Delta_s)^n \qquad \text{where } s = 1, \ldots N \qquad (5.25)$$

Thus, N simultaneous equations in b_{11}, and λ_n's are obtained which can be solved to get b_{11}. One can go on increasing the value of N to get a converged value of b_{11}. However, if Δ_s is taken sufficiently small, a very low value (around 3 or 4) of N is needed for convergence. However, too small a value of Δ_s is also discouraged in order to avoid computational errors that occur while handling small numbers. Other elements of [B] can also be similarly calculated. For the elements of the first column, we need perturbations like $\Delta_s \{ 1 \ 0 \ 0 \}^T$. Similarly, for the second and third columns we use $\Delta_s \{ 0 \ 1 \ 0 \}^T$ and $\Delta_s \{ 0 \ 0 \ 1 \}^T$, respectively. Once $D\tilde{P}$ is constructed numerically, then the movements of the eigenvalues of $D\tilde{P}$ near the boundary of the unit circle give an indication of the nature of the impending bifurcation.

5.5 Results and Discussions

It may be noted that the parameter d_0 characterizes the non-linearity of the damper. Thus, it is pertinent to analyse the dynamic transitions under the control of the parameter d_0. The whole discussion has been divided into two parts. In the first part, the existence , stability and bifurcations of the basic

periodic solutions with higher (> 2) number of impacts are discussed. The nature of the interwindow chaos occurring between two basic windows are also analysed. Unlike the motions with higher number of impacts, the solutions consisting of two impacts per cycle show several distinct bifurcational behaviours which are very sensitive to the other parameter values. Therefore, a separate treatment of this type of motions is required. The second part is directed to a detailed discussion of the stability and bifurcations of the periodic solutions with such two symmetric impacts per cycle.

5.5.1 Bifurcations of the Periodic Solutions with More than Two Impacts

In this section, the stability of the basic periodic solution with four impacts per cycle for the piecewise constant self-exciting force is investigated. The periodic solutions with higher number of impacts and other continuous self-exciting functions are treated numerically.

5.5.1.1 Analytical Results

The bifurcation structure of the symmetric motion with four impacts per cycle is studied in the (χ, d_0) parameter space. The stability boundaries in the parameter space are delineated in Figure 5.4. The eigenvalues, at both the right and left stability boundaries, are seen to cross the unit circle along the positive real axis. Beyond the right stability boundary, the non-existence of any solution implies the occurrence of a saddle-node
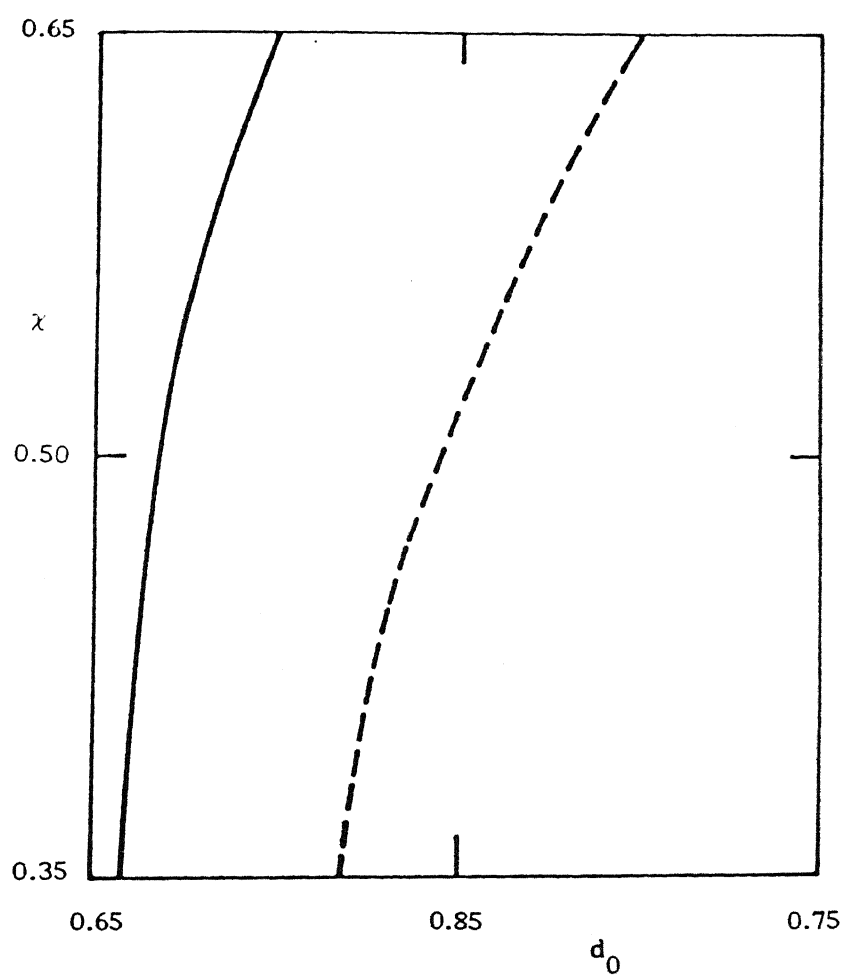
Figure 5.4 Stability boundaries of symmetric four impacts per cycle solution. - - - saddle-node boundary, —— pitch-fork boundary. $\varepsilon = 0.07$, $r_m = 0.1$.

bifurcation. This saddle-node bifurcation is best depicted in Figure 5.5, where the limit cycle amplitude is plotted against the control parameter d_0. The details of the consequence of such a bifurcation are discussed later. An unstable solution continuing beyond the left stability boundary (shown in FIgure 5.4) implies the occurrence of a pitchfork (symmetry-breaking) bifurcation. The consequence of a pitchfork bifurcation (supercritical) is the evolution of an asymmetric solution with four impacts per cycle.

5.5.1.2 Numerical Results

For numerically integrating the equation of motion, a fourth order Runge-Kutta-Merson algorithm (NAG routine) with variable step size control has been used. This numerical scheme has also been used for zero contact-time model (Figure 5.1(a)) which has been treated analytically in section 5.3.1. The amplitudes of the limit cycle obtained (a_ℓ) analytically and numerically are shown in Figure 5.5. It may be concluded from this figure that equations (5.1a) and (5.1b) with a high value of r_1(= 20000 in the present study) can adequately represent the impact phenomenon. All subsequent results are obtained by numerically integrating equations (5.1) which allow for a finite contact time during the collision. As mentioned earlier, the numerical simulation revealed the existence of several windows of periodic solution, each with a specific number of collisions per cycle, in the χ - d_0 plane. As shown in Figure 5.6, these windows are separated by zones where the oscillation undergoes a series of bifurcations.
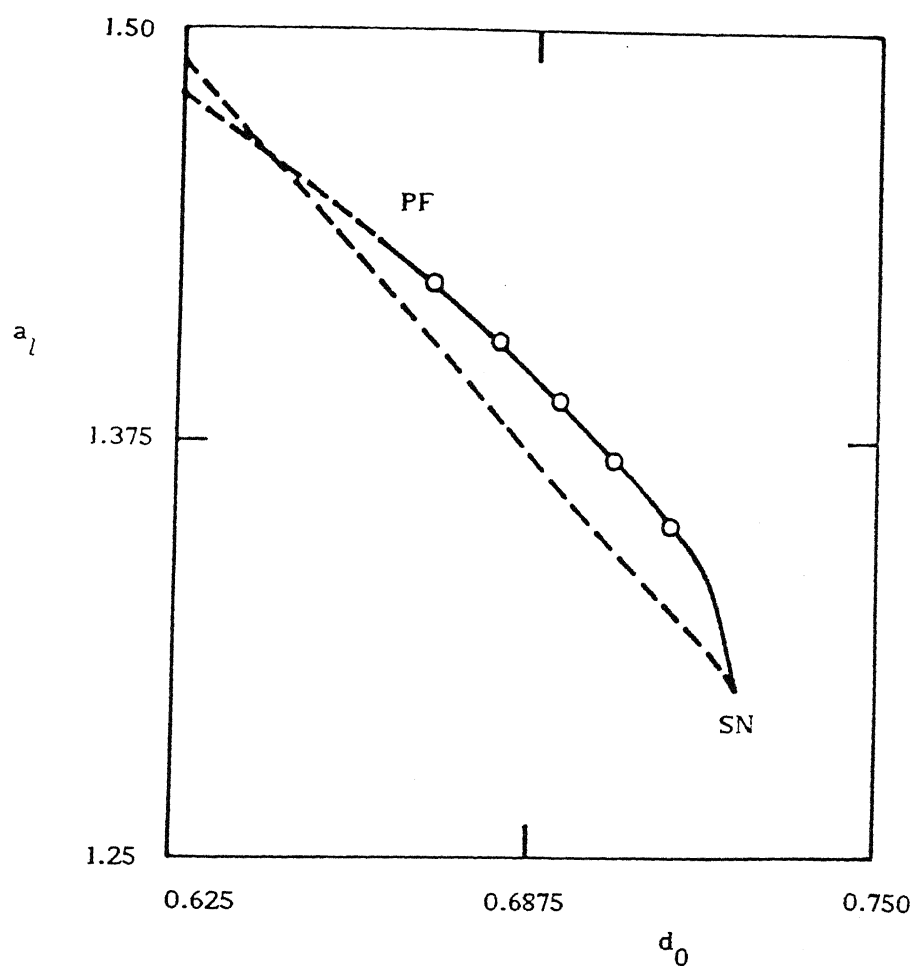
Figure 5.5 Bifurcation diagram of symmetric four impacts per cycle motion. χ =0.39, ε = 0.07, r_m = 0.1. ——— stable solution, - - - unstable solution. SN - saddle-node instability, PF - pitch-fork instability. o - results obtained via numerically integrating equation 5.1 for r_1 = 20000.
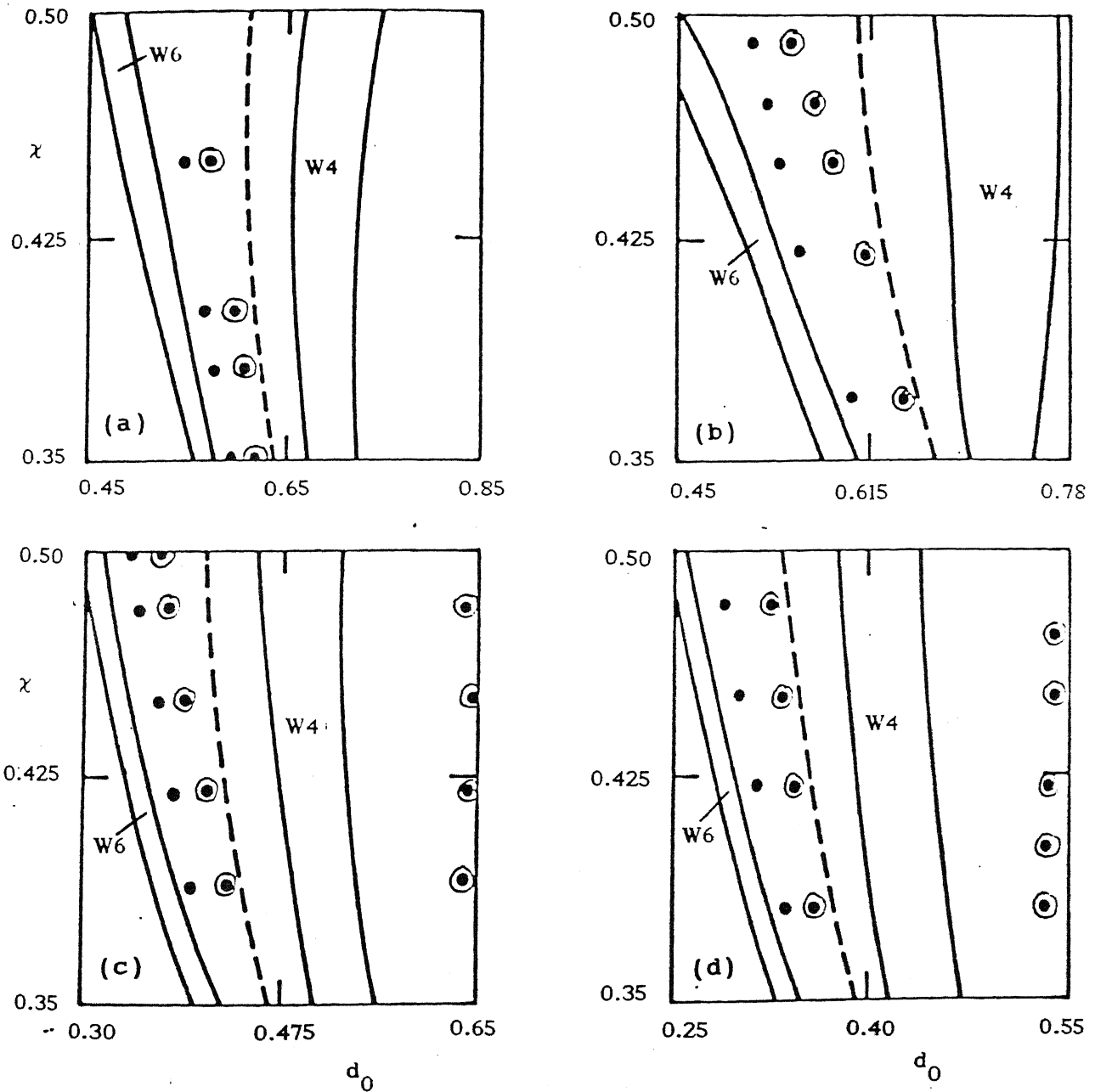
Figure 5.6   Stability boundaries for $r_m = 0.1$ with the form of f as shown in Figure a) 5.2(d), $\varepsilon = 0.07$; b) 5.2(b), $\varepsilon = 0.1$; c) 5.2(c), $\varepsilon = 0.15$; d) 5.2(a), $\varepsilon = 0.15$. w6 denotes the window of six impacts per cycle symmetric motion, w4 denotes the window of four impacts per cycle symmetric motion. - - - flip bifurcation line. ● symmetric period-three solution; ⊙ asymmetric period-three solution.

The periodic solution of each window undergoes a transition to chaos via intermittency when d_0 is increased beyond a critical value (for a fixed value of χ). The intermittency has been identified by its typical signature of a long, laminar, almost regular phase of oscillation interrupted by relatively short chaotic bursts as shown in Figure 5.7.

A nice phenomenological description of the origin of intermittency can be found in the references [115-117]. This description was with particular reference to non-linear maps which are equivalent to a Poincare map of the dynamic evolution of a system described by differential equations. Three different types of intermittency, based on the local bifurcation of a periodic solution, have so far been identified. Mathematically, type I intermittency is associated with a saddle-node (tangent) bifurcation, whereas types II and III are preceded, respectively, by subcritical Hopf and flip bifurcations.

In the analytical study presented in section 5.5.1, a saddle-node bifurcation was revealed at the right boundary of the window of the four impacts per cycle symmetric solution. The occurrence of a saddle-node bifurcation at the right boundary of every window, independent of the form of function f, has been confirmed by the numerical method outlined in section 5.4. So the ensuing intermittency is classified as type I.

Another way of testing a type I intermittency is to plot a Poincare map and detect the well-known narrow channeling effect [117]. A Poincare map shown in Figure 5.8 clearly demonstrates this narrow channeling effect.
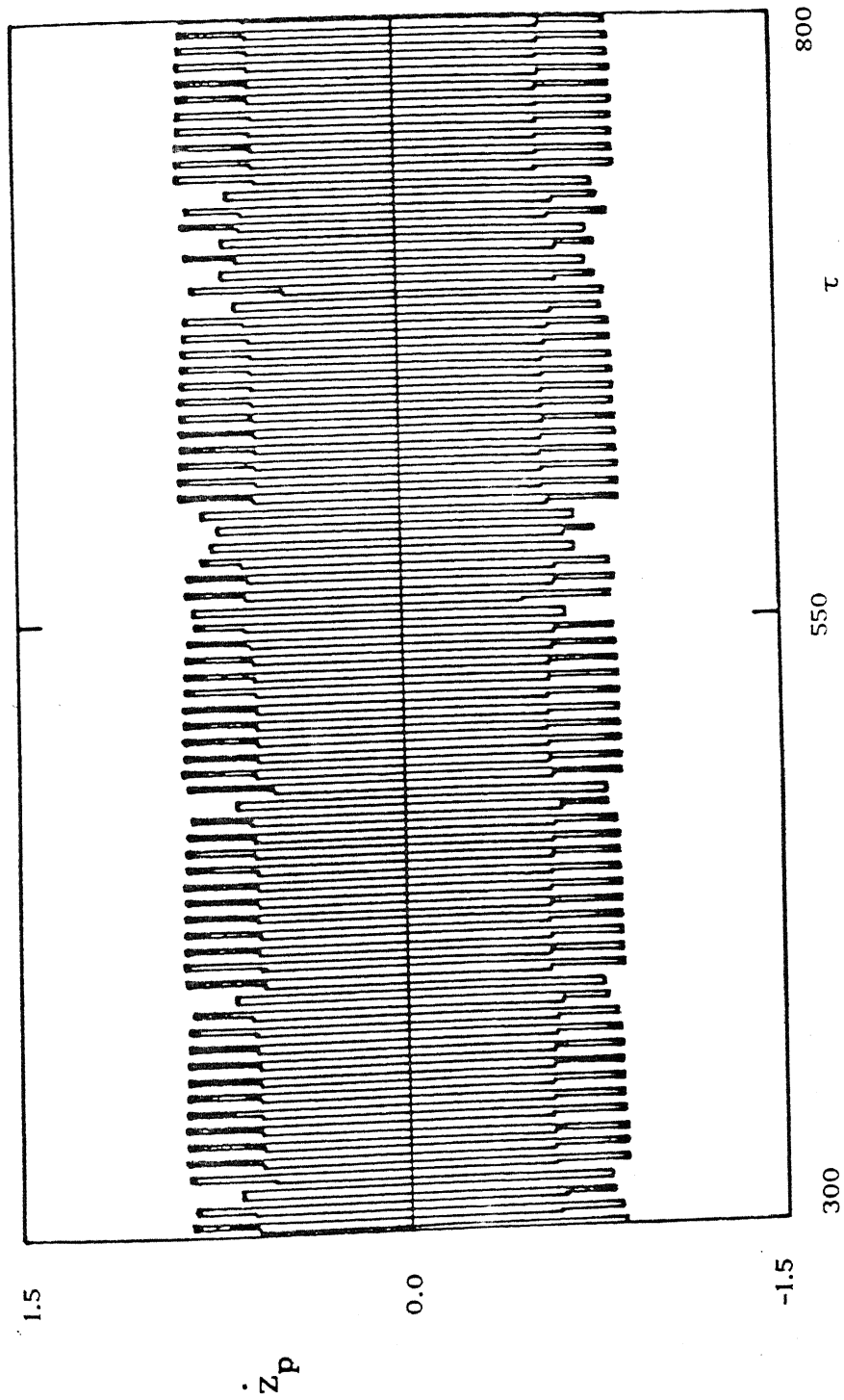
Figure 5.7 Signature of intermittency. Form of f is as shown in Figure 5.2(a). $\varepsilon = 0.15$, $r_m = 0.1$, $\chi = 0.35$, $d_o = 0.473$.
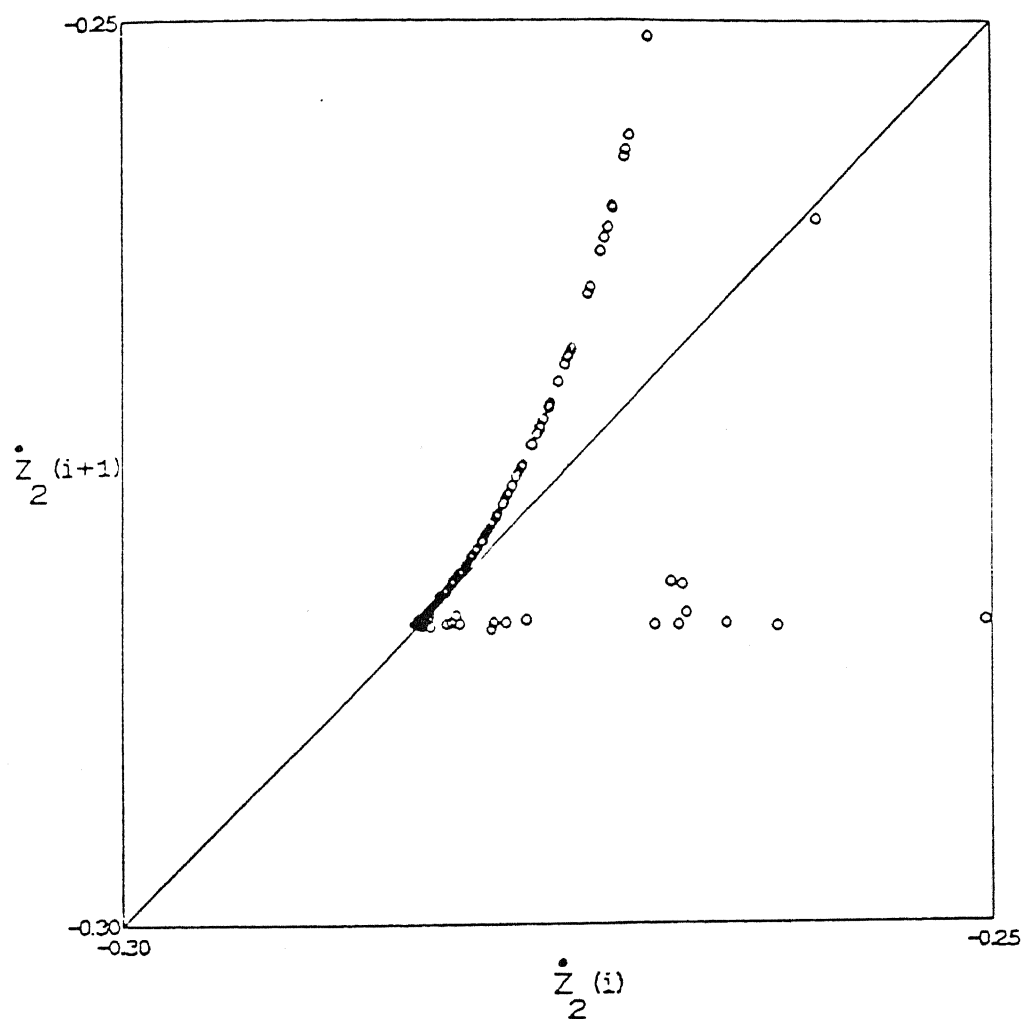
Figure 5.8 Narrow channeling effect. Form of f is as shown in Figure 5.2(a). $\varepsilon = 0.15$, $r_m = 0.1$, $\chi = 0.45$, $d_o = 0.4505$, $\gamma = 0.5$.

Another set of Poincare map $\pi \circ \Sigma_p$, with π denoting the projection on (Z_2, $\dot{Z}_2$) plane, has been plotted in Figure 5.9. These plots clearly show a high measure density (in some measure theoretic sense) near the ghost of the fixed point which existed prior to the bifurcation and a low measure density elsewhere. The points with a high measure density are associated with the local dynamics (laminar phase) whereas those with a low measure density are related to the global excursion i.e., the chaotic bursts. It should be mentioned that the structure of the attractor shown in Figure 5.9 is insensitive to the models of the self-exciting mechanism. Somewhat detailed study of this chaotic attractor will be presented later.

The statistical properties associated with the intermittent signature have also been calculated. The following scaling law is obtained :

$$<\ell> \sim \varepsilon_c^{-\delta} \; , \; \delta \sim 0.52$$

where $<\ell>$ is the average laminar length and $\varepsilon_c = d_0 - d_0^c$ and d_0^c is the critical value of the parameter d_0 at the onset of intermittency. The above scaling law is very close to what has been predicted analytically ($\delta = 0.5$) by Pomeau et al.[117]. If d_0 is increased beyond the right boundary of a window (see Figure 5.6), the intermittent oscillation encounters frequent chaotic bursts giving rise to chaos. Some chaotic attractors are shown in Figure 5.10. The shapes of these attractors are very similar to those shown in Figures 5.9. The only difference is that the points
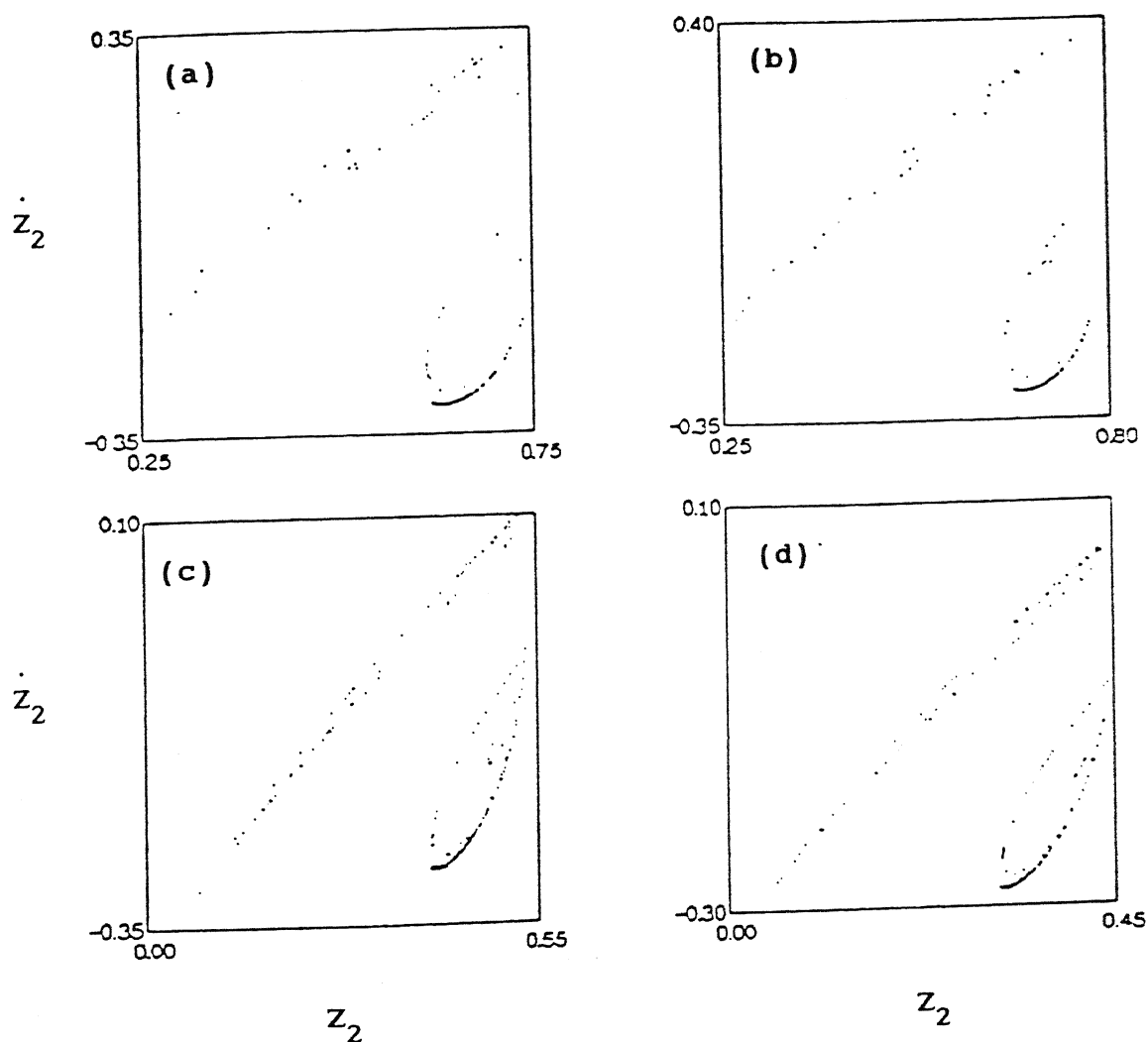
Figure 5.9 Poincare sections corresponding to intermittency. $\chi =$ 0.45, $r_m = 0.1$, $\gamma = 0.5$. a) f - as in Figure 5.2(d), $\varepsilon = 0.07$, $d_o = 0.736$; b) f - as in Figure 5.2(b), $\varepsilon = 0.1$, $d_o = 0.773$; c) f- as in Figure 5.2(c), $\varepsilon = 0.15$, $d_o = 0.532$; d) f- as in Figure 5.2(a), $\varepsilon = 0.15$, $d_o = 0.4505$.
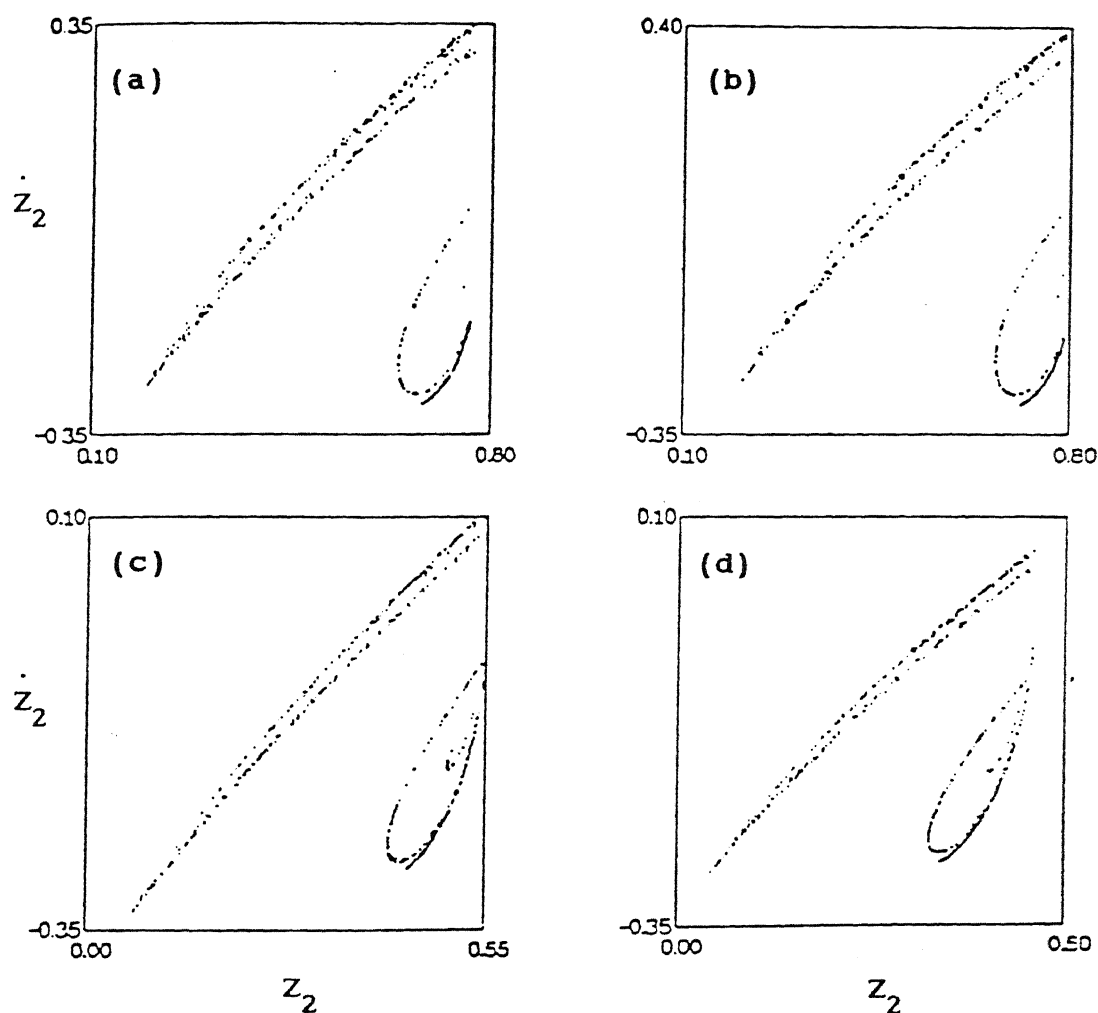
Figure 5.10   Poincare sections corresponding to chaos ensuing intermittency. $\chi = 0.45$, $r_m = 0.1$, $\gamma = 0.5$. a) f - as in Figure 5.2(d), $\varepsilon = 0.07$, $d_o = 0.76$; b) f - as in Figure 5.2(b), $\varepsilon = 0.1$, $d_o = 0.79$; c) f- as in Figure 5.2(c), $\varepsilon = 0.15$, $d_o = 0.55$; d) f- as in Figure 5.2(a), $\varepsilon = 0.15$, $d_o = 0.46$.

on the attractors in Figure 5.10 are more evenly distributed. Thus the saddle-node bifurcation followed by type I intermittency is seen to be persistent and is independent of the details of the form of the function f.

It has already been noticed in section 5.5.1.1, that the left stability boundary of the symmetric solution with four impacts per cycle corresponds to a pitchfork bifurcation. The numerical solution has revealed that this feature is also true for all the windows and for all variations of the function f. Two asymmetric solutions follow this pitchfork bifurcation. These asymmetric solutions have the same number of impacts per cycle as that within the window under consideration. With a further decrease in d_0, the asymmetric solutions undergo a flip bifurcation giving rise to a period-doubling sequence (see Figure 5.6). A further decrease in d_0 leads the period-doubling sequence into chaos. The whole dynamical transition is shown in Figure 5.11.

It has already been mentioned that there exist a whole lot of complicated solutions between two windows of basic solutions. One of these solutions is a period-three oscillation. Just like the window of symmetric basic solutions, a window of symmetric, period-three solution is found to exist irrespective of the form of the function f. This window is very narrow and therefore, only a set of representative points indicating the location of the window is shown in Figure 5.6. These symmetric period-three oscillations undergo bifurcations similar to those shown by the basic solutions. Type I intermittency is observed at the right boundary of the window as shown in Figure 5.12. At the left
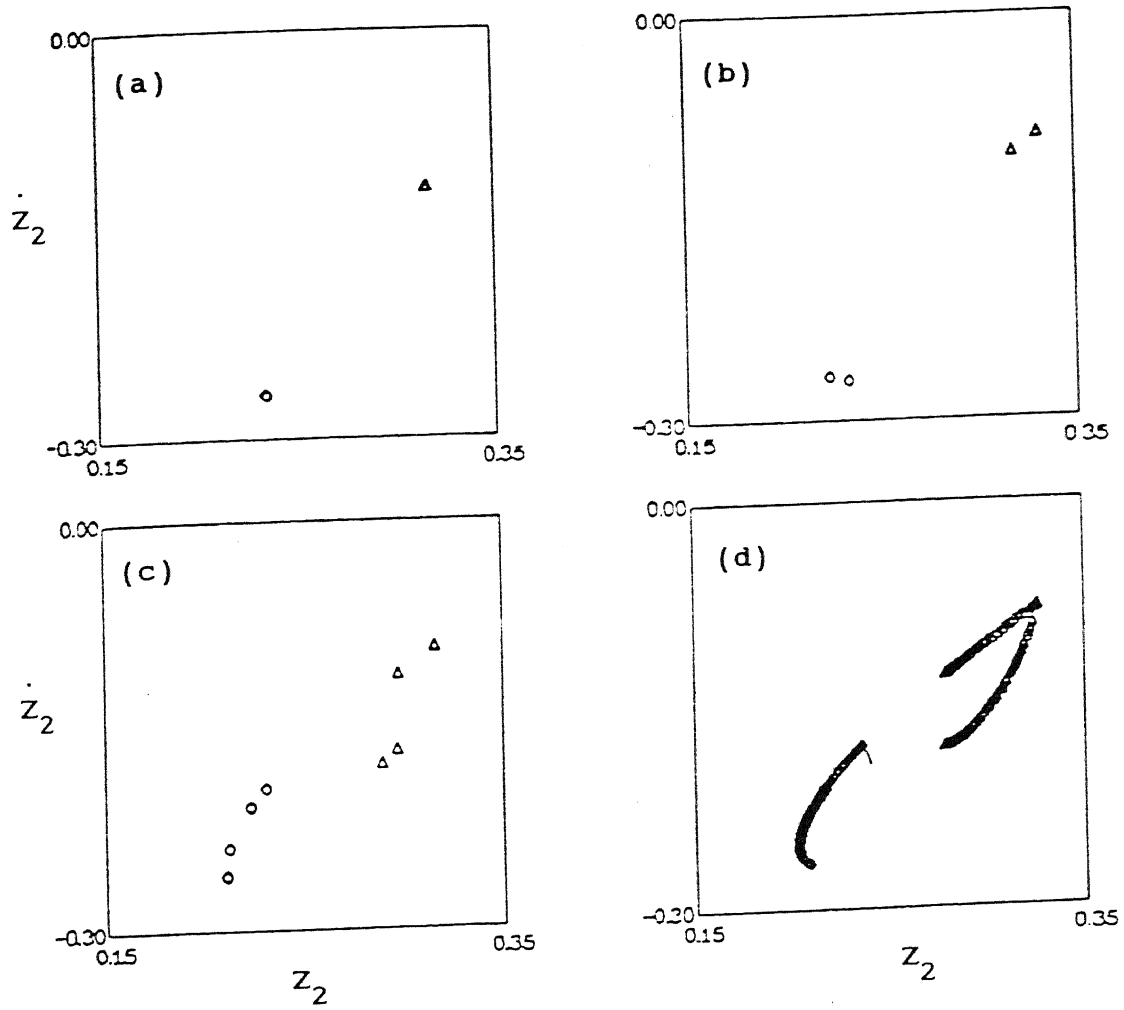
Figure 5.11   Period doubling bifurcation to chaos in poincare plane with $\gamma = 0.5$. f - as shown in Figure 5.2(a), $\varepsilon = 0.15$, $r_m = 0.1$, $\chi = 0.45$. a) $d_o = 0.36$, b) $d_o = 0.35$, c) $d_o = 0.338$, d) $d_o = 0.334$. o and Δ denote two different solutions.
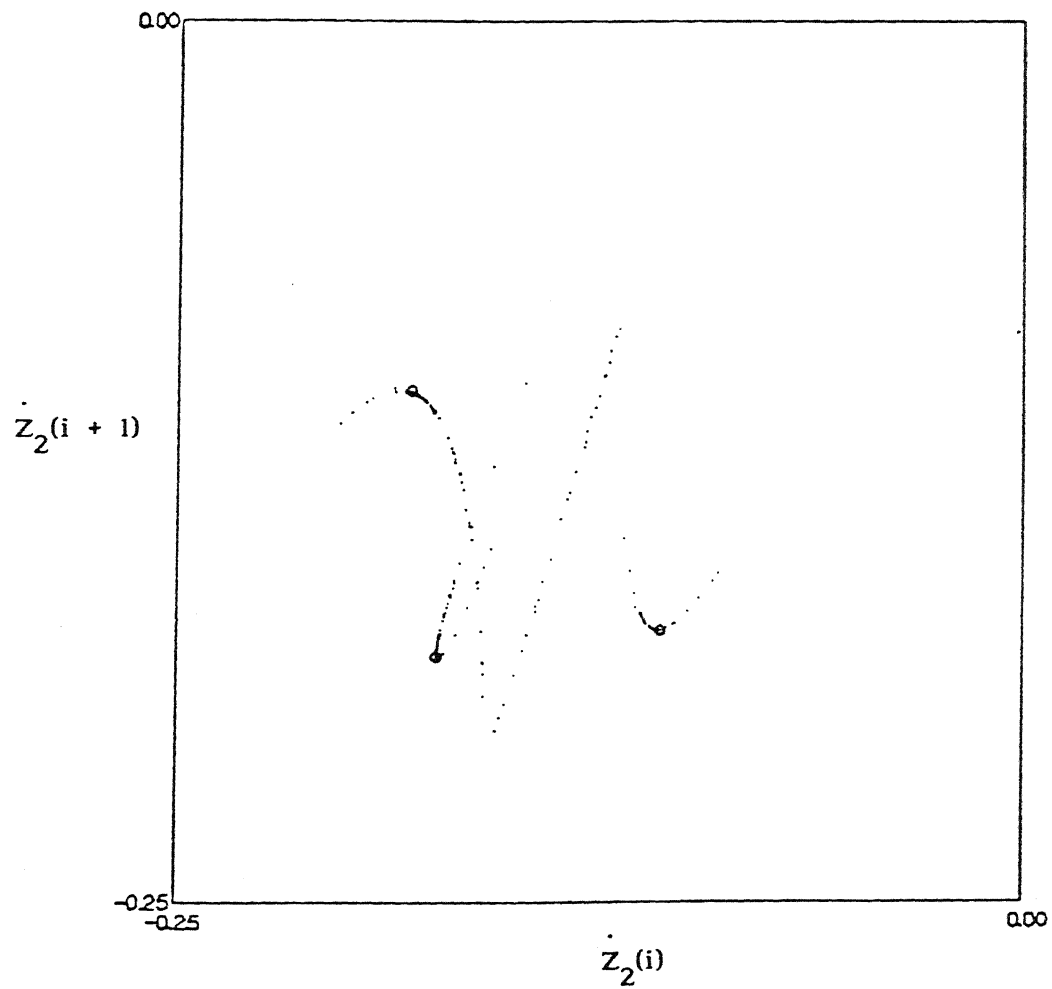
Figure 5.12   Intermittency of symmetric period-three oscillation
in Poincare plane with γ = 0.5. f- as shown in Figure
5.2(a), ε = 0.15, χ = 0.42, r_m = 0.1 , d_o = 0.3211. o
- symmetric period-three oscillation prior to
intermittency at d_o = 0.321

boundary, symmetry-breaking takes place giving birth to a pair of asymmetric period-three oscillations which ultimately lead to chaos via period-doubling bifurcations. A transition of this kind is shown in Figure 5.13.

Besides the symmetric period-three window, an asymmetric period-three window is also seen to exist whose location is again identified by a set of points in Figure 5.6. With decreasing values of d_0 for a fixed χ, such a pair of asymmetric solutions undergo period-doubling bifurcations and ultimately lead to chaos. This transition is shown in Figure 5.14.

The existence of an intermittency route to chaos immediately after a saddle-node bifurcation was mentioned in the beginning of this section. To analyse the structure of the attractor corresponding to this intermittency, let us consider Figures 5.15(a) and 5.15(b). The existence of the region L in Figure 5.15(a) with a high measure density of the return points can be explained by the existence of a saddle-node prior to the bifurcation. But the region G with a low measure density of the return points corresponds to some global phenomena. It may be concluded that this region is the outcome of subharmonic instability, either of the basic solution (see Figure 5.11) or of the period-three solution (see Figures 5.13 and 5.14). Mostly it was found that a period-three solution exists near the saddle-node boundary and the region with a low measure density is related to the subharmonic instability of this solution.
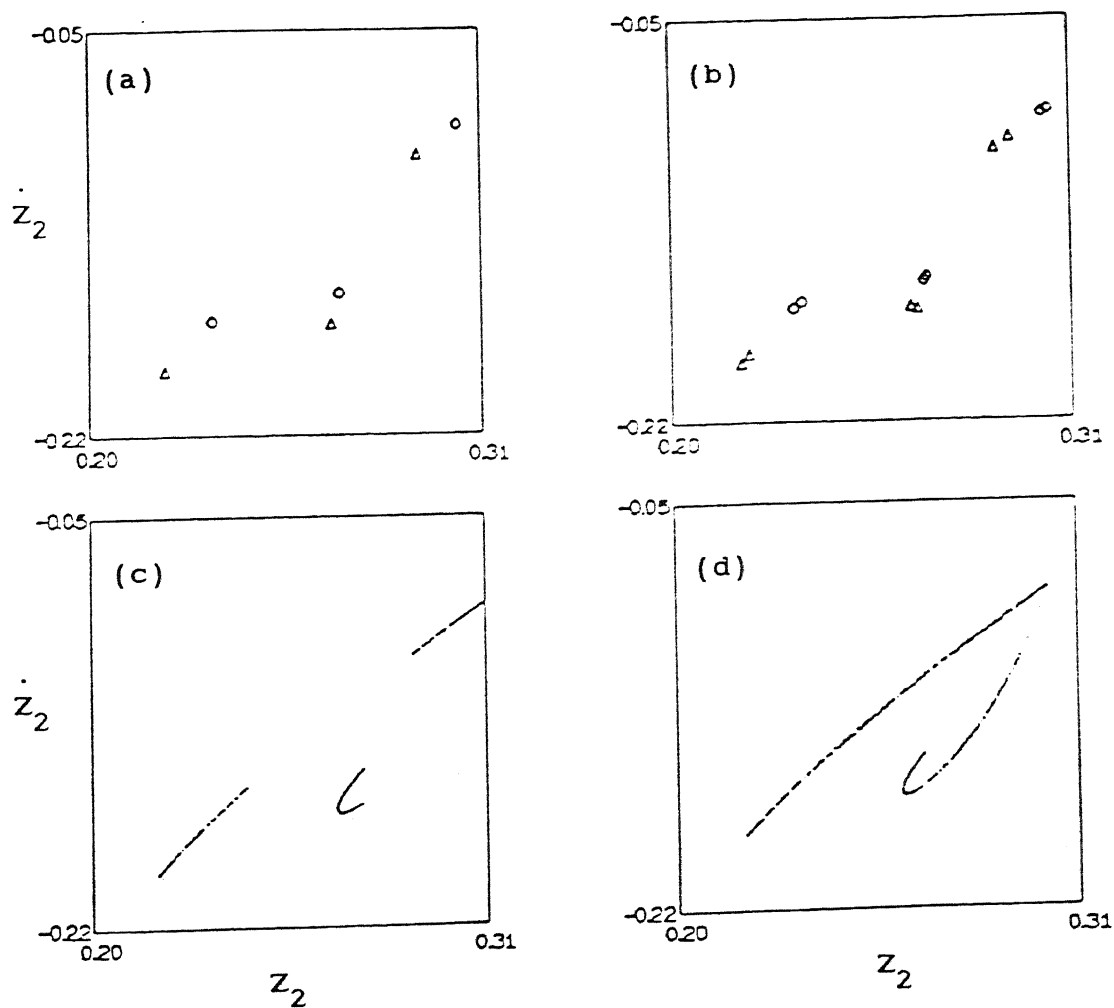
Figure 5.13 Period doubling route to chaos for period-three oscillation in Poincare plane with $\gamma = 0.5$. f - as shown in figure 5.2(a), $\varepsilon = 0.15$, $r_m = 0.1$, $r_1 = 20000$, $\chi = 0.42$. a) $d_o = 0.316$, b) $d_o = 0.3158$, c) $d_o = 0.315$, d) $d_o = 0.311$.
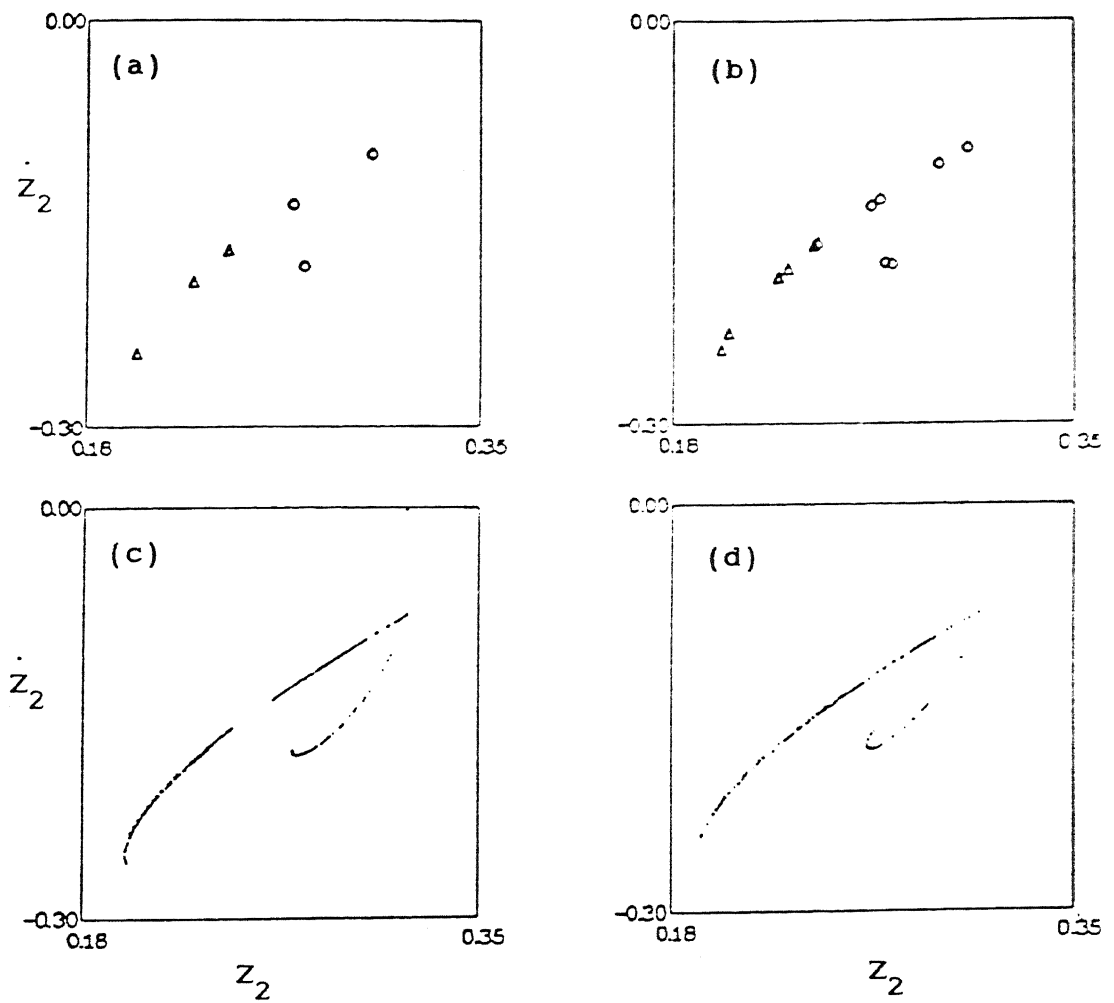
Figure 5.14   Period doubling route to chaos for period-three oscillation in Poincare plane with $\gamma = 0.5$. f - as shown in figure 2(a), $\varepsilon = 0.15$, $r_m = 0.1$, $r_1 = 20000$, $\chi = 0.45$. a) $d_o = 0.33$, b) $d_o = 0.3285$, c) $d_o = 0.327$, d) $d_o = 0.32$.
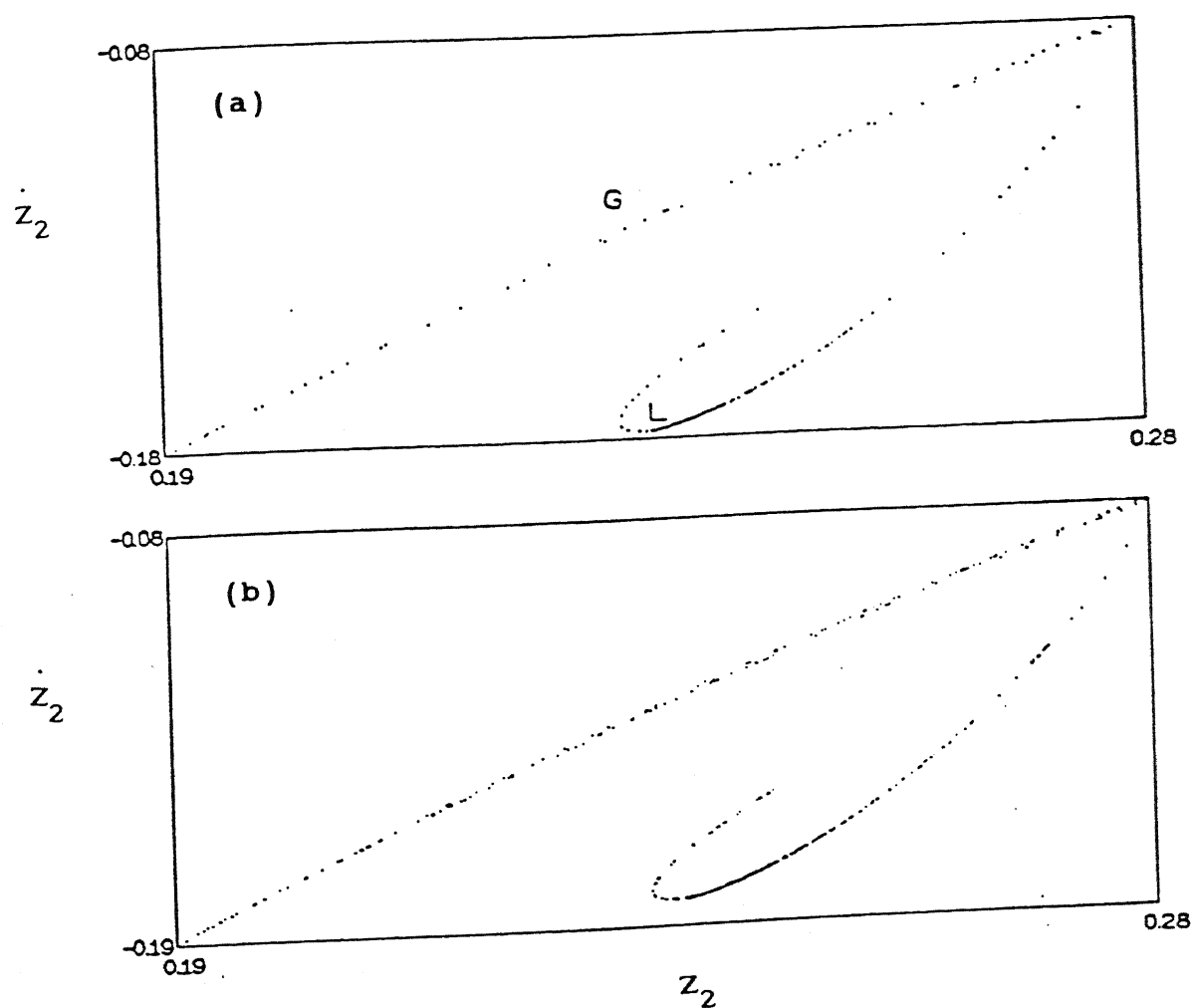
Figure 5.15 Evolution of chaotic attractor via intermittency. χ = 0.45, ε = 0.15, r_m = 0.1. a)intermittency, d_o= 0.2873; b) chaos, d_o= 0.288.

5.5.2 Bifurcations of the Periodic Solutions with Two Symmetric Impacts

So far we have discussed the existence and stability of the periodic solutions with more than two impacts. It is seen that for a fixed combination of (χ, r_m and ε), as d_0 is increased, several windows of periodic solutions (having the basic period) arise. Each of these windows corresponds to a specific number of impacts per cycle . In fact, the number of impacts per cycle corresponding to this basic period is seen to decrease with increasing d_0. Ultimately, if the other parameters are suitably chosen, a symmetric motion with two impacts per cycle appears. In real life applications of an impact damper, this mode of operation is most effective. As suggested by the preliminary numerical simulation, a periodic motion with two impacts per cycle is seen to bifurcate in a number of ways depending on the values of r_m, χ and ε. In what follows, we analyse the bifurcations of this solution and try to show the qualitative equivalence, if any, for all the forms of self-excitation considered hitherto.

5.5.2.1 Analytical Results

To bring out the essential dynamical features of the system, the bifurcational behaviour are studied under the control of the parameter d_0 with fixed values of ε and χ and several choices of the value of r_m. Different bifurcational sequences are observed depending on the value of r_m. The bifurcation diagrams are plotted in the (a_ℓ vs d_0) plane as shown in Figure 5.16. Following observations can be made from this figure:
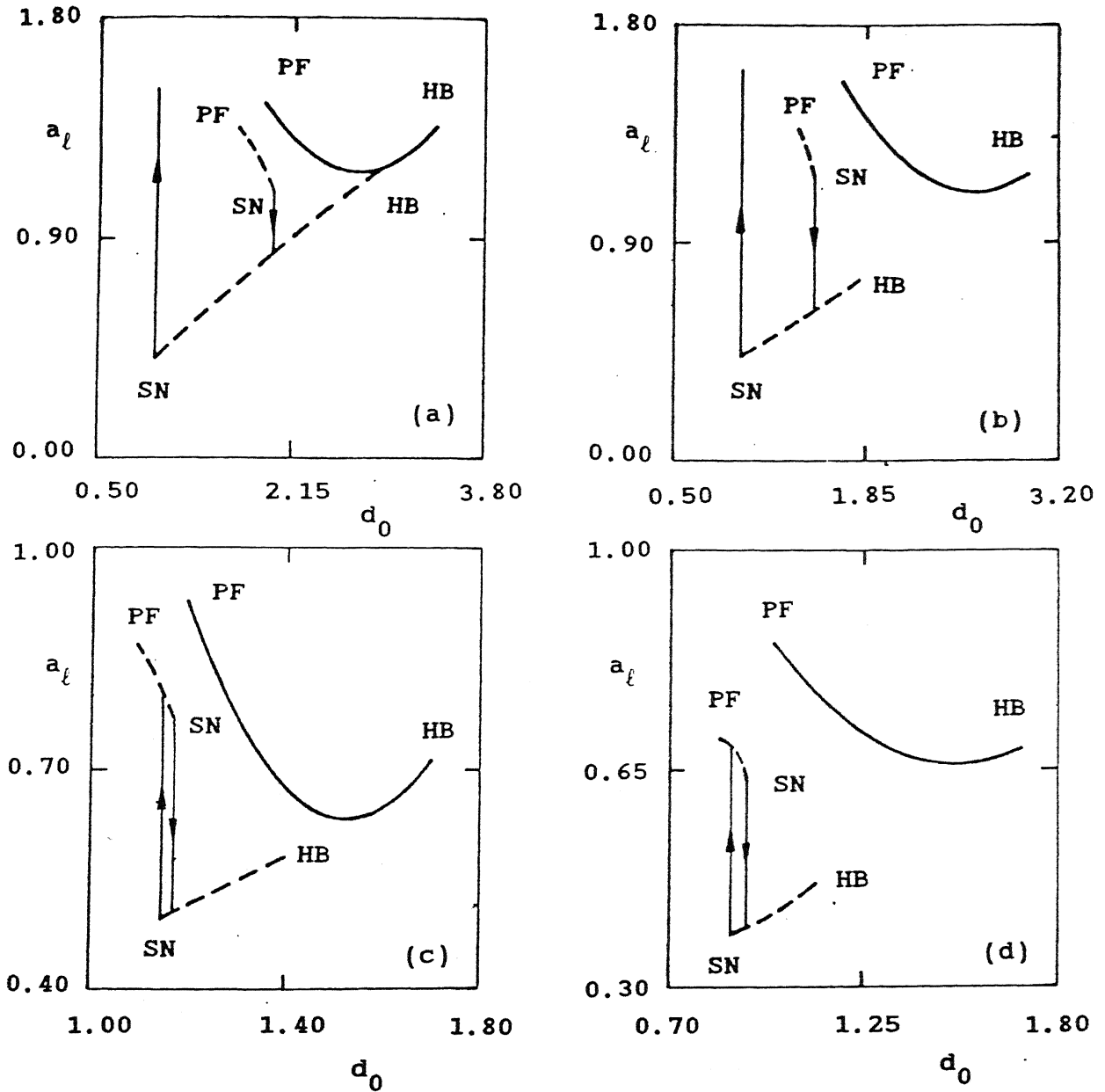
Figure 5.16 Bifurcation diagram of the periodic motion with two symmetric impacts per cycle for various forms of f a) as shown in figure 5.2(d); ε =0.2, χ =0.2, ——— for r_m = 0.1, - - - for r_m = 0.12; b) as shown in figure 5.2(b); χ =0.2, ε = 0.25, ——— for r_m = 0.1, - - - for r_m = 0.14; c) as shown in figure 5.2(c); ε = 0.3, χ = 0.2, ——— for r_m= 0.12, - - - for r_m= 0.14; d) as shown in figure 5.2(a); ε = 0.3, χ = 0.2, ——— for r_m= 0.1, - - - for r_m = 0.15. PF- pitchfork, SN- saddle-node, HB- Hopf bifurcation.

(i) For fixed values of $\varepsilon (<< 1)$ and χ (< 1) and a range of values of r_m, a window of periodic solutions with two impacts per cycle exists.

(ii) For low values of r_m, as d_0 increases beyond a critical value, a symmetric solution with two impacts per cycle is generated via a supercritical pitchfork bifurcation of its asymmetric counterparts. This symmetric solution persists for a range of values of d_0. Beyond another critical value of d_0, the symmetric solution loses its stability via a supercritical Hopf bifurcation.

(iii) For somewhat higher values of r_m, multiple solutions are resulted. The solution branch of higher amplitude is generated by a pitchfork bifurcation and terminated by a saddle-node bifurcation. The solution branch with lower amplitude undergoes a saddle-node bifurcation at the lower end of d_0 and a supercritical Hopf bifurcation at the higher end of d_0.

(iv) For still higher values of r_m, the solutions with two impacts per cycle become either unstable or non-existent.

(v) The bifurcational features of the periodic solutions are seen to be qualitatively equivalent for all types of self-exciting function considered in this paper.

It may be noted that the above mentioned scenario of the bifurcational behaviour can also be seen by varying ε with fixed values of r_m and χ.

5.5.2.2 Numerical Results

The local stability analysis, discussed in the previous section, has revealed different kinds of bifurcations of a symmetric periodic solution with two impacts per cycle namely, saddle-node , Hopf, pitchfork etc. In this section, numerical results are presented to first unfold the dynamic evolution of the system beyond the above mentioned Hopf bifurcations. These results are shown in terms of Poincare sections in Figures 5.17-5.19 for the three different types of self-exciting functions shown in Figures 5.2(a)-5.2(c), respectively.

The Hopf bifurcation of a symmetric solution with two impacts per cycle gives rise to a quasiperiodic attractor which is identified by a closed curve in the Poincare section Σ_p. It is to be noted that the quasiperiodic attractor is smooth in nature near the bifurcation point (Figures 5.17(a),5.18(a),5.19(a)). However, when the control parameter d_0 is increased further, the smoothness of the attractor is destroyed (Figures 5.17(b), 5.18(b), 5.19(b),). Such non-smooth attractors are typical of dynamical systems having piecewise smooth characteristics and have been studied by several investigators [41]. With further increase in d_0, the quasiperiodic motion gets locked into a periodic attractor of higher (than the basic) period which subsequently becomes unstable and chaotic. Such a quasiperiodic route to chaos via frequency locking is apparent in Figures 5.17-5.19. This particular route to chaos is found to be qualitatively very much in accordance with the dynamics of Curry-Yorke model and several
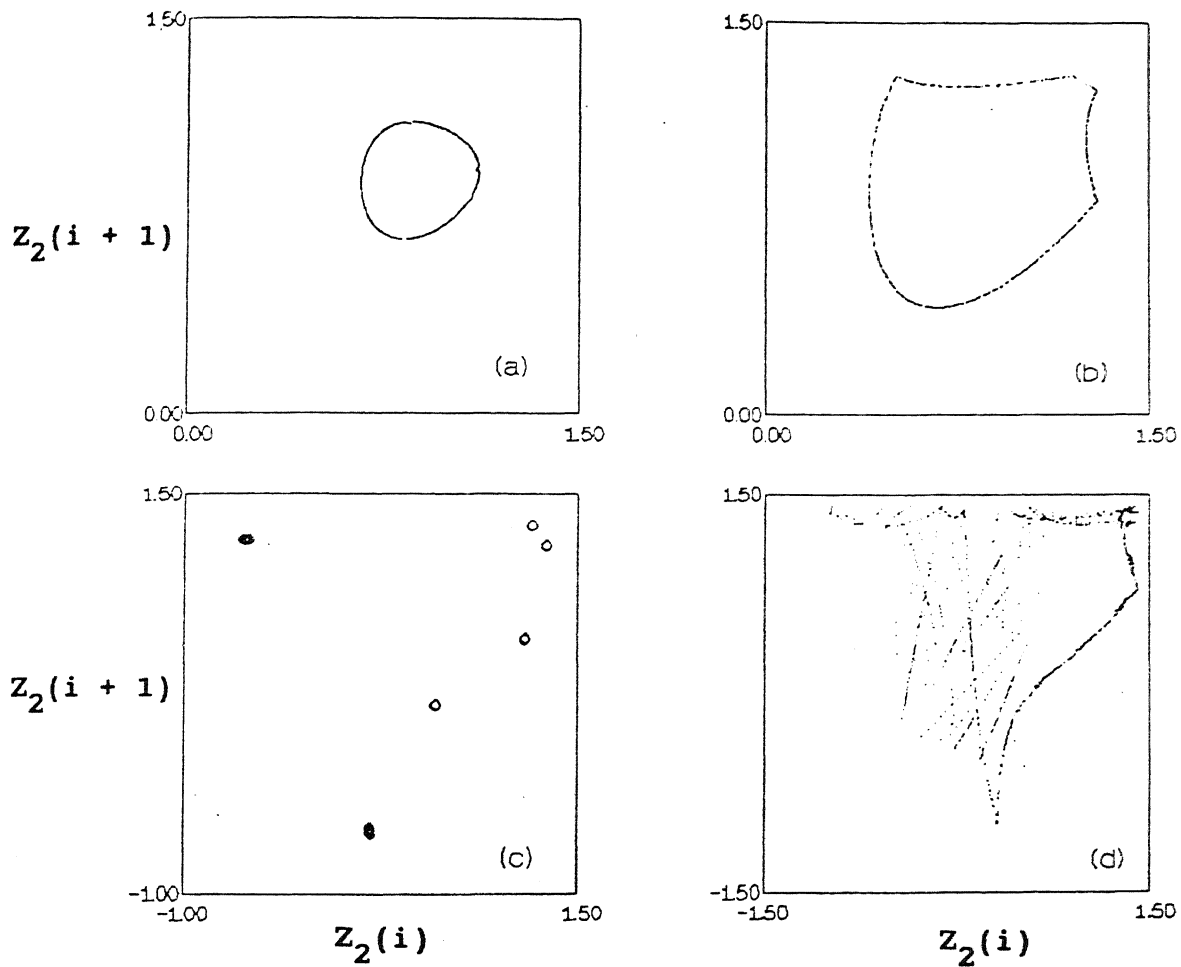
Figure 5.17 Quasiperiodic route to chaos in Poincare plane for the form of the function shown in Figure 5.2(a) with various values of d_0. $\gamma = 0.1$, $\varepsilon = 0.3$, $r_m = 0.15$, $\chi = 0.2$. a) $d_0 = 1.2$, b) $d_0 = 1.3$, c) $d_0 = 1.37$, d) $d_0 = 1.41$.
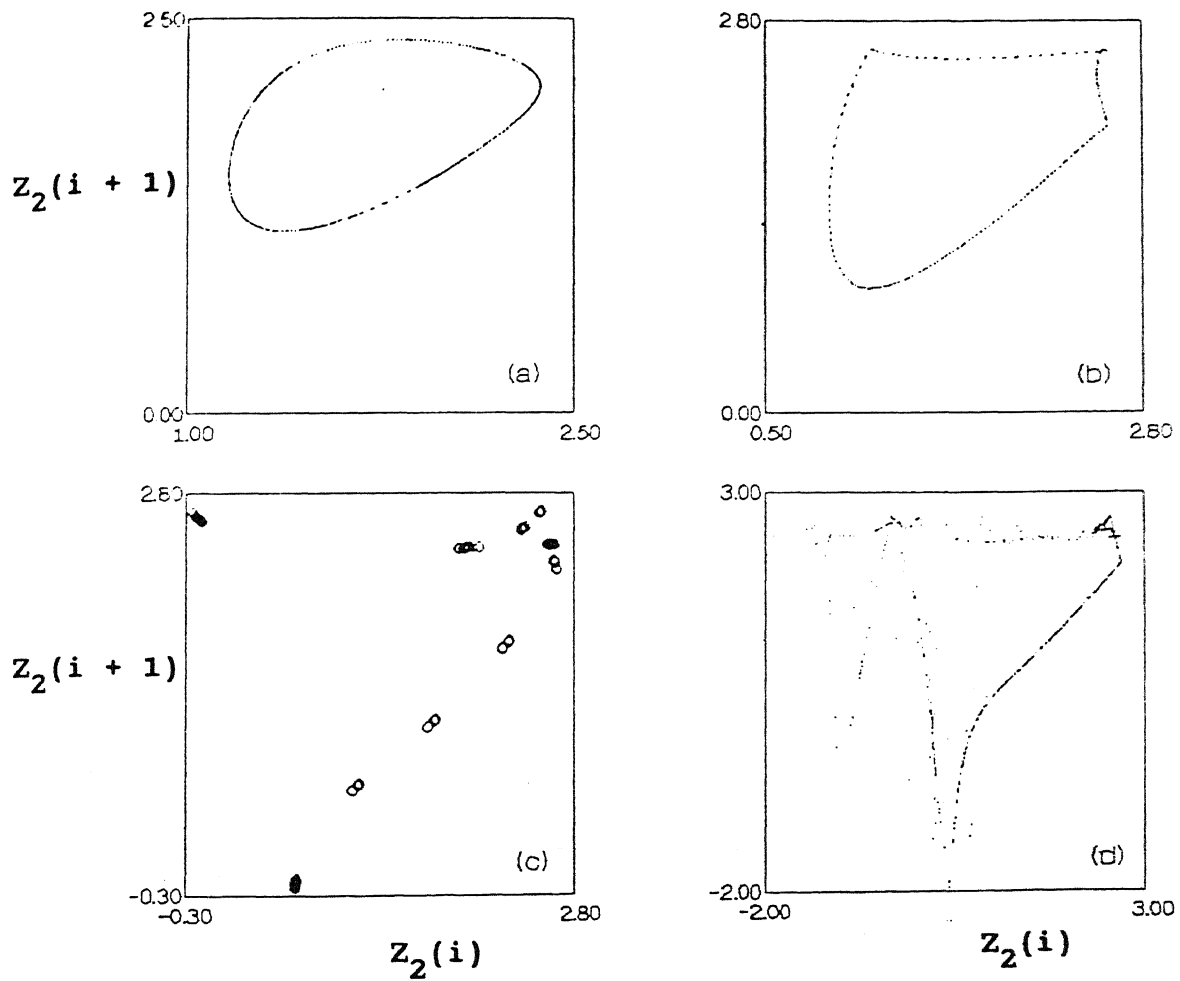
Figure 5.18 Quasiperiodic route to chaos in Poincare plane for the form of the function shown in Figure 5.2(b) with various values of d_0. γ =0.1, ε =0.15, r_m = 0.075, χ = 0.2. a) d_0 = 2.5, b) d_0 = 2.6, c) d_0 = 2.68, d) d_0 = 2.7.
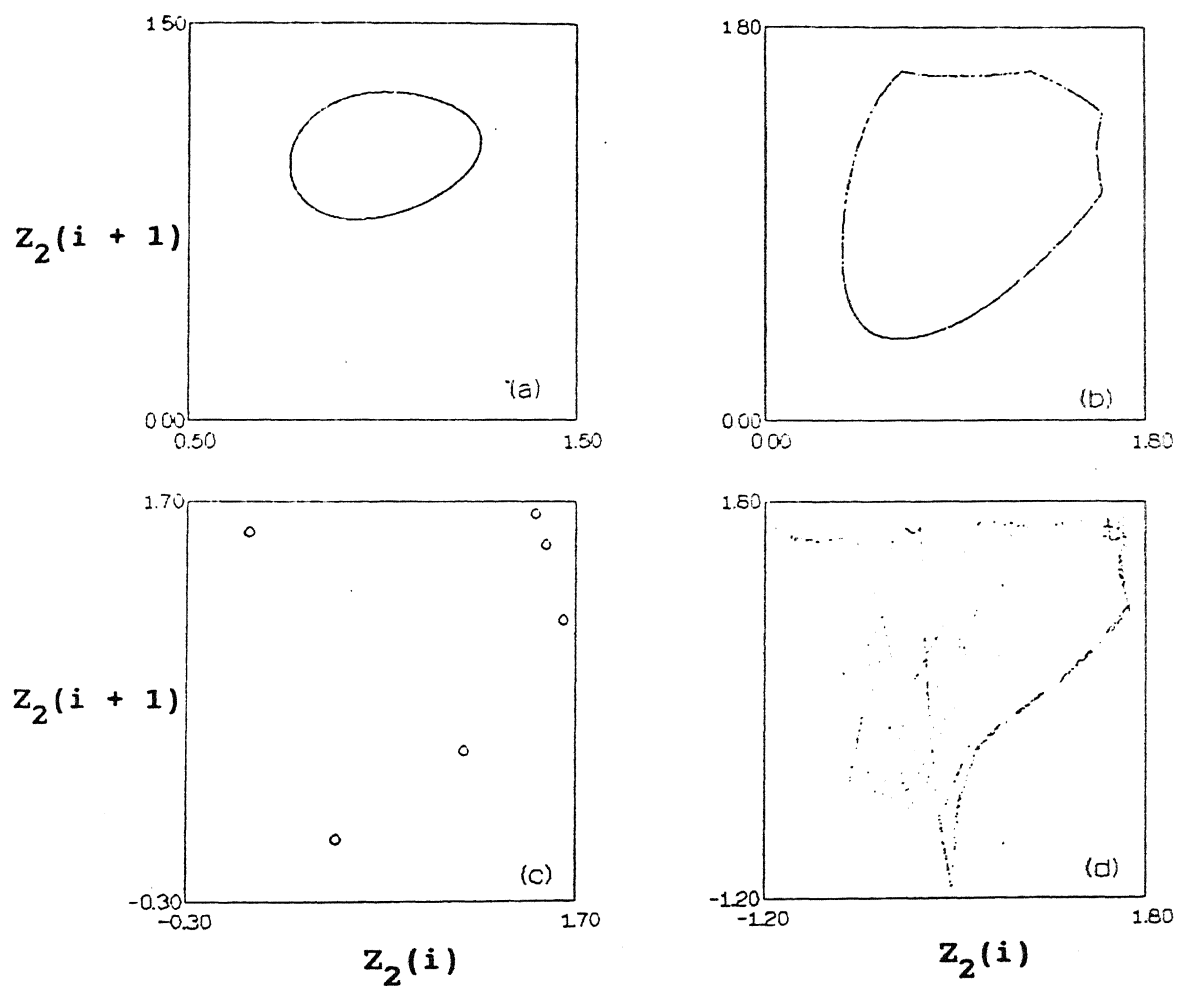
Figure 5.19   Quasiperiodic route to chaos in Poincare plane for the form of the function shown in Figure 5.2(c) with various values of d_0. $\gamma = 0.1$, $\varepsilon.=0.3$, $r_m = 0.14$, $\chi = 0.2$. a) $d_0 = 1.5$, b) $d_0 = 1.6$, c) $d_0 = 1.653$, d) $d_0 = 1.67$.

other experimental observations of hydrodynamic instabilities [117].

Now let us return to the numerical results which are analogous to those shown in Figure 5.15. Here $|Z_1|_{max}$, instead of a_1, is plotted again d_0 (Figures 5.20(a)-5.20(d)) for different values of r_m. At low values of r_m, only one value of $|Z_1|_{max}$ is observed (Figure 5.20(a)). However, for somewhat higher values of r_m, multiple solutions are obtained. Depending on the location of the saddle-node points, hysteresis involves jump between different types of solutions as depicted in these figures. For still higher values of r_m, the periodic solutions with a low amplitude may be completely destabilized and are replaced by quasiperiodic solutions or other solutions bifurcating from the same (Figure 5.20(b)). If the value of r_m is increased further, then the lower amplitude solution ceases to exist while the other periodic solution with two impacts per cycle continues. This solution, beyond a critical value of d_0, is terminated by a saddle-node bifurcation giving rise to type I intermittency (Figure 5.20(c)). Ultimately, at some high value of r_m, periodic solutions with two impacts per cycle cease to exist (Figure 5.20(d)).

The delineation of regions of periodic solutions with four impacts per cycle and two impacts per cycle are apparent in Figures 5.20(a)-5.20(d). Complicated transitions take place in the intervening region. We have already discussed similar transitions with reference to the interwindow space between six and four impacts per cycle.
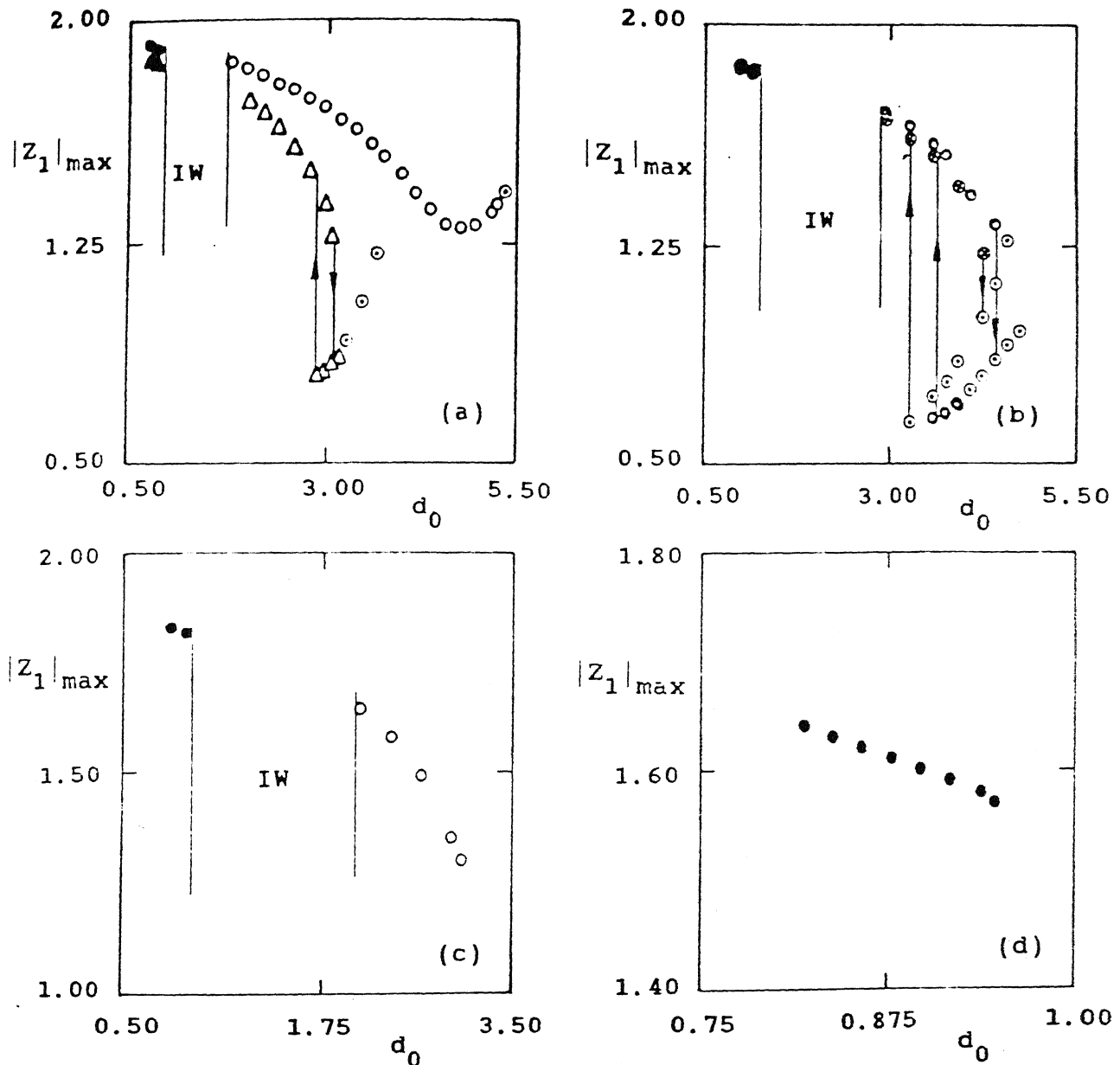
Figure 5.20 Bifurcation diagram of the periodic solutions with two symmetric impacts per cycle for the form of the function f shown in Figure 5.2(b) with various values of r_m. $\chi = 0.4$, $\varepsilon = 0.25$. a) o two impacts per cycle and ● four impacts per cycle for $r_m = 0.05$; Δ two impacts per cycle and ▲ four impacts per cycle for $r_m = 0.075$; ⊙ quasiperiodic motion; b) o two impacts per cycle and ● four impcts per cycle for $r_m = 0.08$; ⊗ two impacts per cycle for $r_m = 0.085$; ⊙ quasiperiodic motion; c) o two impcts per cycle and ● four impacts per cycle for $r_m = 0.09$; d) ● four impacts per cycle , no symmetric two impacts per cycle exists for $r_m = 0.18$. IW represents interwindow space.

5.6 Conclusions

Dynamics and bifurcations of a class of autonomous self-excited systems with momentum transfer mechanism have been studied in detail. Both analytical and numerical results are presented. The chosen parameter space is shown to be spanned by several windows of periodic solutions of a basic period with the interwindow spaces filled up by complicated motions. Each window of periodic solutions corresponds to a specific number of impacts per cycle. The number of impacts per cycle corresponding to a window of basic solution are seen to decrease with increasing d_0. The periodic solutions with higher number of impacts are seen to undergo type I intermittency transition to chaos following a saddle-node bifurcation when a control parameter is increased beyond a critical value. However, the periodic solutions with two symmetric impacts per cycle undergo jump or intermittency (depending on the values of other parameters) after a saddle-node bifurcation . A quasiperiodic route to chaos is preceded by a Hopf bifurcation associated with a symmetric motion with two impacts per cycle. When the control parameter is decreased below a critical value, each symmetric solution of the basic period undergoes a pitchfork bifurcation giving birth to a pair of asymmetric solutions which ultimately generate a chaotic motion through a period-doubling sequence. The symmetric, period-three solutions undergo bifurcations which are similar to those exhibited by the basic solution. All the above phenomena are found to be independent of the model of the self-excitation mechanism.

CHAPTER-6

BIFURCATIONS AND CHAOS IN A HARMONICALLY
FORCED SELF-EXCITED OSCILLATOR WITH IMPACT DAMPING

6.1 Introduction

A detailed account of the optimal design and performance of an impact damper for controlling the high-amplitude vibration of a forced self-excited oscillator is presented in chapter 4. It has been shown that an impact damper may be very effective in neutralising the vibration near and around the harmonic entrainment zone. However, no mention has been made about the types of instabilities that might impair the performance of such an impact damper. None the less, a designer should know the limitations of the device in its operating conditions. Moreover, an impact damper together with its most simplistic low dimensional model also represents a class of mechanical devices with loose sub-components which introduce clearance non-linearity and impact damping in the system. Owing to the presence of non-linearity such systems can exhibit a variety of non-linear instabilities and complex motions which call for an in depth study from theoretical as well as practical points of view. Keeping the above facts in mind, the different types of instabilities, bifurcations, and chaotic motions of a harmonically forced, single degree-of-freedom van der Pol oscillator with an impact damper are investigated.

It has been shown in previous studies that the motion with two symmetric impacts per cycle is the most effective operating

mode of an impact damper. This is true irrespective of the type of damping (dissipative or self-exciting) present in the primary oscillator. Sung et al.[101] have studied the bifurcational behaviour of an impact damper for a forced, linear, strictly dissipative oscillator near its operating mode with two impacts per cycle. Several types of codimension one bifurcations viz., pitchfork, saddle-node and Hopf etc. have been detected. Cascades of period doubling bifurcations along with global bifurcations such as homoclinic tangle of stable and unstable manifolds have also been studied. Chatterjee et al. [114] have investigated the super structure of the bifurcational behaviour of an autonomous, self-excited oscillator with impact damping. However, no studies concerning the bifurcations of a forced self-excited oscillator with impact damping are known to have been reported.

6.2 Equations of Motion and Method of Solution

Equations of motion of a forced self-excited oscillator with an impact damper are already given by equations (4.1) and (4.2). As motions with symmetric, two impacts per cycle are relevant from the practical point of view, the present study is mainly centered around this type of motion. The EPL method described in section 4.4.1 is used to construct the periodic solution and the method of error propagation elaborated in section 4.4.2 is applied to analyse the stability and bifurcation of the solutions.

6.3 Theoretical Results

In this section we present different possible bifurcations obtained analytically using the EPL technique and the associated error-propagation method. There are several parameters in the the model of the system. In practice, it is very difficult to handle all of these simultaneously. However, as we are interested in the local bifurcations of codimension one, the parameters are selected so as to detect all the possible types of bifurcations. Several bifurcation sets are depicted in Figures 6.1 - 6.3 in different parameter spaces. The types of bifurcations (subcritical or super critical) are also delineated. The existence of cusp catastrophes are particularly apparent in Figures 6.2 and 6.3. Single (Figures 6.2(a), 6.2(c)) and double (Figure 6.2(b), $r_m = 0.5$) cusps are seen in the bifurcation sets obtained in $d_0 - \varepsilon$ plane. In the $F_0 - \Omega$ plane (Figure 6.3), however, two (at E and F) or three (at A, B and C) cusps are seen to occur. A direct numerical simulation of the equations of motion are employed to analyse the dynamical bearings of these bifurcations. These results are presented in the following sections.

6.4 Numerical Results

For numerical integration, we have considered equations 4.2 in which the impacts are modelled by springs and dashpots. A fourth order Runge-Kutta-Merson algorithm with adaptive step size control has been employed. Numerical integration revealed different types of intermittent and quasiperiodic routes to chaos as elaborated below.
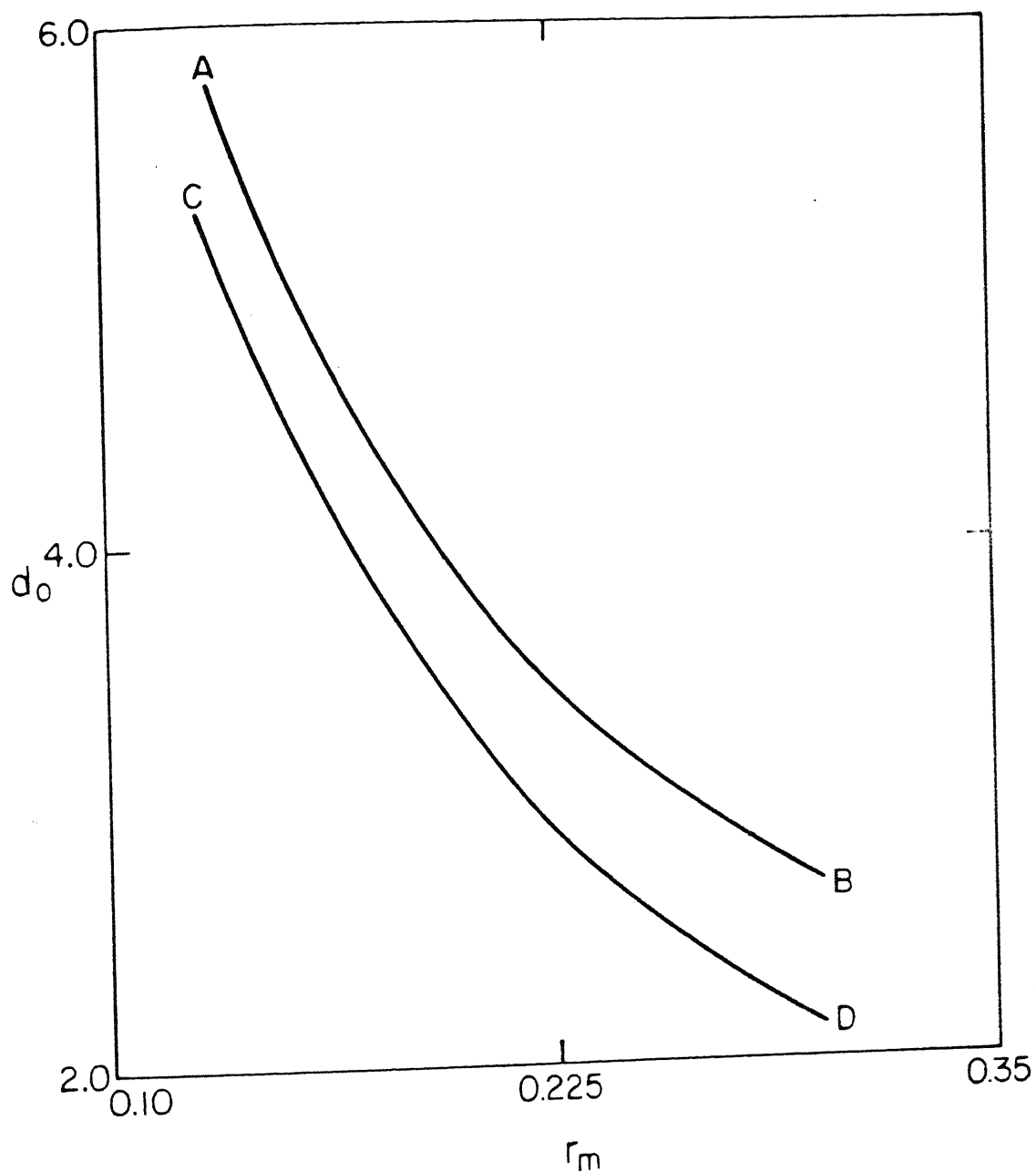
Figure 6.1   Bifurcation set in r_m- d_0 plane. $\Omega = 1$, $\chi = 0.7$, $F_0 = 0.5$, $\varepsilon = 0.1$. The zone enclosed between the lines AB and CD corresponds to stable symmetric motion with two impacts per cycle. AB and CD correspond to supercritical and subcritical Hopf bifurcations, respectively.
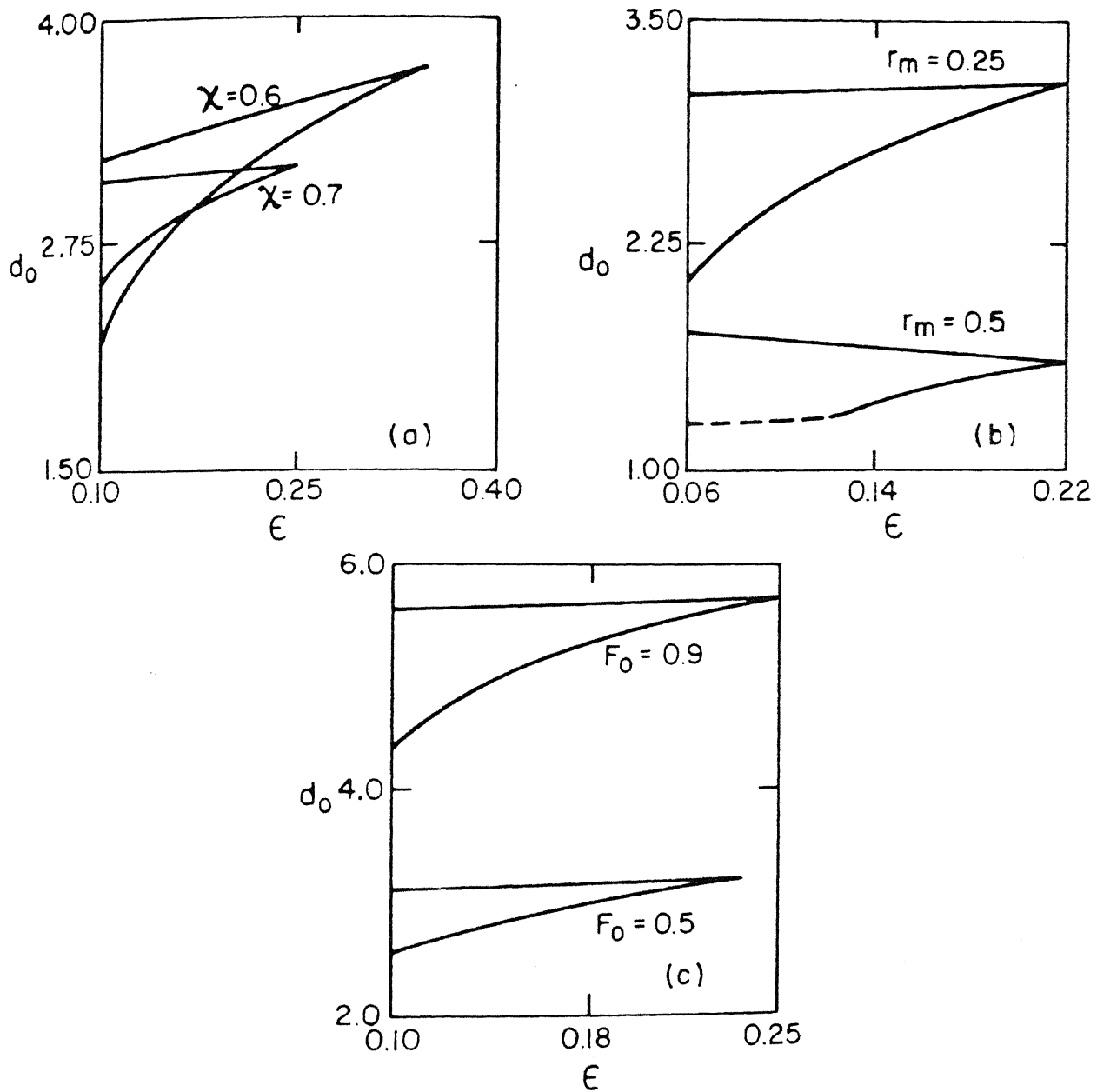
Figure 6.2   Bifurcation sets in ε - d_0 plane. Ω = 1. a) F_0= 0.5, r_m= 0.25; b) F_0= 0.5, χ = 0.7; c) χ = 0.7, r_m= 0.25. ———— Hopf bifurcation (the upper line corresponds to supercritical bifurcation and the lower line corresponds to subcritical bifurcation), - - - pitchfork bifurcation (subcritical).
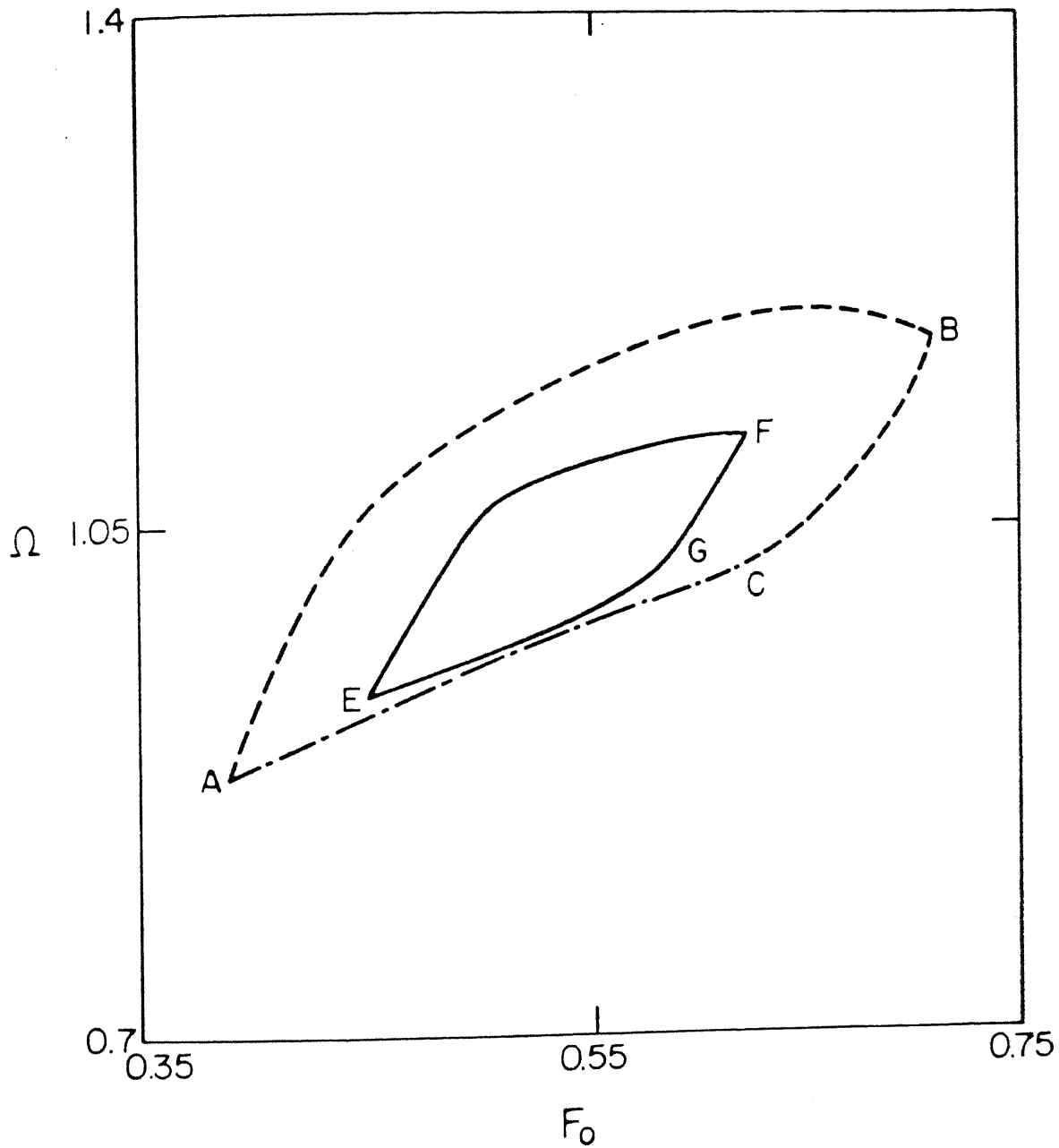
Figure 6.3   Bifurcation set in F_0- Ω plane. χ = 0.7, ϵ = 0.1. AB - supercritical Hopf bifurcation, BC - subcritical Hopf bifurcation, CA - subcritical pitchfork bifurcation : d_0= 1.6, r_m= 0.45. EF - supercritical Hopf bifurcation, EGF - subcritical Hopf bifurcation : d_0 = 2.9, r_m= 0.25.

6.4.1 Type II Intermittency

The zone of stable solutions with symmetric two impacts per cycle is delineated in the $r_m - d_0$ plane as shown in Figure 6.1. The local stability analysis reveals that both the stability boundaries (marked as AB and CD) correspond to Hopf bifurcation. As the non-linear stability analysis turned out to be complicated, the form of the bifurcation could not be established analytically. However, it is well known that two possibilities exist when a periodic motion encounters a Hopf bifurcation (secondary Hopf bifurcation or Neimark bifurcation). Either a quasiperiodic motion results (when the bifurcation is supercritical) or a more complicated evolution (when the bifurcation is subcritical) having a local-global or entirely global feature appears. In the present case, the boundary AB turned out to be a supercritical bifurcation line as the subsequent motion is strictly quasiperiodic. However, when a parameter is varied (here d_0 is decreased while keeping r_m constant) across the boundary CD, an intermittent evolution appears. Such an intermittent signature is shown in Figure 6.4. A closer look into the signature reveals two distinct phases of the motion. One of these consists of frequency modulated oscillation (so called laminar phase) with diverging envelop. Two such phases are punctuated by other phases which are apparently disordered (chaotic phase). According to the classical Pomeau-Manneville [115-117] categorization of different types of intermittencies based on local bifurcations, the present intermittency is of type II as the preceding bifurcation is a Hopf bifurcations. This indirectly implies that the Hopf bifurcation on the boundary CD is
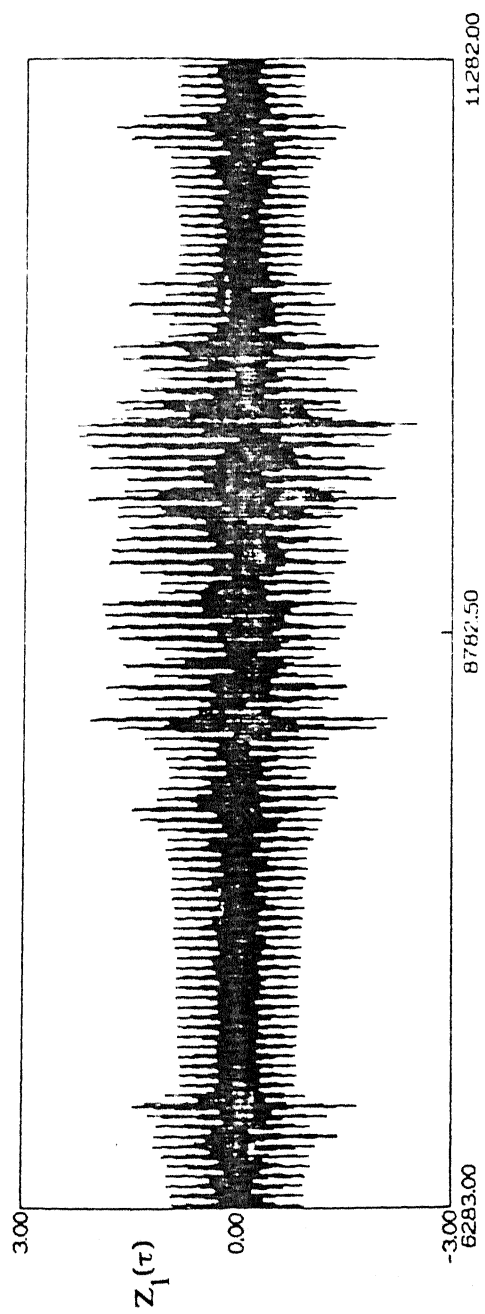
Figure 6.4 Signature of type II intermittency. $\Omega = 1$, $\chi = 0.7$, $F_0 = 0.5$, $r_m = 0.25$, $d_0 = 2.49$.
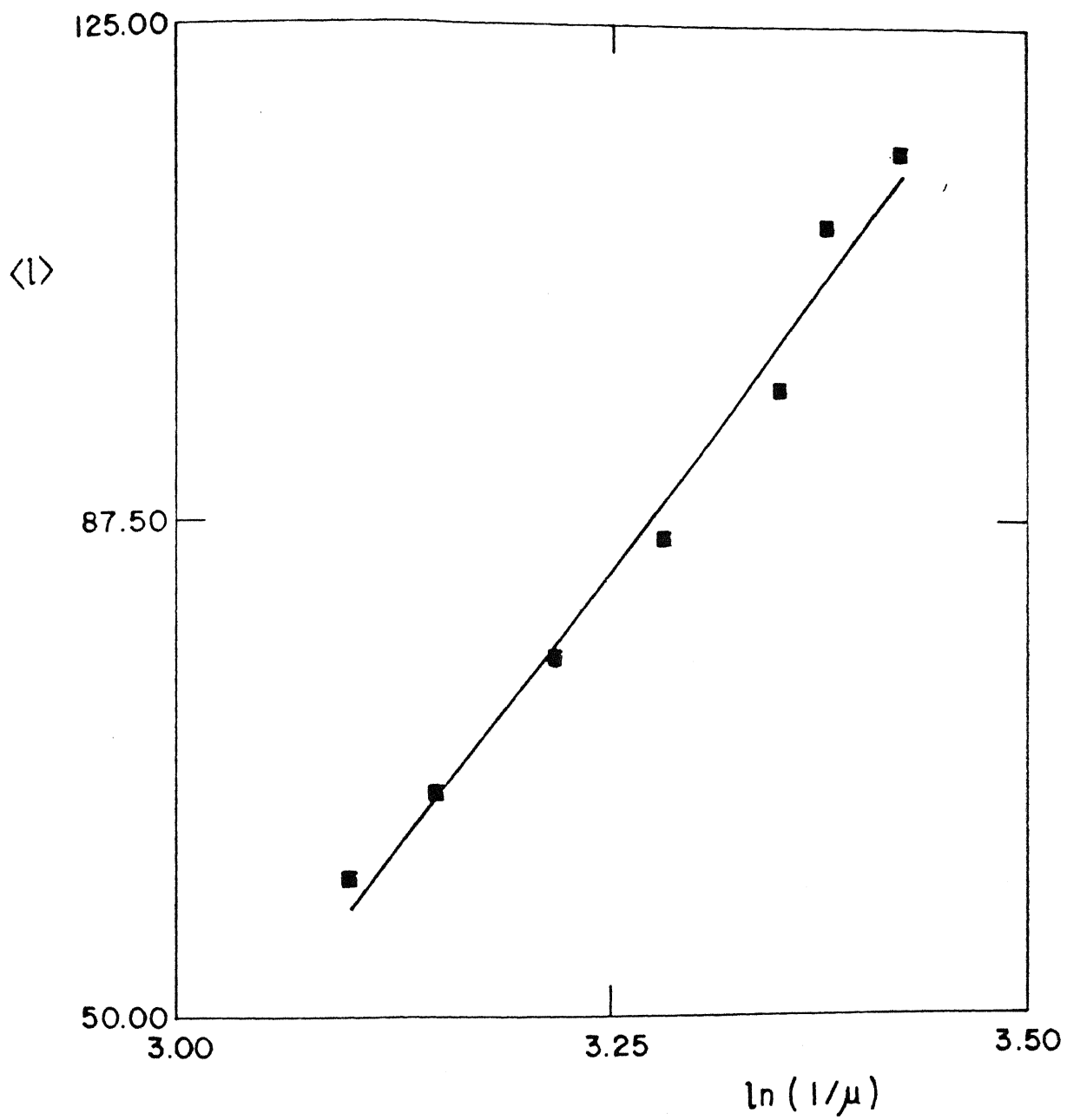
Figure 6.5   Scaling law of type II intermittency. The parameter
values are given in Figure 6.4.

subcritical. The average length $<\ell>$ of the laminar phases is seen to comply with the scaling law (Figure 6.5) predicted by Pomeau-Manneville and described by

$$<\ell> \sim \ln (1/\mu)$$

where $\mu = d_0 - d_0^C$ and d_0^C is the bifurcation threshold. Here, it is worth mentioning that though the type II intermittency is known to exist, it rarely occurs in physical systems. Only very few examples are found in the literature [118-119].

6.4.2 Intermittency After Subcritical Pitchfork Bifurcation

The zones of stable two impacts per cycle solution are delineated in Figure 6.3 in the F_0 vs Ω plane. The boundary AB in this figure can be analytically shown to correspond to a subcritical pitchfork bifurcation. Immediately after this bifurcation (Ω is decreased across the boundary while keeping F_0 constant), another intermittent motion appears as shown in Figure 6.6. In this figure, the time history of the Poincare iterates (so called strobe map with the strobe frequency Ω) is plotted. Such a kind of intermittency created by a subcritical pitchfork bifurcation is not reported so far.

Theoretical models of the dynamics of intermittency have been put forward by Pomeau-Manneville [115-117]. For describing the mechanism of intermittency they used non-linear maps which may stand for a suitable Poincare map of the periodic solutions of an ordinary differential equation. In their model, a kind of narrow channeling effect accounts for the laminar phase and a proper reinjection principle explains the recontinuation of the laminar
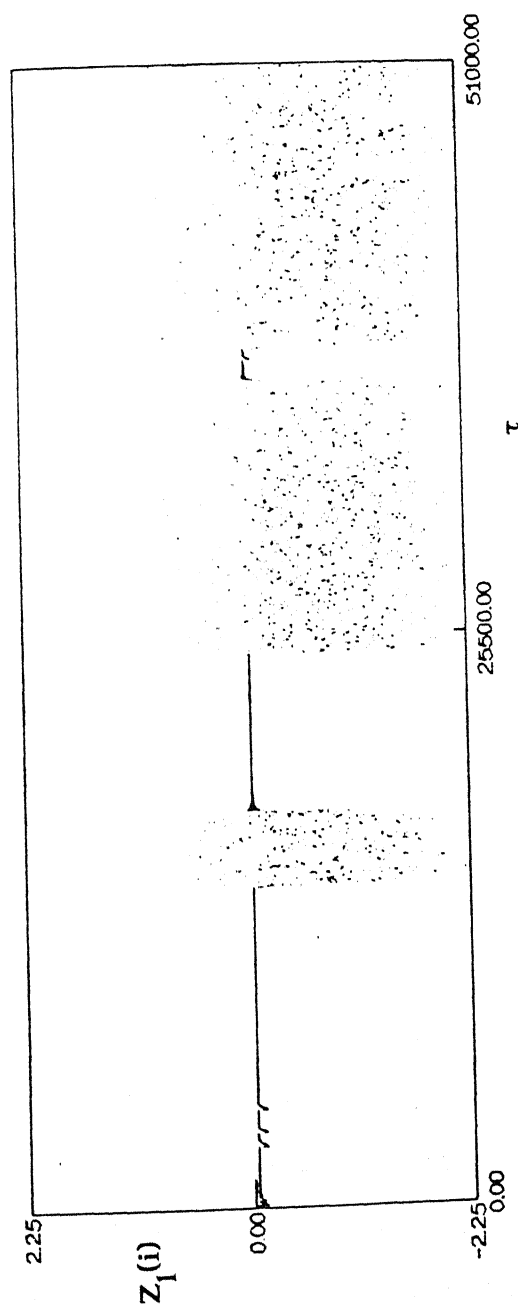
Figure 6.6 Intermittency after subcritical pitchfork (symmetry-breaking) bifurcation. $F_0 = 0.5$, $d_0 = 1.6$, $r_m = 0.45$, $\varepsilon = 0.1$, $\chi = 0.7$, $\Omega = 0.9512$.

phase after a chaotic burst. As the whole mechanism is based on the availability of a suitable non-linear map, only three types of intermittency could be explained each corresponding to a type of local bifurcation viz., saddle-node (type I), subcritical Hopf bifurcation (type II) and subcritical period multiplying bifurcation (type III) of the fixed points of the map. However, the pitchfork bifurcation (or symmetry-breaking) of a periodic solution of a differential equation does not have any counterpart in the bifurcation of a fixed point of a non-linear map. Perhaps this is why no model has been studied for the occurrence of intermittency following a pitchfork bifurcation. Another reason may be that the symmetry breaking is a non-generic bifurcation in the sense that, it is structurally unstable under asymmetric perturbations however small. Of course, for a more detailed study of the mechanism of this type of intermittency a model should be constructed and according to the above discussion such a model should be based on a low dimensional differential equation rather than a non-linear map.

6.4.3 Quasiperiodic Route to chaos

The boundaries corresponding to supercritical Hopf bifurcation are delineated in Figures 6.1 - 6.3. When a parameter is varied (keeping the other constant) across these boundaries, the symmetric, two impacts per cycle solution bifurcates to a quasiperiodic solution. Such quasiperiodic motions can lead to chaos with further variation of the control parameter beyond the bifurcation line. Several routes to chaos via quasiperiodicity

have been reported in the literature [120-122]. In the present study, two distinct routes, as shown in Figures 6.7 and 6.8, are obtained. One of the routes (Figure 6.7) depicts the continuous dispersal of the poincare iterates as the control parameter is increased . This route complies with that of the Rayleigh-Benard convection: structure C described in reference [117]. The other route shown in Figure 6.8 is via frequency locking. The locked motion (period of the locked motion in Figure 6.8(b) is five times that of the forcing) may be destabilized in a number of ways and leads to chaos. However, in the present study, locked modes are seen to undergo intermittent transition to chaos. One such intermittent motion is shown in Figure 6.9 with the help of the time history of Poincare iterates. Such an intermittency is identified to have arisen out of a subcritical half subharmonic instability. Thus, according to PM classification this is type III intermittency. The entire sequence may be summarised as follows:

periodic → quasiperiodic → locked mode → intermittency → chaos. The above route to chaos is seen to be present in a number of situations such as Rayleigh-Benard convection [121].

6.5 Conclusions

Complex dynamics of a forced, self-excited oscillator with impact damping is discussed using theoretical as well as numerical means. Three different types of intermittencies are detected in a single mechanical model. The possibility of the existence of a new kind of intermittency via a subcritical pitchfork bifurcation (symmetry-breaking) is demonstrated through the present model. It
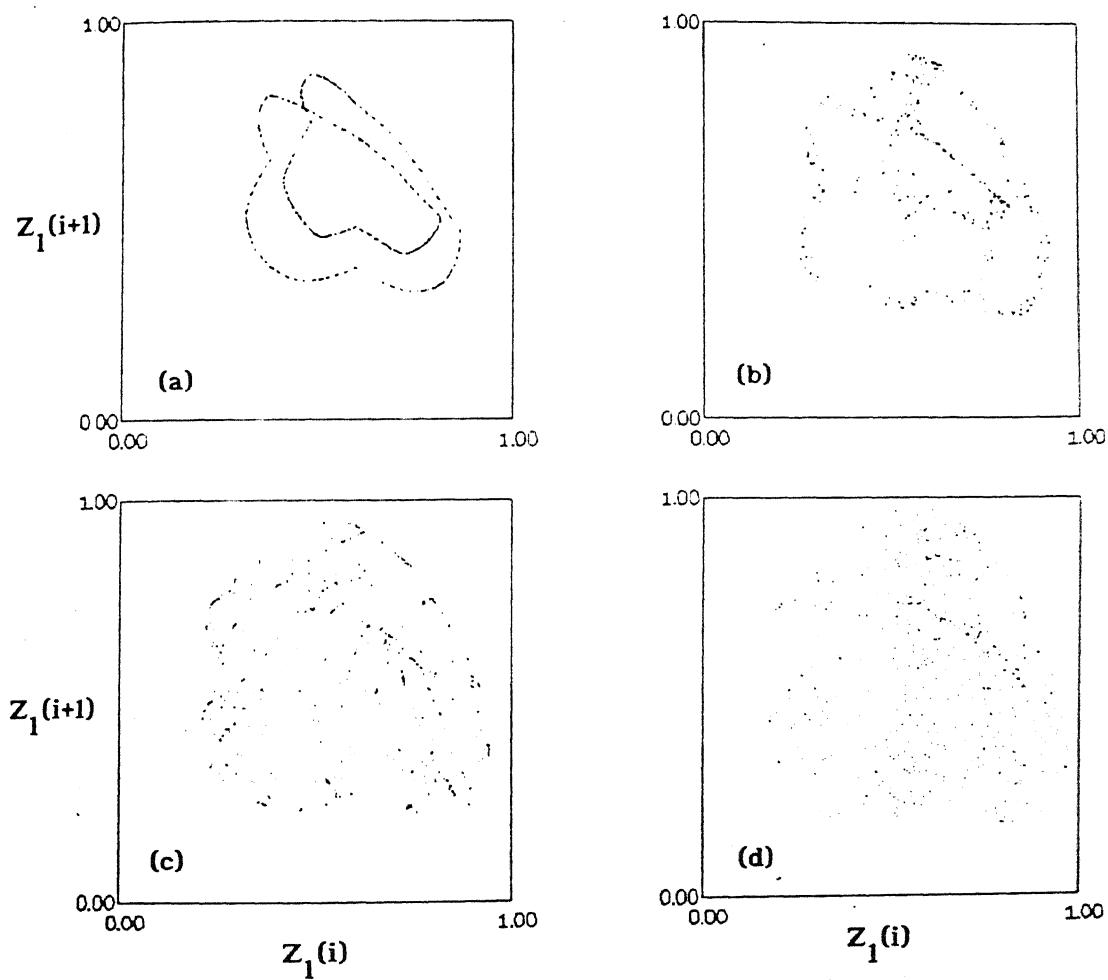
Figure 6.7   Quasiperiodic route to chaos. $F_0 = 0.5$, $\Omega = 1$, $r_m = 0.25$, $\chi = 0.6$, $\varepsilon = 0.1$. a) $d_0 = 3.35$, b) $d_0 = 3.37$, c) $d_0 = 3.38$, d) $d_0 = 3.39$
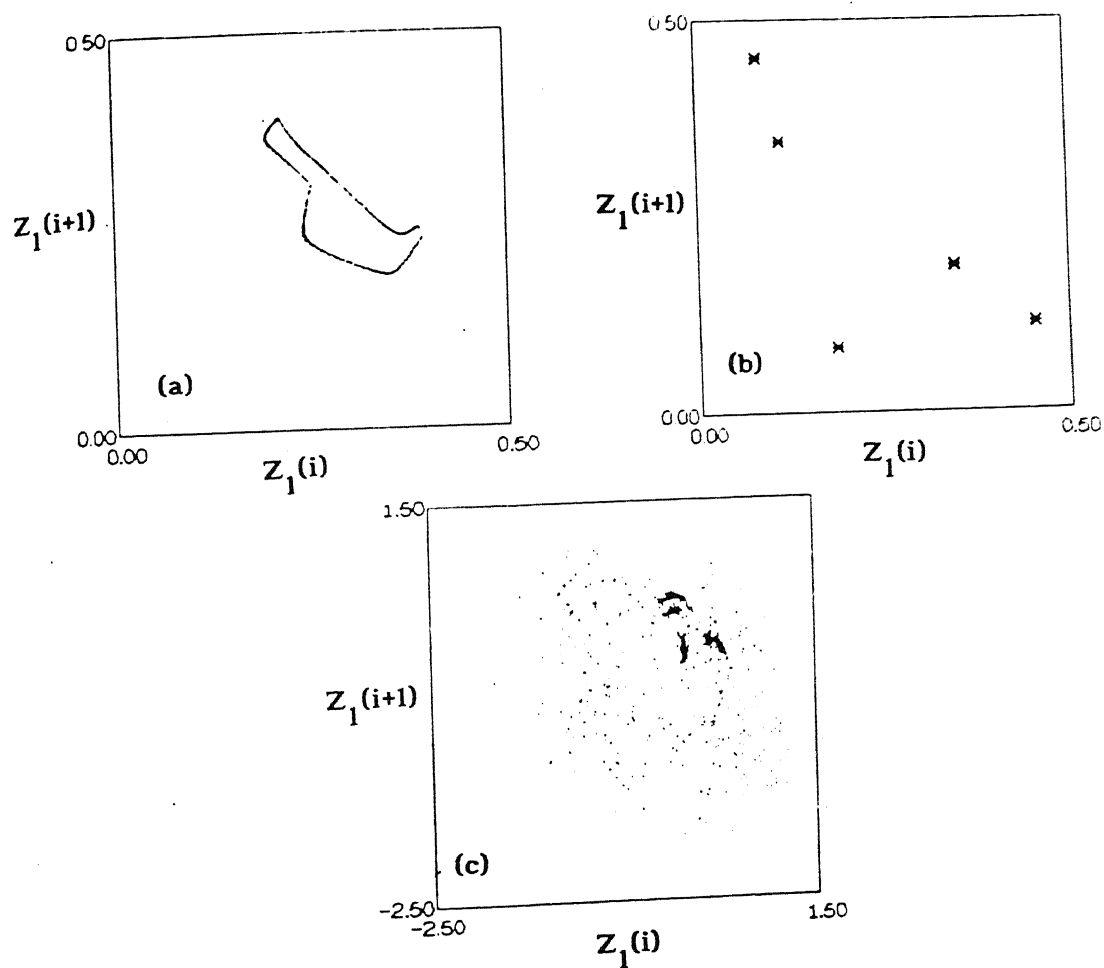
Figure 6.8   Quasiperiodic route to chaos via frequency locking. $F_0 = 0.5$, $d_0 = 1.67$, $r_m = 0.45$, $\varepsilon = 0.1$, $\chi = 0.7$. a) $\Omega = 1.12$, b) $\Omega = 1.125$, c) $\Omega = 1.138$.
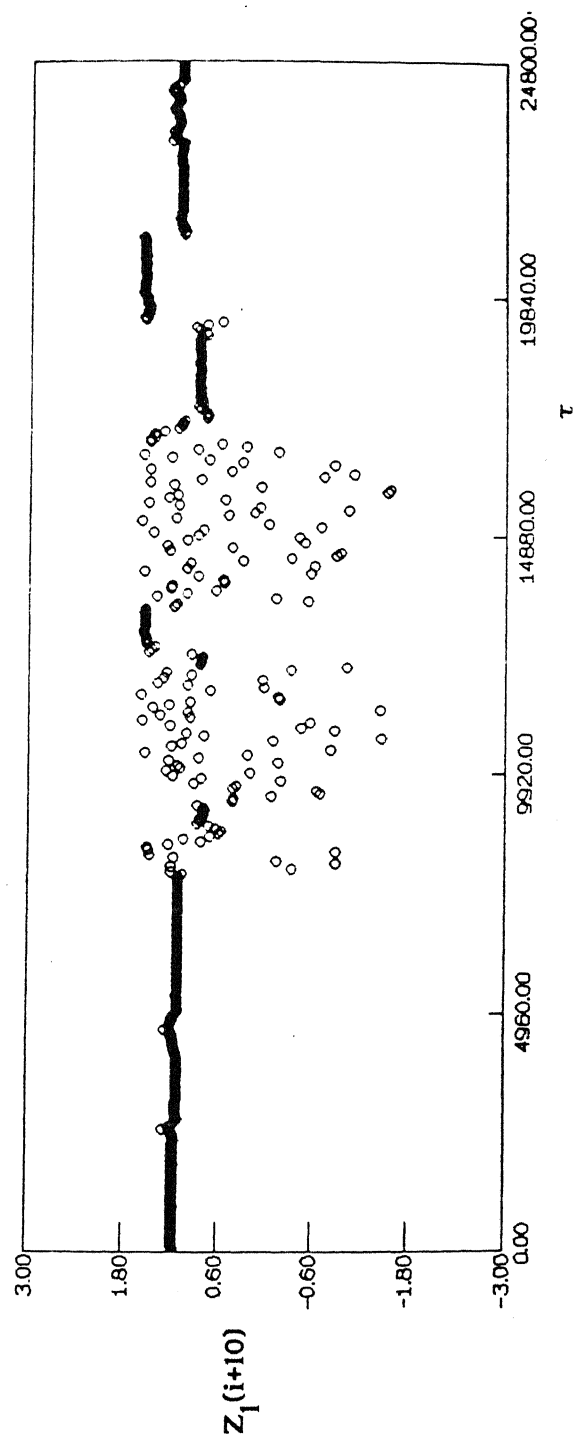
Figure 6.9 Type III intermittency. The parameter values are given in Figure 6.8(c).

is well known that a great deal of hydrodynamic instabilities are related to different kinds of intermittency catastrophes and quasiperiodic transitions. The present model, a purely mechanical one, demonstrates a variety of similar instabilities.

C H A P T E R - 7

CONCLUSIONS

7.1 Conclusions

The major conclusions of the present thesis are listed below.

(i) The proposed EPL technique contains information in both time and frequency domains and consequently gives better results than the HBM which is simply a frequency domain technique. This method is particularly suitable for obtaining the time domain response of a class of piecewise smooth, non-linear systems.

(ii) An impact damper is effective, both in passive and active on-off forms, for controlling the vibration of non-linear systems having Duffing type restoring force characteristics. Both the primary and secondary resonances can be controlled. A simple formula is obtained for providing an initial design and has been shown how to improve upon to obtain a final optimum design.

(iii) An impact damper can be used to control both free and forced self-excited vibrations. Sensitivity of the designed performance towards the inaccuracy of the estimated model parameters is to be incorporated in the design rules. An empirical design formula for an impact damper attached to a forced van der Pol oscillator is provided after a detailed parametric study. The role of the coefficient of restitution for various situations has been clearly brought out.

(iv) Various instabilities occur in an autonomous self-excited system with an impact damper. The gross bifurcation superstructure of the systems under consideration is more or less independent of the exact nature of the model of the self-excitation. A numerical technique has been developed for analysing the eigen properties of the stable solutions.

(v) The dynamics of a harmonically driven van der Pol oscillator with an impact damper is rich with different types of intermittency catastrophes viz., type II, type III etc. A new type of intermittency after a subcritical, symmetry-breaking pitchfork bifurcation is seen to exist in the system under consideration. Several instabilities of the system has a close resemblance to the hydrodynamic instabilities such as Rayleigh-Benard convection etc.

7.2 Suggestions for Future Works

On the basis of the methods developed and results obtained in this thesis, the following suggestions, on research to be carried out in future, can be made:

(i) The suitability of the EPL method for analysing the response of smooth, non-linear systems should be investigated. It should be emphasized, that the piecewise linearization is to be carried out in a dynamic sense where the junction point between the equivalent linear segments has to be left as an unknown quantity to be determined. In the usual static way of piecewise linearization method, this junction point is assumed a priori.

(ii) The effectiveness of an impact damper, used both in passive and active manners discussed in the thesis, for controlling the vibration of non-linear systems should be verified through suitable experimentation.

(iii) The intermittency route via the subcritical, symmetry-breaking pitchfork bifurcation reported in the thesis should be subjected to further investigations. Especially, if possible, a low-dimensional mathematical model for determining its statistical characteristics should be attempted. It may be mentioned that the standard maps, hitherto discussed in the literature, cannot capture such route.

REFERENCES

1. N. Minorsky 1969 *Nonlinear oscillations*. New Delhi: Affiliated East-West Press Pvt. Ltd.

2. S. Maezawa and S. Furukawa 1973 *Bulletin of the Japan Society of Mechanical Engineers* 16, 931-941. Superharmonic resonance in piecewisw linear systems.

3. S. Maezawa 1961 *Bulletin of the Japan Society of Mechanical Engineers* 4, 201-229. Steady forced vibrations unsymmetrical piecewise linear systems.

4. S. Mazewa, H. Kumano and Y. Minakuchi 1980 *Bulletin of the Japan Society of Mechanical Engineers* 23, 68-75. Forced vibrations in an unsymmetric linear system excited by general periodic forcing functions.

5. T. Watanbe 1984 *Bulletin of the Japan Society of Mechanical Engineers* 27, 1493-1498. vibration of non-linear system with symmetrical piecewise linear characteristics.

6. G.R. Tomlinson and J. Lam 1984 *Journal of Sound and vibration* 96, 111-125. Frequency response characteristics of structures with single and multiple clearence type non-linearity.

7. S.W. Shaw and P.J. Holmes 1983 *Journal of Sound and Vibration* 90, 129-155. A periodically forced piecewise linear oscillator.

8. S. Natsiavas 1990 *Journal of Sound and Vibration* 141, 97-102. Stability and bifurcation analysis for oscillators with motion limiting constraints.

9. S. Natsiavas 1990 *International Journal of Non-linear Mechanics* **25**, 535-554. On the dynamics of oscillators with bilinear damping and stiffness.

10. S. Natsiavas and H. Gonzalez 1992 *Transactions of the American Society of Mechanical Engineers, Journal of Applied Mechanics* **59**, Vibration of harmonically excited oscillator with asymmetric constraints.

11. Y.B. Kim and S.T. Noah 1991 *Transactions of the American Society of Mechanical Engineers, Journal of Applied Mechanics* **58**, 545-553. Stability and bifurcation analysis of oscillators with piecewise linear characteristics: a general approach.

12. J.N. Schulman 1983 *Physical Review* **A 28**, 477-479. Chaos in piecewise linear system.

13. J.M.T. Thompson, A.R. Bokaian and R. Ghaffari 1983 *Journal of Applied Mathematics* **31**, 207-234. Subharmonic resonances and chaotic motion of a bilinear sysytem.

14. I.A. Mahfouz and F. Badrakhan 1990 *Journal of Sound and Vibration* **143**, 289-327. Chaotic behaviour of some piecewise linear systems, part I: Systems with set up spring or with unsymmetrical elasticity.

15. I.A. Mahfouz and F. Badrakhan 1990 *Journal of sound and Vibration* **143**, 324-345. Chaotic behaviour of some piecewise linear systems, part II: Systems with clearance.

16. J.M.T. Thompson and H.B. Stewart 1986 *Nonlinear Dynamics and Chaos, Geometric Methods for Engineers and Scientists*. New York: John Wiley and Sons.

17. S.W. Shaw and P.C. Tung 1988 *Transactions of the American Society of Mechanical Engineers, Journal Dynamic systems, Measurement and control* **110**, 278-283. The dynamic response of a system with preloaded complience.

18. H.S. Choi and J.Y.K. Lou 1991 *International Journal of Non-linear Mechanics* **26**, 461-473. Non-linear behaviour and chaotic motions of an sdof system with piecewise non-linear stiffness.

19. S.W. Shaw 1985 *Journal of Sound and Vibration* **99**, 199-212. Forced vibration of a beam with one-sided amplitude constraint: theory and experiment.

20. S.F. Masri, Y.A. Mariarouy and J.C. Anderson 1981 *Transactions of the American Society of Mechanical Engineers, Journal of Applied Mechanics* **48**, 404-410. Dynamic response of a beam with a geometric non-linearity.

21. R.J. Comparin and R. Singh 1989 *Journal of Sound and vibration* **134**, 259-290. Non-linear frequency response characteristics of an impact pair.

22. C.N. Bapat and C. Bapat 1988 *Journal of Sound and Vibration* **120**, 53-61. Impact pair under periodic excitations.

23. C.N. Bapat, N. Popplewell and K. McLachlan 1983 *Journal of Sound and Vibration* **87** ,19-40. Stable periodic motions of an impact pair.

24. C.H. Lee and K.P. Byrne 1987 *Journal of Sound and Vibration* **12**, 268-287. Impact statistics for single rattling system.

25. L.H. Word and K.P. Byrne 1981 *Journal of Sound and Vibration* **78**, 329-345. Analysis of a random repeated impact process.

26. L.H. Word and K.P. Byrne 1982 *journal of Sound and Vibration* **86**, 53-59. Experimental investigations of random repeated impact process.

27. M.S. Heiman, P.J. Sherman and A.K. Bajaj 1987 *Journal of Sound and Vibration* 114, 535-547. On the dynamics of an inclined impact pair.

28. J. Guckenheimer and P.J. Holmes 1983 *Nonlinear Oscillations, Dynamical Systems and Bifurcation of Vector Fields.* New York: Springer.

29. C.N. Bapat and S. Sankar 1986 *Journal of Sound and Vibration* **108**, 99-115. Repeated impacts on a sinusoidally vibrating table reappraised.

30. G.X. Li, R.H. Rand and F.C. Moon 1990 *International Journal of Non-linear Mechanics* 25, 417-432. Bifurcation and chaos in a forced zero stiffness oscillator.

31. M. Senator 1970 *Journal of the Acoustical Society of America* **47**, 1390-1397. Existence and stability of periodic motions of a harmonically forced impacting system.

32. C.C. Fu and B. Paul 1969 *Transactions of the American Society of Mechanical Engineers, Journal of Engineering for Industry* **89**, 1175-1179. Dynamic stability of a vibrating hammer.

33. G.S. Whiston 1979 *Journal of Sound and Vibration* 67, 179-186. Impacting under harmonic excitation.

34. W. Fang and J.A. Wickert 1994 *Journal of Sound and Vibration* **170**, 397-409. Response of a periodically driven impact oscillator.

35. D.T. Nguyen, S.T. Noah and C.F. Kettleborough 1986 *Journal of sound and Vibration* **109**, 293-307. Impact behaviour of an oscillator with limiting stops, Part I : a parametric study.

36. D.T. Nguyen, S.T. Noah and C.F. Kettleborough 1986 *Journal of sound and Vibration* **109**, 309-325. Impact behaviour of an oscillator with limiting stops, Part II : dimensionless design parameters.

37. G.S. Whiston 1992 *Journal of Sound and Vibration* **152**, 427-460. Singularities in vibro-impact dynamics.

38. D.B. Moore and S.W. Shaw 1990 *International Journal of Non-linear Mechanics* **25**, 1-16. The experimental response of an impacting pendulum system.

39. P.V. Bayly and L.N. Virgin 1993 *Journal of Sound and Vibration* **164**, 364-374. An experimental study of an impacting pendulum

40. J.O. Adianpaa and R.B. Gupta 1993 *Journal of Sound and Vibration* **165**, 305-327. Periodic and chaotic behaviour of a threshold limited two-degree-of-freedom system.

41. A.B. Nordmark 1991 *Journal of Sound and Vibration* **145**, 279-297. Non-periodic motion caused by grazing incidence in an impact oscillator.

42. A.P. Ivanov 1993 *Journal of Sound and Vibration* **162**, 562-565. Stabilization of an impact oscillator near grazing incidence owing to resonance.

43. J.M.T. Thompson and R. Ghaffari 1983 *Physical Review* A **27**, 1741-1743. Chaotic dynamics of an impact oscillator.

44. F. Peterka and J. Vacik 1992 *Journal of Sound and Vibration* **154**, 95-115. Transition to chaoic motion in mechanical systems with impacts.

45. F. Hendricks 1983 *IBM Journal of Research and Development* 27, 273-280. Bounce and chaotic motion in print hammers.

46. S.W. Shaw and P.J. Holmes 1983 *Transactions of the American Society of Mechanical Engineers, Journal of Applied Mechanics* **50**, 849-857. A periodic forced impact oscillator with large dissipation.

47. S.W. Shaw 1985 *Transactions of the American Society of Mechanical Engineers* **52**, 453-464. The dynamics of harmonically excited system having rigid amplitude constraint, part 1: Ssubharmonic motions and local bifurcations; part 2 : chaotic motions and global bifurcations.

48. A. Fathi and N. Popplewell 1994 *Journal of Sound and Vibration* **170**, 365-375. Improved approximations for a beam impacting a stop.

49. T.P. Valkering 1994 *Journal of Sound and Vibration* **175**, 397-422. Non-trivial dynamics in a driven string with impact non-linearity.

50. H.S. Jing and K.C. Sheu 1989 *Journal of Sound and Vibration* **141**, 363-373. Exact stationary solutions of the random response of a single-degree-of-freedom vibro-impact system.

51. R. Palej and J. Niziol 1986 *Journal of Sound and Vibration* **108**, 191-198. On direct method of analysing impacting mechanical systems.

52. V.F. Zhuravley 1977 *Mechanics of Solids* 12, 14-18. Investigation of certain vibration-impact systems by the method of non-smooth transformations.

53. H.G. Davies 1980 *Journal of Sound and Vibration* 68, 479-487. Random vibration of beam impacting stops.

54. C.N. Bapat and N. Popplewell 1987 *Journal of Sound and Vibration* 113, 17-28. Several similar vibroimpact systems.

55. S. Natsiavas 1993 *Journal of Sound and Vibration* 165, 439-453. Dynamics of multiple-degree-of-freedom oscillators with colliding components.

56. C. Padmanabhan and R. Singh 1992 *Journal of Sound and Vibration* 155, 209-230. Spectral coupling issues in a two-degree-of-freedom system with clearence non-linearity.

57. R.J. Comparin and R. Singh 1990 *Journal of Sound and Vibration* 142, 101-124. Frequency response characteristics of a MDOF system with clearences.

58. Y.B. Kim, S.T. Noah and Y.S. Choi 1991 *Journal of Sound and Vibration* 144, 381-395. Periodic response of multidisk rotor with bearing clearences.

59. A. Kahraman and R. Singh 1991 *Journal of Sound and Vibration* 146, 135-156. Interactions between time-varying mesh-stiffness and clearence non-linearities in geared system.

60. A. Kahraman and R. Singh 1990 *Journal of Sound and Vibration* 142, 49-75. Non-linear gear dynamics.

61. A. Kahraman and R. Singh 1991 *Journal of Sound and Vibration* 144, 469-506. Non-linear dynamics of a geared rotor-bearing system with multiple clearences.

62. C.W. Stammers and M. Ghazavi 1991 *Journal of Sound and Vibration* 150, 301-315. A theoretical and experimental study of the dynamics of a four-bar chain with bearing clearence: Pin motion, contact loss and impact.

63. M.P. Paidoussis and G.X. Li 1992 *Journal of Sound and Vibration* 152, 305-326. Cross-flow induced chaotic vibrations of heat exchanger tubes impacting on loose supports.

64. M.P. Paidoussis, G.X. Li and F.C. Moon 1989 *Journal of Sound and Vibration* 135, 1-19. Chaotic oscillation of the autonomous system of a constrained pipe conveying fluid.

65. P. Lieber and D.P. Jensen 1945 *Transactions of the American Society of Mechanical Engineers* 67, 523-530. An acceleration damper: development design and some applications.

66. C. Grubin 1956 *Transactions of the American Society of Mechanical Engineers, Journal of Applied Mechanics* 23, 373-378. On the theory of the acceleration damper.

67. G.B. Warburton 1957 *Transactions of the American Society of Mechanical Engineers, Journal of Applied Mechanics* 79, 322-324. On the theory of the acceleration damper.

68. S.F. Masri and T.K. Caughey 1966 *Transactions of the American Society of Mechanical Engineers, Journal of Applied Mechanics* 33, 586-592. On the stability of the impact damper.

69. S.F. Masri 1970 *The Journal of Acoustical Society of America* 47, 229-237. General motion of impact dampers.

70. A.L. Paget 1937 *Engineering* 143, 305-307. Vibration in steam turbine buckets and damping by impact.

71. W.H. Reed 1967 *Wind Effects on Buildings and Structures, Proceedings of International Research Seminar, Ottewa* 2, 283-301. Hanging chain impact dampers - a simple method of damping tall, flexible structures.

72. M.M. Sadek 1972 *Machinery* 120, 152-161. Impact dampers for controlling vibration in machine tools.

73. A.K. Mallik 1990 *Principles of Vibration control.* New Delhi: Affiliated East-West Press Private Limited.

74. M.M. Sadek 1970 *Journal of Mechanical Engineering Science* 12, 268-287. The effect of gravity on the performance of an impact damper: I steady state motion, II stability of vibratory modes.

75. M.A. Dokainish and H. Elmaraghy 1973 *The American Society of Mechanical Engineers Publications* 73, DET 61. Optimum design parameters for impact dampers.

76. P.C. Pinotti and M.M. Sadek 1970 *Proceedings of the 11 th. International Machine Tools Design and Research Conference* A, 181-195. Design procedure and charts for the impact dampers.

77. C.N. Bapat and S. Sankar 1985 *Journal of Sound and Vibration* 99, 85-94. Single unit impact damper in free and forced vibration.

78. W.M. Mansour and D.R.T. Filho 1974 *Journal of Sound and Vibration* 33, 247-265. Impact dampers with coulomb friction.

79. K. Yasuda and M. Toyoda 1978 *Bulletin of the Japan Society of Mechanical Engineers* 21, 424-430. The damping effect of an impact damper.

80. S.F. Masri and A.M. Ibrahim 1973 *The journal of Acoustical Society of America* 53, 200-211. Response of the impact damper to stationary random excitation.

81. S.E. Semercigil and N. Popplewell 1988 *Journal of Sound and Vibration* 12, 178-184. Impact damping of random vibration.

82. S.F. Masri 1972 *Transactions of the American Society of Mechanical Engineers, Journal of Applied Mechanics* 39, 563-568.Theory of the dynamic vibration neutralizer with motion limiting stops.

83. M.D. Thomas and M.M. Sadek 1974 *Journal of Mechanical Engineering Science* 16, 109-116. The effectiveness of the impact damper with a spring supported auxiliary mass.

84. L. Chen and S.E. Semercigil 1992 *Journal of S and Vibration* 156, 445-459. A new tuned vibration absorber for wide band excitations.

86. N.Popplewell and S.E. Semercigil 1989 *Journal of Sound and Vibration* 133, 193-223. Performance of the bean bag impact damper for a sinusoidal external force.

87. C. Pang, N. Popplewell and S.E. Semercigil 1989 *Journal of Sound and Vibration* 133, 359-363. An overview of a bean bag damper.

88. S. Chatterjee, A.K. Mallik and A. Ghosh 1994 *Accepted for Publication in Journal of Sound and Vibration.* On impact dampers for non-linear vibrating systems.

89. S.F. Masri 1967 *Transactions of the American Society of Mechanical Engineers, Journal of Applied Mechanics* 34,

506-507. Motion and stability of two-particle single container impact damper.

90. S.F. Masri 1969 *Journal of Acoustical Society of America* **45**, 1111-1117. Analytical and experimental studies of multi-unit impact dampers.

91. C.N. Bapat, S. Sankar and N. Popplewell 1983 *53 rd. Shock and Vibration Bulletin* **4**, 1-12. Experimental investigations of controlling vibrations using multi-unit impact damper.

92. C.N. Bapat and S. Sankar 1985 *Journal of Sound and Vibration* **103**, 457-469. Multi-unit impact damper - reexamined.

93. C.Z. Cempel 1974 *Journal of Sound and Vibration* **34**, 199-209. The multi-unit impact damper: equivalent continuous force approach.

94. C.Z. Cempel 1975 *Journal of Sound and Vibration* **40**, 249-266. Receptance based model of the multi-unit impact neutralizer-MUVIN.

95. M.M. Nigm and A.A. Shabana 1983 *Journal of Sound and Vibration* **89**, 541-557. Effect of an impact damper on a multi-degree-of-freedom system.

96. R. Chelmers and S.E. Semercigil 1991 *Journal of Sound and Vibration* **146**, 157-161. Impact damping the second mode of a cantilever beam.

97. R. Chelmers and S.E. semercigil 1988 *Journal of Sound and Vibration* **126**, 221-235. The dynamic response of a centrifugal pendulum vibration neutralizer with motion limiting stops.

98. S.F. Masri, R.K. Miller, T.J. Dehghanyar and T.K. Caughey 1986 *Trnasactions of the American Society of Mechanical*

Engineers, Journal of Applied Mechanics 53, 658-666. Active parameter control of non-linear vibrating structures.

99. M.P. Karyeaclis and T.K. caughey 1987 *Trnasactions of the American Society of Mechanical Engineers, Journal of Applied Mechanics* 54. Stability of a semiactive impact damper.

100. J. Shaw and S.W. Shaw 1989 *Transactions of the American Society of Mechanical Engineers, Journal of Applied Mechanics* 56, 168-174. The onset of chaos in a two degree-of-freedom impacting system.

101. C.K. sung and W.S. Yu 1992 *Journal of Sound and Vibration* 158, 317-329. dynamics of a harmonically excited impact damper: bifurcation and chaotic motion.

102. S.L. Lau and W.S. Zhang 1992 *Transactions of the American Society of Mechanical Engineers, Journal of Applied mechanics* 59, 153-160. Non-linear vibration of piecewise linear systems by incremental harmonic balance method.

103. E.A. Jackson 1991 *Physica* D 50, 341-366. On the control of complex dynamic system.

104 L.KOCAREV, A.SHANG and L.O. CHUA 1993 *International Journal of Bifurcation and Chaos* 3, 479-483. Transitions in dynamical regimes by driving: a unified method of control and synchronization of chaos.

105. T.FANG and E.H. DOWELL 1987 *International Journal of Non-Linear Mechanics* 22, 267-274. Numerical simulations of jump phenomena in stable duffing system.

106. W.M. Mansour 1972 *Journal of Sound and Vibration* 25, 395-405. Quenching of limit cycles of a van der Pol oscillator.

107. A. Tondl 1975 *Journal of sound and Vibration* **42**, 251-260. Quenching of self-excited vibrations; equilibrium aspects.

108. A. Tondl 1980 *International journal of Nonlinear Mechanics* **15**, 417-428. Determination of the limit of initiation of self-excited vibrations of rotors.

109. A. Tondl 1976 *Journal of Sound and Vibration* **45**, 285-294. Quenching of self-excited systems: effect of dry friction.

110. K.R. Asfar 1989 *Transctions of the American Society of Mechanical Engineers, Journal of Vibration, Acoustics, Stress, and Reliability in Design* **111**, 130-133. Quenching of self-excited vibrations.

111. C. Hayashi 1964 *Nonlinear Oscillations in Physical Systems.* New York: McGraw-Hill Book Co.

112. J.D.CRAWFORD 1991 *Reviews of Modern Physics* **63**, 991-1037.Introduction to bifurcation theory.

113. B.RAVINDRA and A.K.MALLIK 1994 *Physical Review E* **49**,4950-4954. Role of non-linear dissipation in soft Duffing oscillators.

114. S. Chatterjee and A.K. Mallik 1995 accepted for publication in *Journal of sound and Vibration.* Bifurcation and chaos in autonomous self-excited oscillators with impact damping.

115. Y. Pomeau and P. Manneville 1980 *Communications in Mathematical Physics* **74**, 189-197. Intermittent transition to turbulence in dissipative dynamical systems.

116. P. Manneville and Y. Pomeau 1980 *Physica 1D*, 219-221. Diffrent ways to turbulence in dissipative dynamical systems.

116. P. Manneville and Y. Pomeau 1980 *Physica* 1D, 219-221. Diffrent ways to turbulence in dissipative dynamical systems.

117. P. Berge, Y. Pomeau and C. Vidal 1984 *Order Within Chaos, Towards a Deterministic approach to Turbulence. New York : A wiley interscience Publication, JOHN WILEY & SONS.

118. E. Ringuet, C. Roze and G. Gouesbet 1993 *Physical Review* 47E, 1405-1407. Experimental observation of type II intermittency in a hydrodynamic system.

119. B. Blazejczyk, T. Kapitaniak and J. Wojewoda 1994 *Journal of Sound and Vibration* 178, 272-275. Experimental observation of intermittent chaos in a mechanical system with impacts.

120. D.A. Rand, S. Ostlund, J. Sethna and E. Siggia 1982 *Physical Review letters* 49, 132-135 and *Physica* 8D, 303-306(1983). Universal transition from quasiperiodicity to chaos in dissipative systems.

121. R. Ecke and H. Haucke 1989 *Journal of Statistical Physics* 54, 1153-1172. Noise-induced intermittency in the quasiperiodic regime of Rayleigh-Benard convection.

122. J.P. Gollub and S.V. Benson 1980 *Journal of Fluid Mechanics* 100, 449-460. Many routes to turbulent convections.

123. S. Chatterjee, A.K. Mallik and A. Ghosh 1995 accepted for publication in *Journal of Sound and Vibration.* Impact dampers for controlling self-excited oscillation.

124. S. Chatterjee, A.K. Mallik and A. Ghosh 1995 accepted for publication in *Journal of Sound and Vibration.* Periodic response of piecewise non-linear oscillators under harmonic excitation.

APPENDIX - A

The elements of the Jacobian J of the right-hand-side of equations (3.17) are as follows:

$$J = \begin{bmatrix} J_{11} & J_{12} & J_{13} & J_{14} \\ J_{21} & J_{22} & J_{23} & J_{24} \\ J_{31} & J_{32} & J_{33} & J_{34} \\ J_{41} & J_{42} & J_{43} & J_{44} \end{bmatrix}$$

where

$$J_{11} = -\frac{h}{2} \quad ,$$

$$J_{12} = \frac{r_1 B(b)}{2\Omega} \cos(\theta_2 - \theta_1) - \frac{1}{2\Omega} \cos\theta_1 \quad ,$$

$$J_{13} = -\frac{r_1}{2\Omega} \sin(\theta_2 - \theta_1) \frac{\partial B(b)}{\partial b} \quad ,$$

$$J_{14} = -\frac{r_1 B(b)}{2\Omega} \cos(\theta_2 - \theta_1) \quad ,$$

$$J_{21} = \frac{\cos\theta_1 - r_1 B(b)\cos(\theta_2-\theta_1)}{2a^2\Omega} + \frac{3}{4}\frac{a}{\Omega} \quad ,$$

$$J_{22} = -\frac{1}{2a\Omega}\left\{ -\sin\theta_1 - r_1 B(b) \sin(\theta_2-\theta_1) \right\} \quad ,$$

$$J_{23} = \frac{r_1 \cos(\theta_2-\theta_1)}{2a\Omega} \frac{\partial B(b)}{\partial b} \quad ,$$

$$J_{24} = -\frac{r_1 B(b)}{2a\Omega} \sin(\theta_2 - \theta_1) \quad ,$$

$$J_{31} = -\frac{h}{2} \cos(\theta_1 - \theta_2) - \left(\frac{9a^2}{8\Omega} + \frac{\omega_\ell^2}{2\Omega} \right) \sin(\theta_1 - \theta_2)$$

$$J_{32} = \frac{ha}{2} \sin (\theta_1 - \theta_2) - (\frac{3a^3}{8\Omega} + \frac{a\omega_\ell^2}{2\Omega}) \cos (\theta_1 - \theta_2) \quad ,$$

$$J_{33} = 0 \quad ,$$

$$J_{34} = -\frac{1}{2\Omega} \left\{ \cos \theta_2 + h\,a\,\Omega \sin (\theta_1 - \theta_2) - (a\omega_\ell^2 + \frac{3}{4} a^3) \cos (\theta_1 - \theta_2) \right\} \quad ,$$

$$J_{41} = -\frac{1}{2b\Omega} \left\{ h\,\Omega \sin(\theta_1 - \theta_2) - (\omega_\ell^2 + \frac{9}{4} a^2) \cos (\theta_2 - \theta_1) \right\} \quad ,$$

$$J_{42} = -\frac{1}{2b\Omega} \left\{ h\,a\,\Omega \cos (\theta_1 - \theta_2) - (a\omega_\ell^2 + \frac{3}{4} a^3) \sin (\theta_2 - \theta_1) \right\} \quad ,$$

$$J_{43} = -\frac{1}{2b^2\Omega} \left\{ b (\Omega^2 - (\frac{1}{r_m} + 1)\, r_1 \frac{\partial B(b)}{\partial b}) - f_5 \right\} \quad ,$$

$$J_{44} = \frac{ha}{2b} \cos (\theta_1 - \theta_2) - (\frac{a\omega_\ell^2}{2\Omega b} + \frac{3a^3}{8b\Omega}) \sin (\theta_2 - \theta_1)$$
$$+ \frac{1}{2b\Omega} \sin \theta_2$$

and $f_5 = b\Omega^2 - r_1 B(b) (1 + \frac{1}{r_m})\, ha\,\Omega \sin (\theta_1 - \theta_2)$

$$- (a\omega_\ell^2 + \frac{3}{4} a^3) \cos (\theta_2 - \theta_1) + \cos \theta_2 \quad .$$

A P P E N D I X - B

The mathematical model of an impact pair is shown in Figure B.1 The contact dynamics of the two masses m_2 and m_1 are represented by the differential equations

$$m_2\ddot{X}_2 + C_2\ (\dot{X}_2 - \dot{X}_1) + K_2\ (X_2 - X_1) = 0 \qquad (B.1)$$

and

$$m_1\ddot{X}_1 + C_2\ (\dot{X}_1 - \dot{X}_2) + K_2\ (X_1 - X_2) = 0 \qquad (B.2)$$

Where the dot denotes the differentiation with respect to time t.

Substituting $Y_c = X_2 - X_1$ and $r_m = m_2/m_1$ in equations (B.1) and (B.2) we get

$$\ddot{Y}_c + 2\ \bar{\xi}\ \omega_n \dot{Y}_c + \omega_n^2\ Y_c = 0 \qquad (B.3)$$

where $\quad \bar{\xi} = \dfrac{C_2\sqrt{1 + r_m}}{2\sqrt{m_2\ K_2}} \quad$ and $\quad \omega_n = \sqrt{\dfrac{K_2}{m_2}(1 + r_m)}\quad$.

At the beginning of the contact phase we can write

$$\text{at} \quad t = 0, \quad Y_c = 0, \quad \dot{Y}_c = -V$$

and at the end of the contact phase, when Y_c is again zero, one gets

$$\dot{Y}_c = V\ e^{-\bar{\xi}\ \omega_n \pi / \omega_d}$$

where $\quad \omega_d = \omega_n\ \sqrt{1 - \bar{\xi}^{\,2}}$

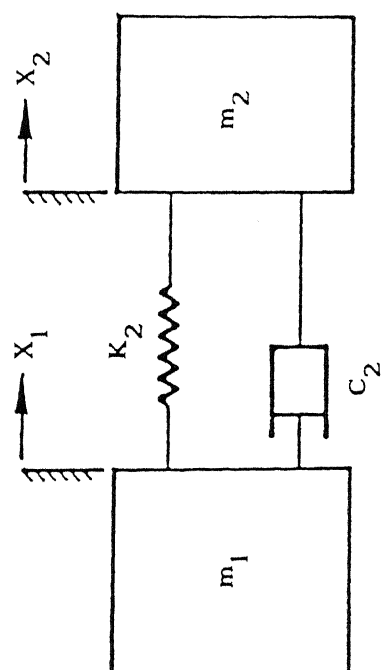Thus, according to the definition of the coefficient of restitution (χ)

Figure B.1   Model of an impact pair.

$$\chi = \exp \left[- \pi \, \bar{\xi} \, / \, \sqrt{1 - \bar{\xi}^2} \; \right]$$

which gives $\quad \xi_c = \dfrac{C_2}{2\sqrt{K_2 m_2}} = - \dfrac{\ln(\chi)}{[\pi^2 + \ln(\chi)^2]^{1/2} (1 + r_m)^{1/2}}$

The above model of an impact pair is seen to be satisfactory only for high values of the coefficient of restitution. The model seems to fail for low values of χ implying a high value of ξ_c. A high value of damping enhances the time of contact and thus violates the condition of zero contact time during impact.

A P P E N D I X - C

Let us consider the system discussed in section 3.5 with $\chi = 1$ (i.e. $C_2 = 0$ in Figure 3.9). The time response of the primary oscillator, given by various methods are shown in Figure C.1. It is clearly seen from this figure that, the HBM while providing a good estimate of the maximum value of the response during a cycle fails to predict the time history accurately. The EPL technique, containing information in both time and frequency domains, is capable of producing the entire time history of the response very accurately. It is expected that this method may work very well even for a smooth, strongly non-linear oscillator, an aspect which is worth further investigations.
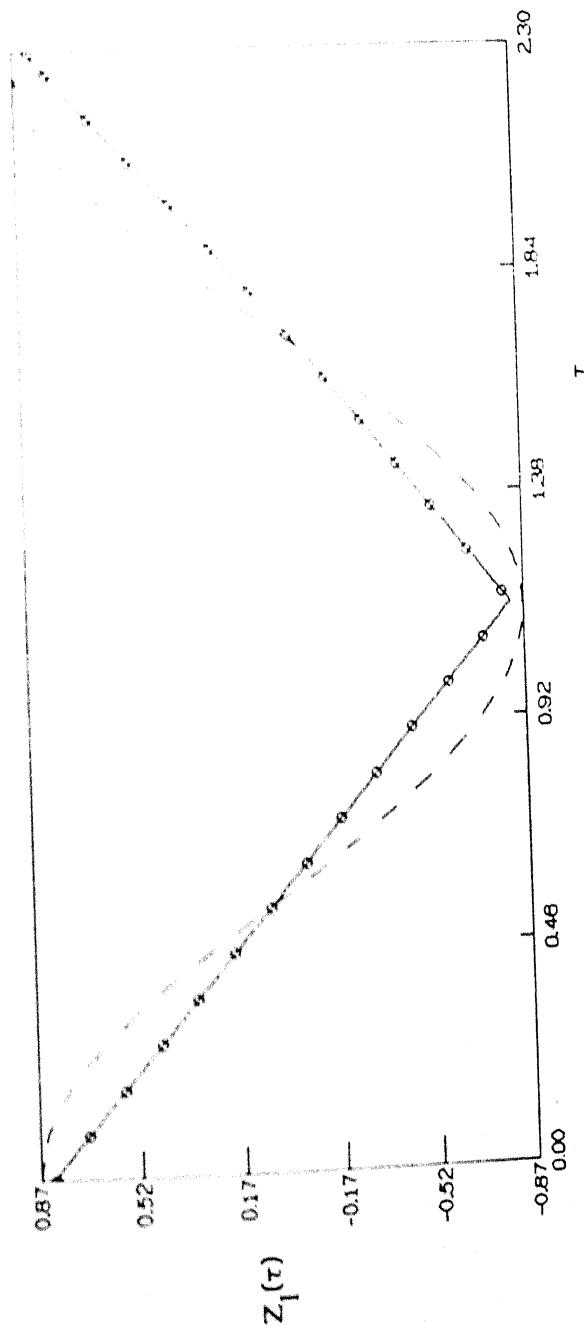
Figure C.1   Time response of the Duffing's oscillator with an impact damper. $\Omega = 2.75$, $h = 0.2$, $\omega_{\ell} = 1$, $\chi = 1$, $d_0 = 17$, $r_m = 0.05$. ——— EPL, – – – HBM, o numerical integration.